

**Micro-Manipulation and Bandwidth Characterization of
Ionic Polymer Actuators**

by

Curt S. Kothera

Thesis submitted to the Faculty of the
Virginia Polytechnic Institute and State University
in partial fulfillment of the requirements for the degree of

Master of Science

in

Mechanical Engineering

Donald J. Leo, Chair
Harry H. Robertshaw
William R. Saunders

December 2002
Blacksburg, Virginia

Keywords: ionic polymer, electroactive polymer, IPMC, bandwidth, micro-manipulation

Copyright by Curt S. Kothera, 2002

Abstract

Micro-Manipulation and Bandwidth Characterization of Ionic Polymer Actuators

Curt S. Kothera

Ionic polymer materials are a class of electroactive polymers that have been used in recent applications that take advantage of their large bending deflection. Although these materials have been around since the 1960s, it has only been in the last decade that their electromechanical coupling has been discovered. Because their life as a transducer has been relatively short, the underlying mechanisms for their mechanical motion have not yet been fully characterized. Modeling has been performed with ionic polymers, but there is no existing model, to date, that explains all the physical phenomena associated them.

The work presented in this document will contribute to the characterization of these materials. To better understand the dehydration effect of ionic polymers operating in an open air environment, research was performed to help characterize this effect. Through the use of frequency response analysis, trends were established showing how the material's response characteristics varied with time, as the polymer dehydrated. These tests were also run at different humidity levels to assess the impact environmental conditions had on the response. It was shown that lower humidity levels cause the system parameters to shift at a higher rate.

The two configurations tested were clamped-free and clamped-clamped, in an effort to bound the performance of the actuators for engineering applications. The clamped-clamped condition also facilitated applying tension to the polymers for evaluation of the dehydrating effects. Several comparisons to beam theory were made throughout the analysis, using it as a baseline condition illustrator. Though qualitative results were obtained

with the polymers, there was much discrepancy in quantitative measures. This was to be expected though, because ionic polymers are composite actuators that exhibit nonlinear behavior, while uniform beams are linear.

Environmental testing was not all that was done, however. Control techniques were applied to improve the closed-loop performance of the actuators. Using proportional-integral control, it was demonstrated that ionic polymers are capable of tracking reference inputs better than it was previously thought. This result will validate future experimentation with ionic polymers for micro-manipulation applications. The simplicity of integral control also eliminated the need for cumbersome model derivations and control system designs, reducing the time necessary to implement and test an actuator. Through the use of this control algorithm, the closed-loop bandwidth was also characterized for the cantilever and clamped-clamped polymers.

Acknowledgments

I would first like to acknowledge my thesis advisor Dr. Donald J. Leo, whose knowledge and guidance has helped me throughout this research process, both in experimentation and in writing. I would also like to thank the other members of my committee, Dr. Harry H. Robertshaw and Dr. William R. Saunders, for their additional advice.

For financial support, I would like to thank the Air Force Research Laboratory in Albuquerque, New Mexico, where, in addition to funding, they offered me a summer position to conduct much of the required experimental work. In particular, I would like to thank Dr. Lawrence M. Robertson for serving as a mentor while I carried out my research at AFRL, and Dr. Benjamin K. Henderson for allocating the necessary funds.

Back at the Center for Intelligent Material Systems and Structures at Virginia Tech, I would first like to express my gratitude to Matt Bennett, who not only introduced me to the laboratory equipment, but also manufactured the ionic polymer samples that made my research possible. I would also like to extend thanks to Kenn Newbury, Kevin Farinholt, Barbar Akle, and John Franklin for the numerous discussions of their work with ionic polymer materials and the help they provided me with in the laboratory.

In memory of Catherine and Karl Lorenz

Contents

List of Tables	ix
List of Figures	xi
Nomenclature	xv
Chapter 1 Introduction	1
1.1 Background	1
1.1.1 History	1
1.1.2 Physical Nature of the Material	4
1.1.3 Comparison of Intelligent Materials	7
1.2 Manufacture of Ionic Polymer-Metal Composites	9
1.3 Applications	12
1.3.1 Robotics	12
1.3.2 Biomedical	14
1.3.3 Space Systems	15
1.4 Motivation	17
1.5 Technical Objectives and Contributions	18
1.6 Thesis Overview	19
Chapter 2 Dynamic Response	20
2.1 Time Response	20
2.1.1 Test Setup	20
2.1.2 Step Displacement Results	23
2.1.3 Sinusoidal Displacement Results	29
2.2 Frequency Response	31

2.2.1	Test Setup	32
2.2.2	Transfer Function Results	32
2.3	Summary	39
Chapter 3 Effects on Open-Loop Bandwidth		40
3.1	Test Setup	40
3.2	Humidity Effects	43
3.2.1	Testing Method	44
3.2.2	Cantilever Results	45
3.2.3	Clamped-Clamped Results	50
3.2.4	Discussion	54
3.3	Tension Effects	56
3.3.1	Testing Method	57
3.3.2	Tensioning Results	57
3.3.3	Discussion	64
3.4	Summary	65
Chapter 4 Control Techniques		66
4.1	State-Space Control	66
4.1.1	Method and Design Basics	67
4.1.2	Previous Results	69
4.2	Proportional-Integral Control	70
4.2.1	Modeling and Simulations	71
4.2.2	Test Setup	78
4.2.3	Single-Layer Step Response	80
4.2.4	Single-Layer Sinusoidal Response	83
4.2.5	Multi-Layer Step Response	87
4.2.6	Multi-Layer Sinusoidal Response	90
4.2.7	Discussion	92
4.3	Adaptive Control	100
4.3.1	Reference Model Selection	101
4.3.2	Controller Design and Analysis	102
4.3.3	MRAC Simulation	106

4.3.4	Test Setup	107
4.3.5	Experimental Results	108
4.4	Summary	111
Chapter 5	Conclusions	113
5.1	Conclusions of Research	113
5.2	Contributions	114
5.3	Future Work Recommendations	115
Bibliography		118
Appendix A	Humidity Effects Data Plots	123
Appendix B	Tension Effects Data Plots	128
Appendix C	Control Scheme Block Diagrams	130
Vita		133

List of Tables

1.1	Property Comparison of Bender-Type Smart Materials.	9
2.1	Step Response Characteristics for Cantilevered Ionic Polymer Actuators. . .	29
2.2	Sinusoidal Time Response Characteristics for Ionic Polymer Actuators. . . .	30
2.3	Data Collection Settings for Frequency Response Testing.	33
2.4	Weighted Natural Frequencies for Clamped-Free and Clamped-Clamped Beams.	38
3.1	Summary of Data for Humidity Effects on the Natural Frequency of Ionic Polymers.	55
3.2	Force Conversion Values for Load Cell Outputs.	58
3.3	Natural Frequency Comparison of a Clamped-Clamped Uniform Beam with Polymer Properties to an Ionic Polymer.	60
4.1	Averaged Parameter Values used for State-Space Model with Integral Control.	72
4.2	Results from Pole Placement Iterations using Integral Control.	75
4.3	Summary of Integral Control Results for Single-Layer Ionic Polymers under a Step Input.	84
4.4	Summary of Integral Control Results for Single-Layer Ionic Polymers under a Sinusoidal Input.	86
4.5	Summary of Integral Control Results for Multi-Layer Ionic Polymers under a Step Input.	89
4.6	Summary of Integral Control Results for Multi-Layer Ionic Polymers under a Sinusoidal Input.	92
4.7	Characteristic Cantilevered Frequency Response Values.	94
4.8	Comparison of Controlled Cantilevered Response to Predicted Response. . .	95

4.9	Characteristic Clamped-Clamped Frequency Response Values.	96
4.10	Comparison of Controlled Clamped-Clamped Response to Predicted Response.	97
4.11	Summary of Closed-Loop Bandwidth Characterization Results.	99

List of Figures

1.1	Ionic polymer bender. The large bending deflection of an ionic polymer demonstrates the electromechanical coupling of the material.	3
1.2	Chemistry of Nafion TM . The chemical structure of Nafion TM includes fluorocarbons, oxygen, sulfonate groups, and a mobile cation, which is often hydrogen. In the figure, a varies from 5 to 11 and b is usually 1.	5
1.3	Ionic motion of the membrane. The bending motion in an ionic polymer occurs when an electric field is applied across its thickness. Initially the polymer is straight (a), but when the voltage is applied, it bends toward the side of the positive electrode (b) as the cations are attracted to the negative electrode.	7
1.4	Cross-section of ionic polymer actuator. A scanning electron micrograph of the cross-section (a) and zoomed in on one side (b) show the dendritic electrodes produced from the co-reduction process. The thin gold layer can also be seen.	11
2.1	Time response testing equipment used to measure the displacement of the ionic polymer as a function of time.	21
2.2	Under small deflections (a), the laser vibrometer is able to track the motion, but for larger deflections (b), it is unable to measure the polymer's position.	22
2.3	Close-up of test fixture showing the two clamps and the unislide, used for different testing configurations.	23
2.4	Typical step response of a cantilevered IPMC (a) compared to a more unusual response (b).	25

2.5	Step responses of 4-stack IPMC cantilever showing a slow increase (<i>a</i>) and slow decrease (<i>b</i>).	26
2.6	Cantilever step responses of packaged, 2-stack actuators showing different ending positions.	27
2.7	Clamped-clamped ionic polymer step responses.	28
2.8	Cantilevered ionic polymer responses to sinusoidal input of 300 microns at 0.5Hz (<i>a</i>) and 4Hz (<i>b</i>). Note that the time scales are different.	29
2.9	Clamped-clamped sinusoidal time response for a 2 micron wave at 0.16Hz (<i>a</i>) and 3Hz (<i>b</i>).	31
2.10	Natural frequency comparison of ionic polymer benders. The short polymer is (8 x 5 x 0.2)mm and the long polymer is (24 x 5 x 0.2)mm.	34
2.11	Cantilever (<i>a</i>) and clamped-clamped (<i>b</i>) frequency response functions shifting with time.	36
3.1	Test setup for controlled humidity experiments. Note that the signal analyzer is not included in the figure.	41
3.2	Close-up of the test fixture points out the pertinent devices used in the testing configurations.	42
3.3	Natural frequency as a function of time and humidity for cantilever polymer.	46
3.4	Cantilever peak magnitude as a function of time and humidity.	47
3.5	Cantilever natural frequency shift with increased input voltage.	48
3.6	Magnitude plots of cantilever for increased input.	48
3.7	Percent difference plots comparing initial to final values for frequency and magnitude at each humidity level.	49
3.8	Clamped-clamped frequency shift as a function of time and humidity.	50
3.9	Magnitude results for clamped-clamped polymer actuator.	51
3.10	Clamped-clamped frequency shift for an increased input.	52
3.11	Clamped-clamped magnitude shift for an increased input.	53
3.12	Percent difference for the clamped-clamped ionic polymer.	54
3.13	Tensioned ionic polymer frequency shift as a function of time and humidity.	60
3.14	Tensioned magnitude results of clamped-clamped ionic polymer.	61
3.15	Transfer functions of clamped-clamped polymer with 800mV tension.	62

3.16	Low frequency magnitude plots for 600mV tension (a) pointing out magnitude values at 4Hz (b).	63
4.1	LQR control results using a linear observer-estimator.	70
4.2	Full-state feedback integral control simulation results (a) and associated control voltage (b).	74
4.3	Block diagram model of integral control.	75
4.4	Simulation results for integral control in transfer function form (a) and control voltage (b).	78
4.5	Schematic of the control experiment setup.	79
4.6	Open-loop step response (a) of cantilevered ionic polymer compared to result using integral control with a gain of 16 (b).	81
4.7	Open-loop step response (a) of a clamped-clamped ionic polymer compared to result using integral control with a gain of 20 (b).	82
4.8	Cantilevered polymer displaying its position holding capability (a) and corresponding control voltage (b).	83
4.9	Integral control of cantilevered polymer used to track sinusoidal inputs. The 25 μ m input wave is at 5Hz (a) and 15Hz (b).	85
4.10	Clamped-clamped polymer tracking a 2 μ m sine wave at 2Hz (a) and 6Hz (b).	86
4.11	Packaged stack of two ionic polymer cantilevers open-loop response (a) compared to result using integral control (b).	88
4.12	Stack of four ionic polymer cantilevers open-loop response (a) and result using integral control (b).	89
4.13	Sinusoidal tracking of packaged 2-stack actuator with integral control for a 10 μ m wave at 1Hz (a) and 5Hz (b).	90
4.14	Sinusoidal tracking of 4-stack cantilevered actuator using integral control for a 10 μ m wave at 1Hz (a) and 5Hz (b).	91
4.15	Transfer functions for cantilevered (20 x 5 x 0.2)mm ionic polymer actuator.	93
4.16	Transfer functions for clamped-clamped (20 x 5 x 0.2)mm ionic polymer actuator.	96
4.17	Transfer functions for “short” (8 x 5 x 0.2)mm cantilevered ionic polymer.	99
4.18	Integral control results (a) compared with a more ideal system model (b).	101

4.19	Simulation results of MRAC system given a reference step input (left) and a sinusoidal input (right). The adaptation gain in this example is 20.	106
4.20	Step response with MRAC system using an adaptation gain of 50.	109
4.21	Step response with MRAC system using an adaptation gain of 80.	110
4.22	MRAC system results for a sinusoidal input.	111
A.1	Natural Frequency Shift as a Function of Time for Cantilever Ionic Polymer with 500mV-rms Input.	124
A.2	Magnitude Shift as a Function of Time for Cantilever Ionic Polymer with 500mV-rms Input.	124
A.3	Natural Frequency Shift as a Function of Time for Cantilever Ionic Polymer with 750mV-rms Input.	125
A.4	Magnitude Shift as a Function of Time for Cantilever Ionic Polymer with 750mV-rms Input.	125
A.5	Natural Frequency Shift as a Function of Time for Clamped-Clamped Ionic Polymer with 500mV-rms Input.	126
A.6	Magnitude Shift as a Function of Time for Clamped-Clamped Ionic Polymer with 500mV-rms Input.	126
A.7	Natural Frequency Shift as a Function of Time for Clamped-Clamped Ionic Polymer with 1V-rms Input.	127
A.8	Magnitude Shift as a Function of Time for Clamped-Clamped Ionic Polymer with 1V-rms Input.	127
B.1	Natural Frequency Shift as a Function of Time and Tension for Clamped-Clamped Ionic Polymer with 1V-rms Input. Tensions given in milli-Volts.	129
B.2	Magnitude Shift as a Function of Time and Tension for Clamped-Clamped Ionic Polymer with 1V-rms Input. Tensions given in milli-Volts.	129
C.1	Proportional-Integral Control Block Diagram.	131
C.2	Model-Reference Adaptive Control Block Diagram.	132

Nomenclature

m - mass

ρ - material mass density

L - length

I - moment of inertia

k - stiffness

ζ - damping ratio

E - elastic modulus (Young's modulus)

e_m - energy mass density

f - frequency in Hertz [Hz]

ω - frequency in radians per second [rad/s]

λ - natural frequency parameter

F_T - applied tensile load

F_b - buckling load

ϑ - load cell output

t - time variable

s - Laplace variable

$y(t)$ - output vector

$u(t)$ - input vector

$r(t)$ - reference input vector
 $e(t)$ - error, difference between reference and output
 $x(t)$ - state vector
 $u(t)$ - control signal
 $\hat{x}(t)$ - observer state vector
 $x_I(t)$ - integral term

A, B, C, D - state-space matrices
 Q, R - linear quadratic regulator weighting matrices
 q, r - linear quadratic regulator design variables
 I - identity matrix
 P - controllability matrix

$Y(s)$ - system output, Laplace domain
 $U(s)$ - system input, Laplace domain
 $R(s)$ - reference input, Laplace domain
 $E(s)$ - error signal, Laplace domain

T_I - integral time
 t_0 - initial time
 t_r - rise time

K - control gains
 G - full-state feedback gains
 G_r - feedforward gains

$K(s)$ - controller transfer function
 $G(s)$ - system transfer function

A_m, B_m - model parameters
 A_p, B_p - plant parameters
 $\hat{A}(t)$ - variable model parameter

A^* - ideal model parameter

$\tilde{A}(t)$ - parameter errors

ξ - adaptation gain

$V(\cdot)$ - Lyapunov function

Chapter 1

Introduction

Ionic polymer materials are a class of electroactive polymers that fall under the greater regime of smart or intelligent materials. Although the materials have been used for some time, the electromechanical coupling of ionic polymers was only recently discovered. Therefore, being a relatively new material, the mechanisms responsible for their motion are not yet fully understood. Though several models have been proposed, none fully account for all the dynamics associated with these materials. Another aspect of ionic polymers that makes them a challenging material for engineers to model and implement is the high degree of nonlinearity involved. The research presented in this work is aimed to gain more insight into the dynamic nature of the material, and to show that some implementation can be achieved, even without a fully realized model.

1.1 Background

As a starting point, the background of ionic polymers will be discussed to show how the material has reached its current state-of-the-art. Following the brief history of ionic polymers, features of the material that are understood will be discussed. Then, they will be compared to other similar intelligent materials, where advantages and disadvantages will be discussed.

1.1.1 History

It is difficult to discuss the history of ionic polymers without any mention of the base material NafionTM and fuel cell technology. The birth of fuel cells dates back over a century

ago to 1839 when William Grove first made their discovery (Grove, 1839). His discovery of the fuel cell used hydrogen as fuel and oxygen to produce electricity. Despite the numerous advantages to using fuel cells, including clean emission and high efficiency, no major technological breakthroughs occurred for nearly another hundred years. However, in 1933, Cambridge University's F. Thomas Bacon had laid the groundwork for their future integration into spacecraft (Bacon, 1954). While this basis was primarily built upon Grove's discovery and not necessarily the type of fuel cell that would be used in spacecraft, it was important because it would spark the research and development of the fuel cell field.

Around this time, 1938 to be exact, some unrelated work was being done at DuPont in the United States. Roy Plunkett had been working with gases related to refrigerants when he discovered that a compressed, frozen sample of tetrafluoroethylene had spontaneously polymerized. The result was the solid polytetrafluoroethylene, which in 1945 would become the registered trademark TeflonTM. While TeflonTM would not be directly related to advancements in fuel cell technology, it would provide the base material.

Further development of these technologies leads fuel cells and DuPont into the 1960s. By modifying TeflonTM, Walther Grot was able to develop the first synthetic polymer with ionic properties, which would come to create a new class of polymers known as ionomers. This material was called NafionTM and is considered a perfluorosulfonate ionomer. Both TeflonTM and NafionTM are registered trademarks of E. I. DuPont de Nemours.

Having TeflonTM as its base material, which has uses in several fields itself, NafionTM's properties play host to a variety of applications. Some of these properties include high working temperatures, high resistance to chemical attack, high permeability to water, and it is a super-acid catalyst. Initially developed for the chlor-alkali industry as a water electrolyzer, NafionTM's applicability has greatly expanded to use in fine chemicals production, selective gas humidifiers or dehumidifiers, and fuel cells. The type of fuel cell that NafionTM is classified as is called either a proton exchange membrane or a polymer electrolyte membrane, abbreviated as PEM.

The initial success of fuel cell implementation by NASA, both in Gemini and Apollo missions, kept their development moving in a forward direction into the 1970s energy crisis, where the variety of fuel cell types increased in an effort to reduce fossil fuel consumption. With government support to develop fuel cells and the increasing variety of different types, PEMs took a backseat in this phase because of their extremely high cost. However, research

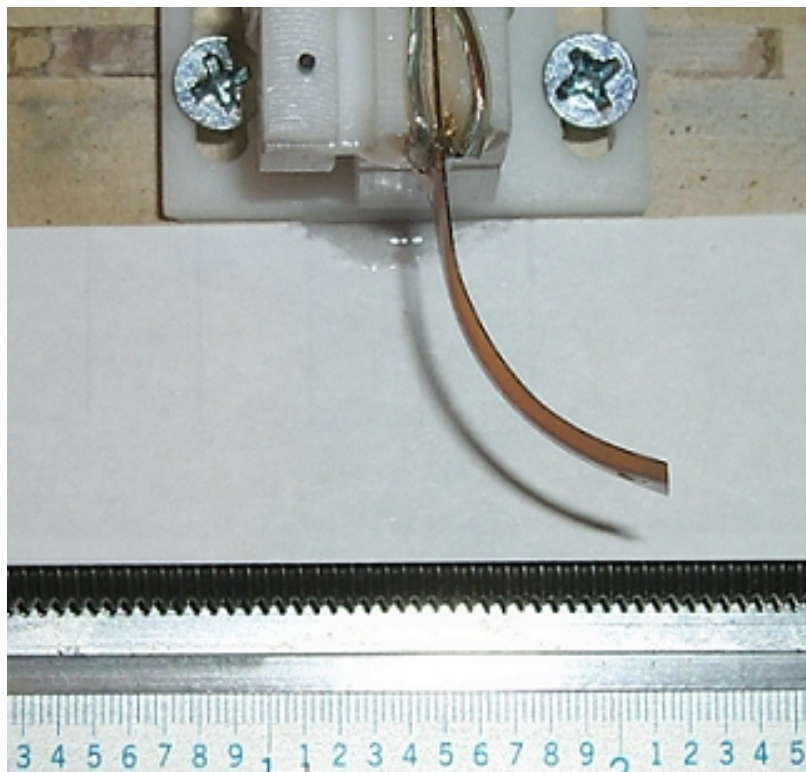


Figure 1.1: Ionic polymer bender. The large bending deflection of an ionic polymer demonstrates the electromechanical coupling of the material.

did continue with PEMs, and during the 1980s, two independent groups discovered how to substantially reduce cost, thus increasing the commerciability of this type of fuel cell. These groups were at Los Alamos National Laboratory and Texas A&M University, and they contributed to opening the door of fuel cell technology for automobiles, where NafionTM is widely used today. Automotive applications favor the use of PEM fuel cells because they are comparably light in weight and can operate at temperatures lower than 175 degrees Celsius.

With the automotive industry leaders all researching PEM fuel cells, NafionTM had become more readily available for other research as well. Fuel cells use the chemoelectric coupling properties of PEMs to produce electric energy, but that is not the only application for materials like NafionTM. In the early 1990s, three research groups demonstrated the transduction properties of ionic polymer materials in terms of electromechanical effects. One group in Japan (Oguro et al., 1992) and one group in the United States (Shahinpoor, 1992) presented actuation results with ionic polymers, while another group in the United States showed the sensing capability of ionic polymers (Sadeghipour et al., 1992).

The results were that by applying a voltage across the thickness of the material, it would mechanically deform, and conversely, by deforming the material, a measurable charge flow was produced. This means that in addition to chemoelectric fuel cell power generation, ionic polymers could be used as electromechanical actuators and sensors. Figure 1.1 illustrates the electromechanical actuation of an ionic polymer bender. The polymer in the figure is about 30mm long and the tip is shown to bend 16mm when 3 Volts are applied.

Being that an entirely new field of research was created following the discovery of the electromechanical coupling of ionic polymers, the applications that could benefit from these materials were left to the imagination of the engineers and researchers investigating them. Ionic polymers are now considered a smart or intelligent material and are classified as an electroactive polymer (EAP). The EAP branch of smart materials can be divided even further into two separate groups depending on the driving forces. These two groups are either electric EAP or ionic EAP, where the material is driven solely by the applied electric field or Coulomb forces, or if the motion involves mobility or diffusion of ions, respectively. The ionic EAP category consists of ionic polymer gels (IPG), ionomeric polymer-metal composites (IPMC), conductive polymers (CP), carbon nanotubes (CNT), and electro-rheological fluids (ERF) (Bar-Cohen, 2001). Of these types, IPMCs are the specific ionic EAP used in the research presented in this work.

Research and support have continued to progress in the field of ionic polymers and have led to even more interesting and challenging ideas. There are now entire conferences and symposia dedicated specifically to the future development of electroactive polymers, covering all aspects of the research. Some of the areas of research include electromechanical modeling, reduction of manufacturing cost, integration as a sensor/actuator pair, and control.

1.1.2 Physical Nature of the Material

Being a relatively new material in terms of electromechanical effects, the mechanisms responsible for the motion of ionic polymers are still being debated. While several models have been proposed with experimental verification, there is no single model that is able to realize all the dynamics of ionic polymers over all operating conditions.

Most of the known aspects of ionic polymer materials have to do with the chemoelectric properties from fuel cell research. For the purpose of gaining a broader background

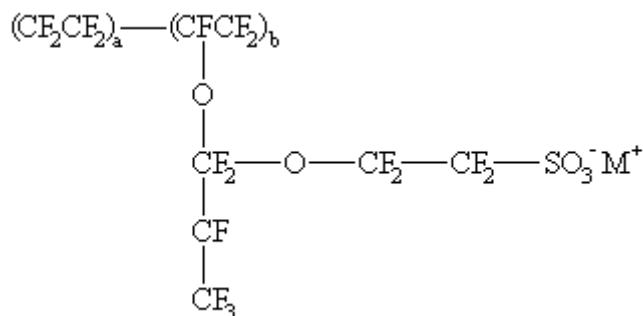


Figure 1.2: Chemistry of Nafion™. The chemical structure of Nafion™ includes fluorocarbons, oxygen, sulfonate groups, and a mobile cation, which is often hydrogen. In the figure, a varies from 5 to 11 and b is usually 1.

of the materials, the electric power generation of ionic polymers will be briefly discussed, prior to discussing what is known about their mechanical motion. The type of fuel cell characteristics to be reviewed are those for a PEM fuel cell, which is also known as the solid polymer electrolyte (SPE™). SPE™ is a registered trademark of General Electric.

Nafion™ is one of the most common polymer electrolyte membranes, and as the type implies, it is a very thin material. It typically ranges from about 50 to 180 microns, which is about the same thickness as a few sheets of plastic wrap. As mentioned before, the membrane is a solid perfluorosulfonate ionomer consisting of three main regions. Since Nafion™ is a co-polymer of Teflon™, the membrane has a Teflon™-like fluorocarbon backbone, side groups containing oxygen, in addition to carbon and fluorine, and sulfonic acid ion clusters. In the ion clusters, the negatively charged ions, or anions, SO_3^- are fixed to the side groups, while the positively charged ions, or cations, H^+ are mobile when the membrane is hydrated with water. When mobile, the cations jump from fixed anion to fixed anion, moving from one side of the membrane to the other, through the thickness of the material. Figure 1.2 shows the chemical structure of the Nafion™ polymer membrane.

In a PEM fuel cell, the two sides of the membrane are kept separate with one having an anode reaction and the other having a cathode reaction. This creates a single direction of ion migration in the material, which is important for the operation of the fuel cell. The anode reaction starts with hydrogen and separates it into two cations and two electrons, and the cathode reaction starts with oxygen, hydrogen cations, and electrons, and yields water. The actual power generation comes from the electrons that are removed by an external

load. Restated, hydrogen is first ionized, passing the cations through the membrane and drawing the electrons out by a load, creating power. Then, the cations and electrons are reunited with the addition of oxygen to produce water, the byproduct of the process. Each membrane itself does not produce too much power, but they can be stacked together making a multi-layered fuel cell that increases the output, where their high power to weight ratio becomes advantageous. For a much more comprehensive review of PEM fuel cells and how they function, the reader is referred to Thomas and Zalbowitz (1999).

Switching emphasis from chemoelectrical to electromechanical coupling, some of the knowledge of the physical nature of the material can be applied to try to understand how ionic polymers move. The ionic polymer-metal composites consist of a NafionTM membrane that has been electroded on each side. Typically, the ionic polymer is cut into a strip and placed in an electroded clamp at one end, leaving the other end free to move. The clamp is then connected to a power source or signal generator and a voltage is applied across the polymer's thickness. Contrary to the fuel cell application, the transducers do not have separate sides. The direction of the applied voltage dictates the direction that the cantilever moves. This means that either side can be the anode or cathode, or it can change with time. This ability of bi-direction ion migration in ionic polymers is a favorable characteristic for their use as transducers.

Since the mechanisms of motion in ionic polymers are yet to be fully understood, no equations will be presented on the matter. Rather, the most widely accepted concept of the bending motion of the polymers will be illustrated. As determined from the development of PEM fuel cell technology, it is known that the cations are mobile and that they move from one side of the membrane to the other. What is highly regarded as the fundamental mechanism of motion has to do with this ion migration through the membrane material. When an electric field is applied across the thickness, one side of the ionic polymer becomes positively charged and the other becomes negatively charged. Because the mobile cations are positively charged, they are attracted to the negatively charged surface, toward which they begin to migrate. As the cations move through the hydrated polymer, they drag water with them to the negatively charged surface. This negative surface then becomes swollen, while the positive surface has lost some of its water and cations. The negatively charged surface now has an accumulation of water molecules and cations that have migrated from the positively charged surface. This makes the negative surface want to stretch, while the

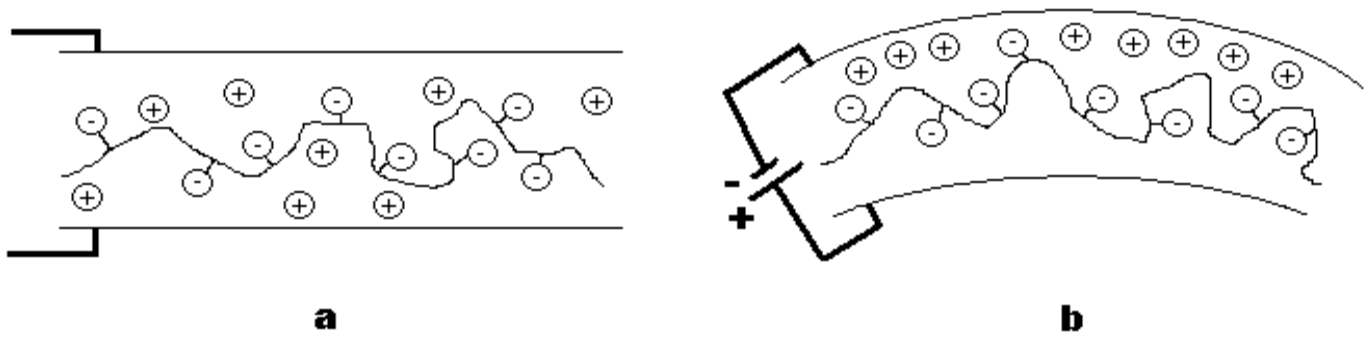


Figure 1.3: Ionic motion of the membrane. The bending motion in an ionic polymer occurs when an electric field is applied across its thickness. Initially the polymer is straight (*a*), but when the voltage is applied, it bends toward the side of the positive electrode (*b*) as the cations are attracted to the negative electrode.

positive surface wants to shrink. Thus, the polymer bends toward the positive side. A sketch of this can be seen in Figure 1.3. This phenomenon has also been described in terms of a pressure gradient in the material, high at the negative electrode and low at the positive electrode.

Having presented the physical nature of the material, in addition to mentioning that ionic polymers a class of smart materials, it may be of interest to see how ionic polymers compare to other smart material technology. This is the subject of the following section.

1.1.3 Comparison of Intelligent Materials

With so many different intelligent materials on the market, one may begin to wonder why research continues with ionic polymer materials. After all, with other smart materials, the underlying mechanisms are well understood and the various types of transducers have been used in engineering applications for a long time. Some of these types of materials are piezoelectrics, shape memory alloys, magneto-rheological fluids, and electro-strictive materials.

One of the key advantages to using ionic polymers has to do with the required actuation voltage. It is known for piezoceramics, which move in the microstrain regime, that massive power electronics are required to supply the necessary voltage for actuation. Despite their precision positioning and sensing capabilities, piezoceramics are limited in application by their high required power for operation and the increased weight that accompanies

the electronics. Ionic polymers, on the other hand, operate on relatively low voltages. Compared to piezoceramics, ionic polymers require voltage levels two to three orders of magnitude lower. This eliminates the extra mass associated with power electronics, making ionic polymers a lightweight alternative. Basically, piezoelectrics require power supplies and amplifiers, while ionic polymers can run off battery-level voltage. On the other hand, piezoceramics do not require high current with their high voltage, while ionic polymers need relatively high current to go along with their low voltage.

Another pair of transducer properties that are often discussed together are force and displacement. That is, how much force can it produce and how far will it move? The converse is of interest in sensing applications. For this comparison, a piezoelectric bender will be used since the bender, or cantilever configuration, is what has been used most often with ionic polymers. For a common piezo bender, forces in the hundreds of milli-Newtons and displacements near a millimeter are achievable. A common ionic polymer bender may be able to achieve over a centimeter of displacement and a maximum force of around one milli-Newton. These rough numbers do vary with transducer dimensions and voltage level, but what they say is that piezoelectrics are usually considered high force, low displacement transducers, whereas ionic polymers are considered low force, high displacement transducers.

Frequency range is another important characteristic of dynamic sensing and actuation elements. Like the force and displacement values stated above, this also depends on transducer dimensions, but will be reported in terms of the first resonant frequency for typical dimensions. An ionic polymer bender 20mm long has a first natural frequency of about 20Hz, while a piezo bender 70mm long has a first natural frequency of 60Hz. To relate this to a cantilever beam, theory shows that the longer the bender, the lower the natural frequency, and vice versa. Therefore, a piezo bender the same length as the ionic polymer bender would have a much higher natural frequency. Frequency range is, of course, more application specific when determining what is good and what not so good, but a higher frequency range does say that the transducer will respond faster. What can come out of this comparison is that, comparatively, ionic polymers serve as a low frequency transducer.

Material properties are yet to be discussed, so they will be commented on here. Two of the most common material properties discussed are elastic modulus and density. Ionic polymers have a density of around 3000kg/m^3 and an elastic modulus of about 200MPa. Piezoelectrics have a density of about 7800kg/m^3 and a modulus around 66GPa. The density

Table 1.1: Property Comparison of Bender-Type Smart Materials.

Property	Units	IPMC ₀	IPMC ₁	Piezo Bender	PVDF
ρ	kg/m ³	3200	2000	7800	1800
E	GPa	0.20	0.05	66.0	2.0
e_m	mJ/kg	7.0	4.5	27	4.1

gives insight into the relative weights of the materials, while the modulus is the inverse of the material compliance. The compliance, or softness, is one aspect of ionic polymers that is very favorable because they can be used as a soft actuator or sensor. This enables their use in flexible systems, where piezoelectrics are not as good of a choice. Another material that provides some competition for ionic polymers is polyvinylidene fluoride (PVDF), which is a piezo polymer. It has a density of 1800kg/m³ and an elastic modulus of around 2.0GPa. Table 1.1 summarizes these properties for two different ionic polymers, a piezo bender, and PVDF. For the ionic polymers, IPMC₀ refers to an ionic polymer fabricated at the University of New Mexico, while IPMC₁ was manufactured at Virginia Tech using the method described in the following section. Additionally, the piezo bender's base material is 5A4E ceramic. This table also lists the energy density (e_m), which gives an idea of how much work can be done by the material per unit mass.

1.2 Manufacture of Ionic Polymer-Metal Composites

Having addressed the background of ionic polymer materials, the manufacture of ionic polymer-metal composites will now be discussed. As mentioned in the history of the material, fuel cell research found a way to significantly reduce the cost, making them feasible for use in the automotive industry. Likewise, research has been conducted in reducing the manufacturing cost of ionic polymers, in an effort to make them more readily available for more research applications. The reduced cost manufacturing process to be discussed here is the result of the work done by Bennett. For a thorough discussion and evaluation of the process, refer to Bennett (2002).

The manufacture of ionic polymers is a two part process, each with two parts of its own. The first process actually applies the electrodes to the NafionTM membrane, while the second process is performed to protect the electrodes from oxidation. Each will be discussed

in turn.

To electrode the membrane, which is essential to apply or collect a signal to or from the polymer, a combination of impregnation and reduction methods are used. This process will be referred to as co-reduction. The first part of this process basically involves preparing the membrane for treatment. Here, the NafionTM is roughened on each side to improve electrode adhesion. Remember that NafionTM is a co-polymer of TeflonTM, which is the most slippery substance around. Next, the polymer is cleaned ultrasonically, prior to boiling it in hydrochloric acid. Boiling the polymer in HCl accomplishes the task of hydrating the polymer.

Once the pre-treatment is complete, the soaking process is begun. This is where the electrodes are actually deposited on the surface of the membrane. First, the hydrated polymer is soaked in an exchange solution and agitated. This serves the purpose of impregnating the polymer with ions of platinum and copper, the base materials comprising the electrodes. Then the polymer is rinsed in deionized water. Finally, the polymer is soaked and agitated again, but this time it is in a reducing agent solution. This process reduces the impregnated ions into metal electrodes, therefore completing the co-reduction process in manufacturing ionic polymers.

The second process is called electroless plating, and it protects the electrodes from oxidation. Like the co-reduction discussed above, this process also has two parts. The first will be called catalyst plating. The solutions used in this process were provided by Solution Technology Systems. The polymer is initially soaked and agitated in a conditioner in order to remove any debris, followed by a rinse in hot tap water. To displace the rinse water from the membrane's surface and to prevent excess water from being carried into the activator solution, the polymer is soaked in a pre-dip solution. Next is the activator soak. This has the tin/palladium colloidal catalyst in it. The polymer is then rinsed again in hot running tap water before being soaked in an accelerator solution. This solution merges the colloids into a continuous film, and completes the catalyst plating phase of the process.

The final stage of the electroless plating process and therefore the ionic polymer manufacturing process is the gold plating. Solutions in this process were provided by Buehler. The first step involves combining the solutions and heating them up on a hot plate. Once this is done, the membrane is soaked and agitated in the mixed solutions. This plates the membrane with a thin layer of gold, and the ionic polymer is ready for use.

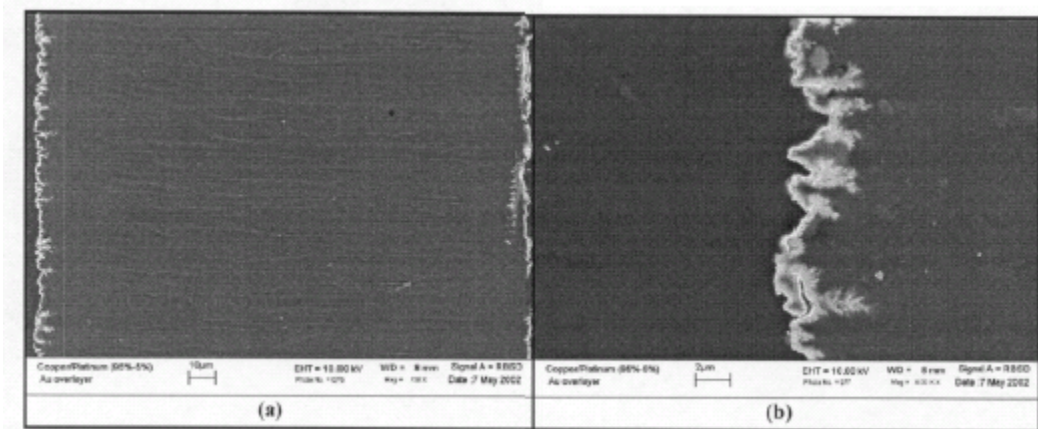


Figure 1.4: Cross-section of ionic polymer actuator. A scanning electron micrograph of the cross-section (*a*) and zoomed in on one side (*b*) show the dendritic electrodes produced from the co-reduction process. The thin gold layer can also be seen.

This process of impregnating the membrane with metal ions and then reducing them into metal electrodes produces dendrites that eliminate any adhesion problems. Figure 1.4 shows two scanning electron micrographs of the cross-section of a polymer manufactured using the co-reduction process. In the figure, (*a*) shows the entire cross-section with the thickness being the displayed length. Part (*b*) shows a zoomed section of the left side. In this figure, the dendrites are more pronounced and the thin layer of gold can be seen. It is the brighter looking surface along the outer edge of the electrode. One aspect of the process that will need to be improved upon if ionic polymers are to go into the low micron and sub-micron precision field is the surface roughness. To put this into perspective, (*a*) is about 180 microns across, while the dendrites in (*b*) extend about 2 microns into the membrane. This figure was adapted from Bennett (2002).

Following the completion of manufacturing ionic polymers, they are typically run through a longevity test to verify that their response does not diminish with time and cycles. This test has been carried out to 150,000 cycles with no sign of much change in the amplitude, when comparing the first data sample with the last. Any material properties testing conducted was usually done after the ionic polymer was completed, too. One property in particular is elastic modulus, which is around 60MPa for this process. Additionally, the mass density is in the neighborhood of 2000kg/m^3 and the energy density is near 5mJ/kg .

Since discussion of the manufacturing process of ionic polymers has finished, it may now be interesting to see the variety of applications in which engineers and researchers have been able to implement them. Nearly all of the applications to be discussed take advantage of a cantilevered ionic polymer actuator. This is the focus of the next section.

1.3 Applications

This section presents current applications of ionic polymers. The applications included are all of the research or academic type, but they show the great potential these materials have and how they can impact a broad array of topics. As the materials become more fully understood and all of their problems are addressed, these application fields will be waiting. The specific areas presented here are for robotics, biomedical, and space systems.

1.3.1 Robotics

Robotics may be the first field that jumped at the chance to develop a soft actuator and sensor. Most of the robotics applications of ionic polymers are described as biomimetics, creating artificial mechanisms intended to mimic, and inspired by, biological ones. Examples of this include wings, fins, and muscles. In fact, Shahinpoor has dedicated his research group to the study of ionic polymers as artificial muscles, which is also closely linked to the biomedical field.

By taking advantage of the compliance of ionic polymers, researchers have been able to successfully construct actuating mechanisms that have many degrees of freedom (DOF). Traditional robotic manipulators are limited in degrees of freedom by their rigidity, and those that do have multiple DOF tend to be large and bulky. Using the flexibility and softness of the materials, both 3-DOF and 6-DOF micro-motion devices have been created using different crossing pattern arrangements of ionic polymer strips (Tadokoro et al., 1999). This same research group in Japan has performed experiments with an elliptic friction drive (EFD) element to produce a traveling wave effect for possible transport or motion applications (Tadokoro et al., 1997). The generated motion would be similar to cilia inside the human body or the legs of a centipede. Continuing work with this distributed actuation device, Tadokoro and colleagues were able to produce a prototype model consisting of several arrays of EFD elements (1998). Distributed arrays are necessary when using ionic polymers

because the material cannot produce large amounts of force to support the traveling object. However, multiple EFD elements divide the weight of the object, enabling the ionic polymers to “carry” the object. Ionic polymers can also be easily miniaturized by simply cutting them into smaller segments, which make them ideal for creating micro-robots.

Similar to this distributed motion concept, underwater propulsion has also been achieved. Present ionic polymer materials operate best in a moist environment because of the water drag phenomenon that causes them to move. Seeing that these materials work best in water and are studied in biomimetics, it is a natural progression to think of making a fish or swimming robot with them. This was, in fact, accomplished (Guo et al., 2000). The ionic polymer actuator was used as the tail fin to propel a buoyancy adjuster through water. This particular robot uses two fins. It was shown that by adjusting the input frequency and amplitude, the speed of the fish-like robot and its floatation level could be controlled. Possible uses for swimming micro-robots include pipeline maintenance, in-body micro-surgery, and biological or marine studies.

Using this novel concept of swimming micro-robots, biomimetic studies of fin motion efficiencies have been carried out (Laurent and Piat, 2001). Laurent and Piat were able to build a millimeter-scale swimming robot with fins made of ionic polymers. Then, performing theoretical fluid dynamic analysis of oscillatory versus undulatory motion, their robot was able to verify the efficiency study. The flexible nature of ionic polymers enables them to perform undulatory motion, in addition to oscillatory motion, like that of a paddle. By performing the swimming experiments, the results show that undulatory motion is more efficient than oscillatory motion.

Another idea that arose from the bending and holding capacity of ionic polymers is an end-effector gripper. A robotic gripper has been built employing four ionic polymer benders as “fingers,” and has demonstrated the ability to grab and lift an object (Shahinpoor et al., 1998). By using a low frequency square wave for actuation, the gripper could grab the object during the first half of the duty cycle and release the object during the second part. This gripper was set up in a two-pincher orientation, where the two pinchers were at right angles with each other to grab the object on four sides.

More recent developments with ionic polymers in robotics try to use advanced techniques to control the locomotion of biomimetic actuators. The type of locomotion sought was for a worm-like robot (Arena et al., 2002). Cellular neural networks (CNNs) by way

of central pattern generators were used on an ionic polymer, electroded using a pattern plating method. This study came about after successful results were obtained using CNNs on other biomimetic robots. The motion generated was undulatory, as each actuator in the robot sequentially bent in a head-to-tail fashion.

While many of these robotic applications just described were biologically inspired, only one was stated to have a possible future in biomedicine. The next section will discuss applications more directly related to the biomedical field.

1.3.2 Biomedical

The robotics field has a great potential for using ionic polymers as actuators and sensors, especially in biomimetics. The biomedical field is also taking advantage of the softness and flexibility of ionic polymers, but they are also ambitious about using ionic polymers because of the ease in which they can be miniaturized. The optimal environment being moist is also advantageous since that is the condition inside the human body. Being biologically inert is another benefit for in-body considerations.

In addition to generating various biomimetic motions, such as a snake and a jellyfish, with different polymer arrangements, the idea of a joy-stick controlled device arrived. This would be particularly useful in surgery scenarios when a doctor was trying to apply a treatment inside the body. An example case given was an active catheter for in-vivo surgery, such as treating a brain aneurysm (Onishi et al., 2000). The ionic polymer actuator tip, which would distribute the medication, was fabricated by adhering four electrodes on a tube. Having four electrodes would enable the physician to have a full range of motion with the actuator tip. The initial work published on this catheter system also listed micro-pumps and valves for inside-body drug delivery systems as possible applications (Sewa et al., 1998).

Concentrating on the topic of a medical micro-pump, research has been conducted on using ionic polymer components inside a pump (Guo et al., 1999). The pump was driven by an ionic polymer diaphragm, while two one-way valves controlled the flow of the solution inside the pump. Model equations of the pump were derived and by assembling a prototype, measurement and calculation of flow versus frequency matched fairly well. Other components of the micro-pump not made of ionic polymers include two pump chambers, a storage tank, and rubber.

Moving away from the actuator-type applications, ionic polymer designs have also

been proposed for medical sensors. Currently, pressure sensors for the spine are available, but they can only be used in select regions because of size factors. Electronic malfunction and sealing problems are also evident. Ionic polymers offer a promising alternative to the conventional pressure sensor, in that they can be placed inside the body without physical harm, and they can be cut as small as necessary. Experiments have been done using a materials testing system to simulate loading conditions in the spine, giving well correlated data (Ferrara et al., 1999). Similar has also been done regarding the sensing of blood pressure, pulse rate, and pulse rhythm (Keshavarzi et al., 1999). By configuring an apparatus to simulate blood pressure and rhythm, sensing results from the ionic polymer showed that consistent readings could be acquired.

The future may also hold a place for ionic polymers in wearable systems. It has been proposed that ionic polymer materials, used in tandem with rubber micro-dispersed carbon phases may lead to producing garments that can record proprioceptive maps (Rossi et al., 2001). Garments of this type may also be able to painlessly stiffen body segments for teleoperation or rehabilitation purposes. The specific active dressware mentioned was an exoskeleton-like glove.

Futuristic systems apply not only to the biomedical and virtual reality realm, but also to space systems that are presently pursuing the use of ionic polymers in inflatable and deployable telescopes and satellites. This discussion follows.

1.3.3 Space Systems

When considering the advancement of technology, one usually looks to outer space. Discoveries are continually being made and the cutting edge of technology is constantly pushed forward. It is no wonder that ionic polymers are being considered for use in the push to make bigger and better things. The shift in telescope technology is going from single mirror optics to membrane optics, and fixed structures to deployable, inflatable structures. The compliance of ionic polymers makes them a promising transducer for this new fleet of flexible, lightweight, and low stow volume systems.

In space there are several factors that can structurally effect spacecraft. Examples of these include temperature gradients and UV exposure. In order to compensate for the deviations caused by these factors, transducer elements are required. Being that the optical reflectors are moving toward becoming membrane materials, ionic polymers are one viable

option for implementation since they are made of a membrane material themselves. A review of recent developments in this field can be found in Salama and Jenkins (2001). This review also covers modeling and control issues, as fully autonomous, intelligent systems are further developed. One technology need that is expressed is the development of transducers with greater sensitivity and larger stroke. This may fuel the research for the practicality of ionic polymer transducers because they are known for their large displacements, when compared to other actuators and sensors.

The majority of present research in these advanced mirror systems focuses on the use of polyvinylidene fluoride (PVDF). This material, like ionic polymers, is classified as an electroactive polymer, but its characteristics differ from those of ionic polymers. It is a more understood material, being a piezoelectric polymer. Aside from the membrane-like nature of PVDF, it does have a common characteristic with ionic polymers in that it has time-dependent properties. An advantage that ionic polymers have over PVDF is that they are much more compliant and may ultimately be able to contribute more to this field of controlling the shape of membrane optics. However, current ionic polymers are restricted by their dependency on water to achieve motion. In space this water would certainly freeze, sacrificing the function of the material. Needless to say, both materials need further development. It is another challenge altogether to then be able to control the reflecting surface to “ $\lambda/20$ ” or sub-wavelength precision. For a review of PVDF trends, the reader is referred to Jenkins and Vinogradov (2000).

In addition to surface shape control, structural health-monitoring systems are also being explored. This is where the detection of degradation or eventual failure of components could be monitored by making localized measurements and assessing the global conditions of the structure. In this area, sensor/actuator pairs are thought to be the best solution. Due to the present limitations with ionic polymer materials, solutions are being developed using micro electro-mechanical systems (MEMS) technology (Witherspoon et al., 2001). Because of the inherent flexible nature of these systems, flexible actuators and sensors would be the ideal solution. Unfortunately, this application will have to wait for ionic polymer technology to improve to where the materials are no longer water-dependent. Despite the material drawback, a concept demonstration was developed by Witherspoon and Tung (2002).

Considering the optical applications for ionic polymers, Leo et al. (2001) have addressed several of the issues for ionic polymers, including their sensing properties. Men-

tioned is the small offset voltage. Pertinent to membrane surface control is the DC sensing capability, which could be made more stable by phasing this offset out of the measurement. This would make it a possibility that ionic polymers could replace piezoresistive sensors in the low frequency range, if this phasing out is fully conceived. An interesting note brought up is how ionic polymers appear differently, in the electrical sense, at different frequency ranges. In the low frequency range, an ionic polymer is a capacitative material, whereas in the high frequency range, it becomes resistive. Relating to the future improvements that need to be made in the material is the standardization of the manufacturing process. It was shown that the sensing characteristics are affected by the physical processes occurring within a few microns of the electrodes.

While ionic polymers are not exactly space-quality materials right now, future improvements in ion transport mechanisms, surface roughness, and physical understanding may lead them to the front line of transducer technologies.

1.4 Motivation

Some of the questions raised in the various applications of ionic polymers have opened several doors to a range of research topics. The motivation for the work presented in this document is based on the fact that ionic polymers are not yet available for space systems. Not having a comprehensive knowledge of the material and the potential for future generation polymers to be used in space are the underlying factors. As previously stated, ionic polymers of today would not be able to survive the harsh environmental conditions in space. This is mostly due to their reliance on water. While technology investigates the use of different solvents that will not freeze in space, research on current ionic polymers will be conducted to form a baseline or stepping stone for future modified materials.

For different control applications, it is of interest to know the bandwidth of the transducer, so the designer will be able to judge how fast the system can respond. One thing that is known about ionic polymers is that their frequency response shifts in time as the material dehydrates. The type of shift that occurs is like a stiffening effect, where the longer the polymer is exposed to an air environment, the higher the resonant frequencies will become. Past literature has commented on this phenomenon and shown illustrative plots, but to date, the effect has not been characterized.

Related to the speed of response of a system, optical reflecting surfaces are required to have extremely tight tolerances, which offer a challenging feat in precision control. Because of their intrinsic compliance and membrane nature, ionic polymers are already being considered as a possible source to control the shape of the membrane optics. Work has been carried out in reducing some of the unfavorable response characteristics of ionic polymers, but it was done on more of a large scale. For sub-wavelength precision, ionic polymers will need to be controlled to strict position requirements. Also, having such a large swing, it is one idea that ionic polymers will be able to rectify the problem of having different control systems for both coarse and fine adjustment. For this reason, different control techniques will be studied with the aim to improve existing methods.

The next section states the specific goals and contributions encouraged by the previous work and possible future for ionic polymer actuators.

1.5 Technical Objectives and Contributions

With motivation given for the research to be presented, it is helpful to state the technical objectives of the work and how they contribute to advancing the state-of-the-art in ionic polymers. This follows in a bulleted format.

- *Investigate Dehydration Effects.* Although this feature has been commented on by researchers, it has not yet been characterized. Also, since many of the applications have to do with wet or moist environments, the dehydration is not a problem. In order to extend the use of ionic polymers to open air environments, it is necessary to have knowledge of the hydration state of the material, so it will be known how the system will be affected. By studying the dehydration effect of ionic polymers, mathematical relationships or trends will be established in relation to the resonant frequencies and input-output relationships. This investigation will play the role of actually quantifying this adverse property of ionic polymers.
- *Examine Boundary Condition Effects.* On the control system design side of ionic polymers, it is important to know the speed of response. To more fully understand how the bandwidth changes, both the cantilever and clamped-clamped conditions will be examined. According to theory, clamping both ends of a beam greatly increases

the natural frequencies from those with one end free, while also greatly reducing the motion. Both of these consequences will be advantageous to micro-manipulation applications, including space optics. Most all previous work with ionic polymer actuators takes advantage of the large bending deflections of the cantilever configuration. However, by clamping the free end and applying tension, the bandwidth increase will be characterized to see how fast ionic polymers can respond.

- *Improve Actuator Tracking Capability.* Some control work has been done in the past with successful results, but there is much more that can be improved upon. The previous work focused on a small time frame, where dehydration effects were negligible. With ionic polymers having time varying characteristics, an interesting control problem is posed. Experimenting with different control schemes has improved the response in the short-term and offered a preliminary design that could expand to longer time frames where dehydration is no longer negligible. By improving the controlled response of ionic polymers, the broad range of potential applications will be more fully realized.

Before starting right into the bandwidth characterization and control schemes studied in this research, some more background about the typical open-loop response will be addressed. The next section gives an overview of the remainder of this work.

1.6 Thesis Overview

To set the scale for why ionic polymers need to be controlled and how much their response needs to be improved, Chapter 2 presents the dynamic response of ionic polymers. Both time response and frequency response characteristics will be discussed. Chapter 3 discusses the characterization of ionic polymers to humidity and dehydration aspects, as well as to tensioning the material. Here the experimental setups are described prior to the results for the different testing configurations considered. Completing characterization, Chapter 4 is dedicated to the task of controlling ionic polymers. To start off, previous control results are discussed, followed by two new schemes that show more evidence to support the use of ionic polymers for precision applications. Finally, Chapter 5 provides conclusions of the work, contributions, and a list of possible future work.

Chapter 2

Dynamic Response

Ionic polymers are known for their undesirable open-loop response and for having at least one time varying parameter. Nearly all of the work published to date has dealt with cantilevered polymers, so that is what these characteristics are based upon. Other configurations may not necessarily have similar problems, however. This chapter will discuss the different response characteristics of ionic polymers in both the time domain and the frequency domain. First will be the time response, followed by the frequency response. To end the chapter, a summary will be given.

2.1 Time Response

This section will discuss the time response characteristics of ionic polymer-metal composites. Results from various test specimens and testing configurations will be presented, beginning with a description of the test apparatus.

2.1.1 Test Setup

To measure the time response of an ionic polymer, a sensing element and unit system must be determined. The actuation mechanism is known to be an applied electric field through the thickness of the membrane. Due to the potential for ionic polymers to be used in micro-manipulation applications, position was chosen as the desired response characteristic, with microns (μm) being the unit of measure.

Because of the lightweight nature and low force output of ionic polymers, a non-contact sensing element was required to minimize the errors associated with mass loading of

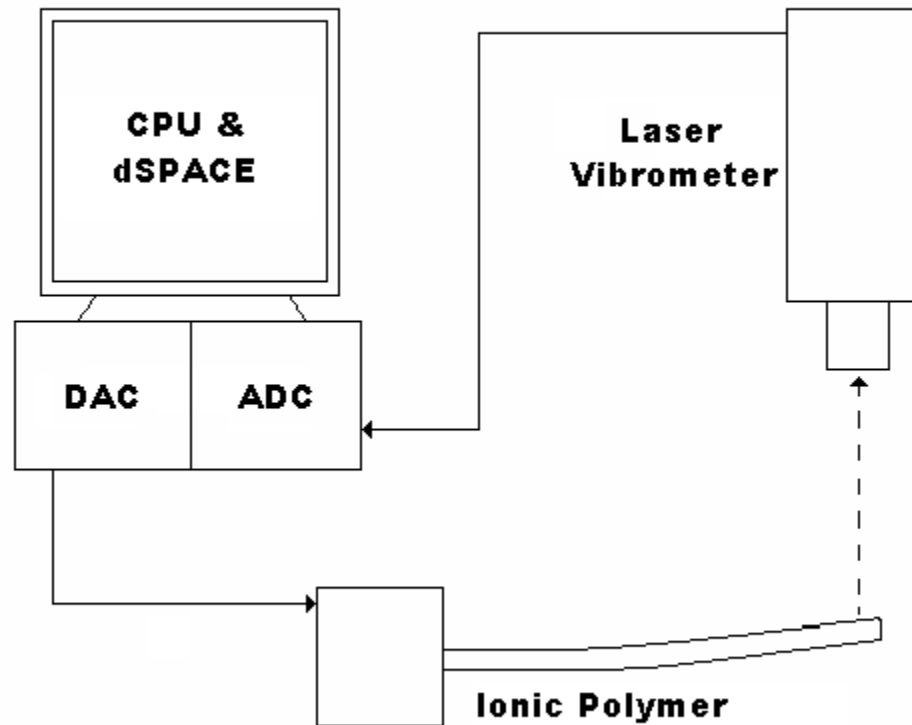


Figure 2.1: Time response testing equipment used to measure the displacement of the ionic polymer as a function of time.

contacting sensors. The chosen equipment was a Polytec OFV 3001 Vibrometer Controller and Polytec OFV 303 Sensor Head, which will be referred to as the laser vibrometer, while the point of measurement was taken to be the tip of the ionic polymer cantilever. The signal was fed into a dSPACE DS2003 Mux analog-to-digital board for storage onto a PC hard disk. The source of actuation voltage was also a dSPACE, Inc. product, the dSPACE DS2103 digital-to-analog converter, passing first through a Hewlett-Packard 6825A Bipolar Power Supply/Amplifier, and then to the polymer. The controls field is known to use dSPACE digital signal processing (DSP) equipment for simulations and experimentation for its ease of implementing Matlab models. ControlDesk software was used, in addition to Simulink, to control the experiment parameters. Figure 2.1 illustrates this testing equipment in a schematic.

One disadvantage of using a laser vibrometer for position measurement of an actuator with such a large bending deflection is that the laser can have a difficult time tracking the

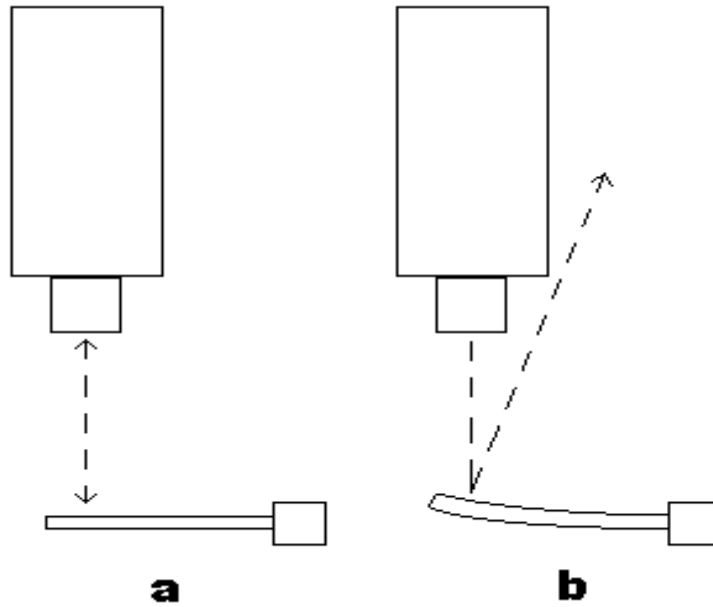


Figure 2.2: Under small deflections (*a*), the laser vibrometer is able to track the motion, but for larger deflections (*b*), it is unable to measure the polymer’s position.

position. This is because the more the polymer (reflecting surface) bends, the farther the reflected signal is from the initial point of emission. This concept is easier to explain by thinking of the polymer as a mirror. If you hold the mirror directly in front of you, perpendicular to your line of sight, and move it back and forth, there is no problem seeing your reflection. However, if you begin to angle the mirror, there quickly comes a point where you can no longer see your reflection. This is the same thing that happens when trying to measure large bending deflections with the laser vibrometer. Therefore, only small displacements were examined. Figure 2.2 helps illustrate this point.

Having discussed the data acquisition equipment, the test fixture will now be described. The fixture has two delrin clamps with gold foil electrodes attached. The gold electrodes are wired to a BNC connection that can be run directly from the DSP for the actuation signal. One of the clamps is screwed to the base, while the other is attached to a Velmex, Inc. unislide. Using the slide enables multi-function of the fixture for both clamped-free (cantilever) and clamped-clamped boundary conditions. For cantilever testing conditions, the movable clamp is backed away to where it will not interfere with the motion of the polymer, and for clamped-clamped conditions, it is placed in a position where it can

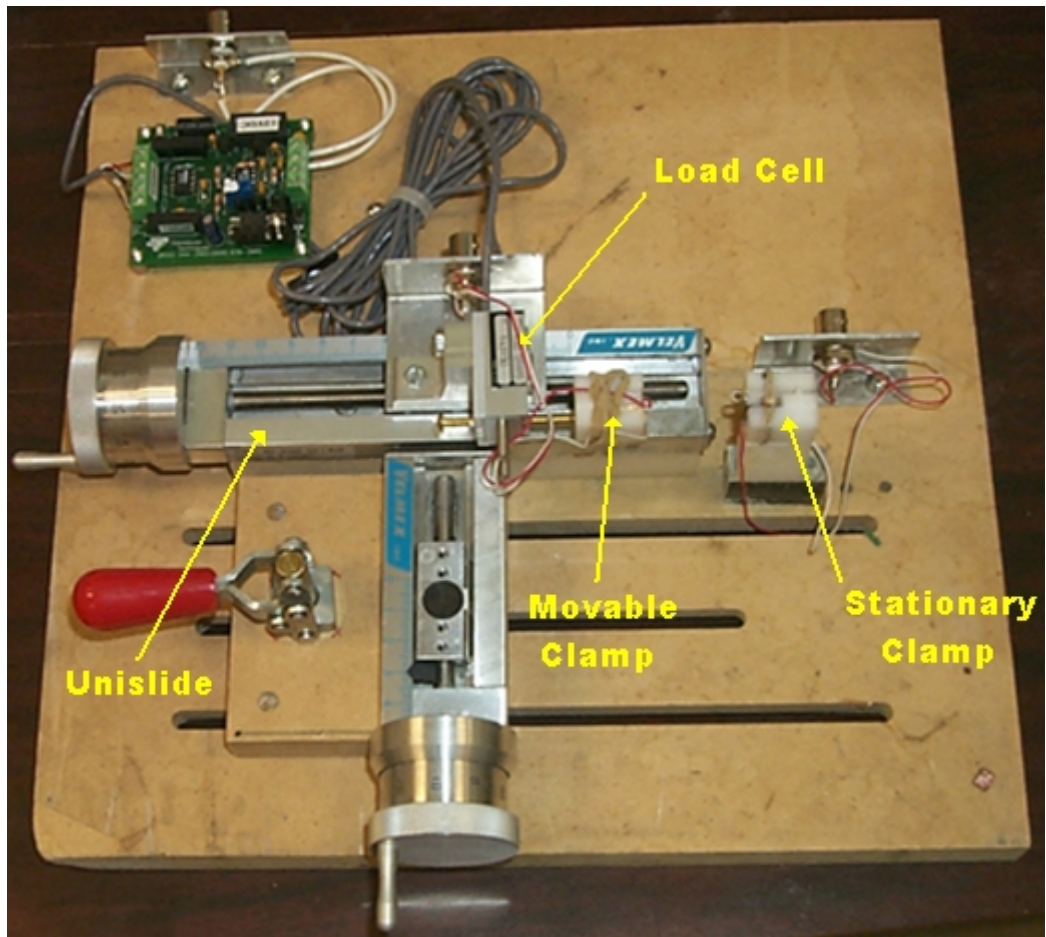


Figure 2.3: Close-up of test fixture showing the two clamps and the unislide, used for different testing configurations.

hold the previously free end of the polymer. The movable clamp was also assembled with a Transducer Techniques, Inc. load cell so that it can measure the tension in the polymer. Tension can be either free or forced, respectively caused from polymer contraction due to dehydration or an applied load due to manually positioning the clamps farther apart. All of these parts are shown visually in Figure 2.3.

With the testing equipment explained and setup, it could now be used to measure the open-loop response of some ionic polymer actuators. The results of these tests will be discussed in the following two sub-sections.

2.1.2 Step Displacement Results

The step response of ionic polymers will now be discussed for various types of actuators. A step response is a measure of how the actuator behaves when a voltage is suddenly

applied and remains at a constant value. The results to be shown have the input voltage converted into its corresponding position, demonstrating that for most cases, the open-loop step response needs to be greatly improved to have good tracking. The voltage to position conversion is done by adjusting the sensitivity of the laser vibrometer to a desired value and dividing the input position by the calibration factor.

Before presenting results, it will be helpful to define some terms that will be used in discussing the step response characteristics. The first term is overshoot. Overshoot is the maximum amount the system rises above the desired value, divided by that desired value, given as a percentage. The desired value for the ionic polymers was chosen to be the calibrated reference input, for both the open-loop results to be shown here, and the control results of Chapter 4. The reason this was chosen for the open-loop, rather than the settling point, was that the repeatability issues yield different settling positions from test to test, which would lead to inconsistent results. In terms of time, there are two parameters to be defined: rise time and settling time. The time it takes a system to get close to the desired value is called the rise time, and it will be quantified as the time it takes the system to get from 10% to 90% of the reference value. In the results to come, there are some instances when the actuator never reaches 90% of the desired reference value, so in these cases, the rise time will be the time it takes to go from 10% to 90% of the peak. Settling time is defined as how long the system takes to settle to within $\pm 2\%$ of the reference value, or how long it takes for the transients to decay. These definitions were referenced from Franklin et al. (1994).

The first result to be presented is the most frequently shown step response, that for a single polymer actuator in the cantilever configuration. As the literature says, the response is dominated by a large overshoot and a slow relaxation time. There is also steady-state error and the nonlinearity of different settling positions. It has been proposed that the slow relaxation time is the result of cation redistribution in the cathode layer of the actuator (Nemat-Nasser, 2002). The length of the actuator also plays a role in the response characteristics. Resonance phenomena tend to become more pronounced as the length of the polymer increases. This follows from longer polymers having lower natural frequencies, which cause resonant modes to be excited.

Figure 2.4 shows a response that is more toward the range of worst-case responses. This polymer is about 20mm long and in (a), it has an overshoot of 470%, a settling

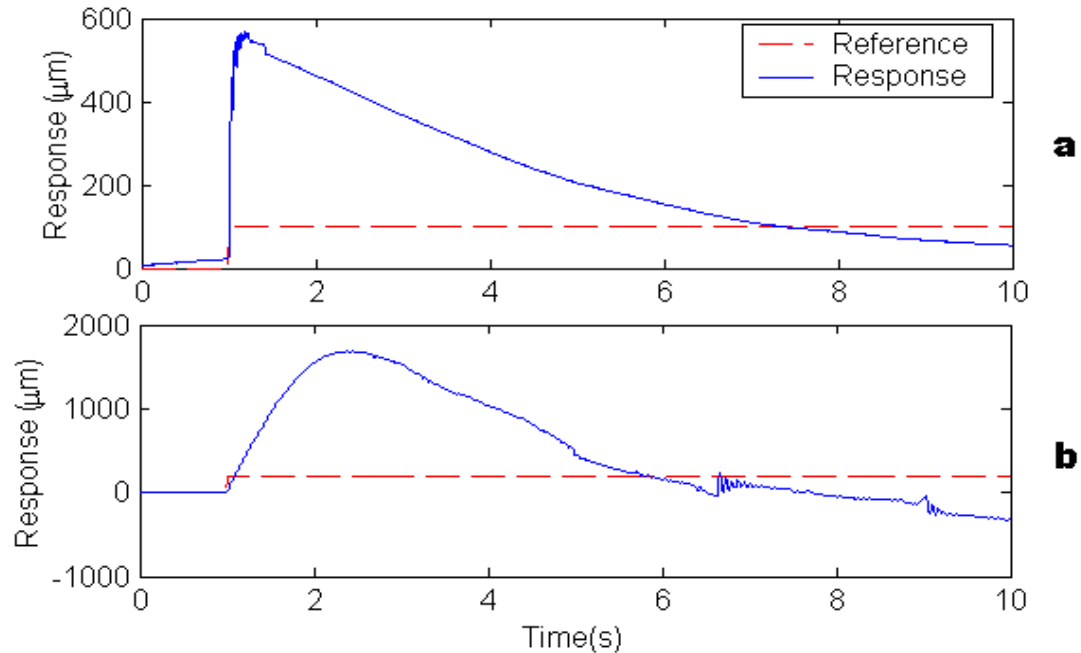


Figure 2.4: Typical step response of a cantilevered IPMC (a) compared to a more unusual response (b).

time of greater than 10 seconds, a rise time around 6 milli-seconds, and some steady-state error. It should be noted that resonance occurs at the peak. Part (b) in the figure shows another, more uncharacteristic, step response that has a slow rise (90ms) and resonance phenomena occurring well after the initial step, in addition to a steady-state resting position in the negative direction. The overshoot reaches 750%, and the settling time is, again, more than 10 seconds. The more typical response is depicted in Figure 2.4a, but Figure 2.4b was included to show the nonlinearity and repeatability issues involved with these materials. Obviously, this poses a great control problem, but that will reserved for discussion in Chapter 4.

There are different types of cantilevered ionic polymer actuators that can be experimented with, however. Studies have been performed attempting to increase the force output by constructing a stack of polymer actuators, wired in parallel (Akle, 2002). Similar to the use of stacked NafionTM membranes in fuel cells to increase power output, stacked polymers do increase the available output force. When compared to a single actuator, the response characteristics are also altered. The alteration of response is one from the more favorable variety, where no overshoot is present. Figure 2.5 illustrates this improved step response.

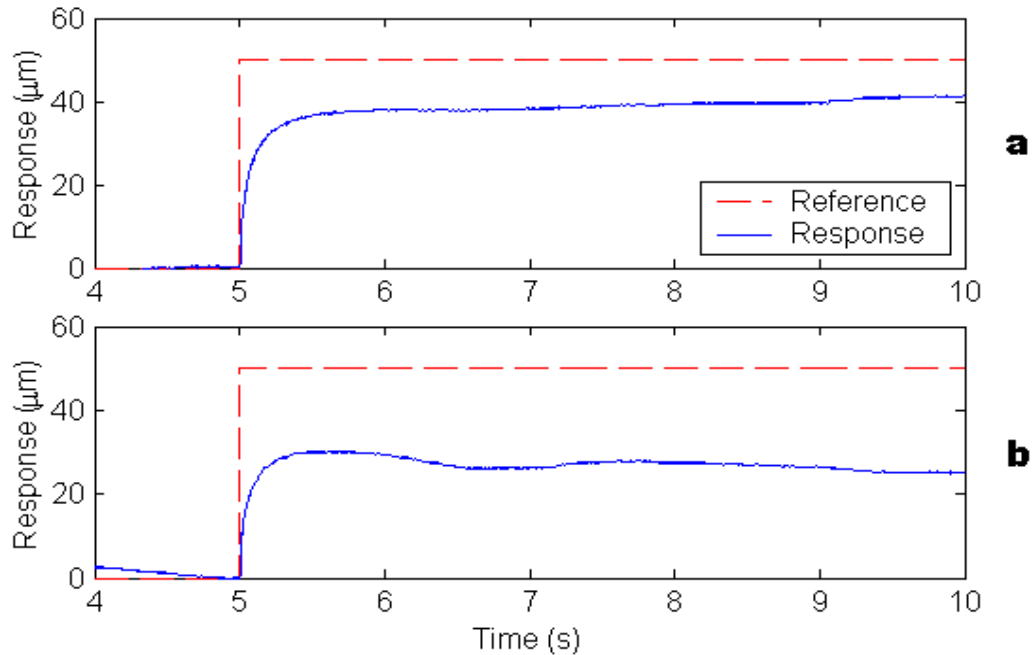


Figure 2.5: Step responses of 4-stack IPMC cantilever showing a slow increase (a) and slow decrease (b).

In the figure it can be seen that there are still some repeatability issues, indicated by the different slopes and positions at 10 seconds. Figure 2.5a shows a slight positive slope, as the polymer’s tip approaches the reference value, while Figure 2.5b has a slightly negative slope, decaying away from the reference step. The steady-state error and settling time are certainly still not up to par to have good tracking, but the overshoot problem is definitely better using a stack of ionic polymers. Figure 2.5a reaches 70% of the reference in 350 milliseconds, and Figure 2.5b only gets to 60% the reference step in about 300 milliseconds. The 4-stack results may best be described as overdamped. With the increased mass and the layers of “dead” material acting as isolation in between each of the polymers, it seems reasonable that the response looks overdamped.

Mentioned as a disadvantage of implementing ionic polymers into a system was their dependency on water to achieve motion. One possible solution that received some attention was to package the actuator in some water-impermeable material to prevent any dehydration of the membrane, therefore extending its use to open air environments. Using plastic wrap as the packaging material, a stack of two ionic polymer actuators was wrapped in a sleeve and tested. It is reasonable to think that this actuator’s step response might fall between that of a single layer and a 4-stack actuator. As displayed by Figure 2.6, an overshoot of

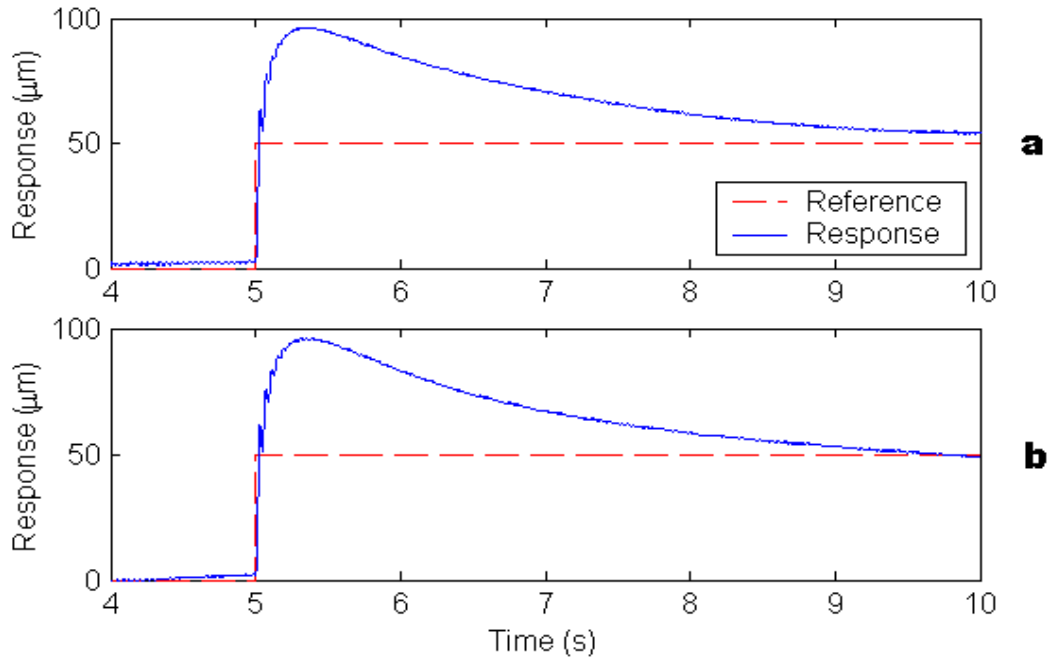


Figure 2.6: Cantilever step responses of packaged, 2-stack actuators showing different ending positions.

about 100% in each case shown is the result. The rise time in Figure 2.6a is 17ms, and that in Figure 2.6b is 14ms. As for the other cantilevers, the settling time is again over 10 seconds. Similar to the other two cantilever responses, the packaged, 2-stack actuator also displays a problem of repeatability of response, as evidenced by the positions of (a) and (b) at the end of the time block.

Now moving to the clamped-clamped configuration, some common characteristics are seen. For these tests, the previously free end of the cantilever is placed in a clamp and the laser vibrometer is focused on the center of the actuator. For both configurations, the point of highest deflection was chosen as the measurement point. Clamping both ends of the ionic polymer does substantially reduce the peak deflection, but some of the response characteristics are similar. One change that had to be made in test settings by going to the clamped-clamped from the clamped-free is the sensitivity of the laser. It had to be adjusted so that more voltage would be applied to the polymer when much smaller displacements were inspected.

Making these adjustments, some step responses were taken for a 20mm long polymer with a width of 5mm. Results are shown in Figure 2.7 for a reference step value of 4 microns. Figure 2.7a has no overshoot, reaching only 50% of the input in 50 milli-seconds,

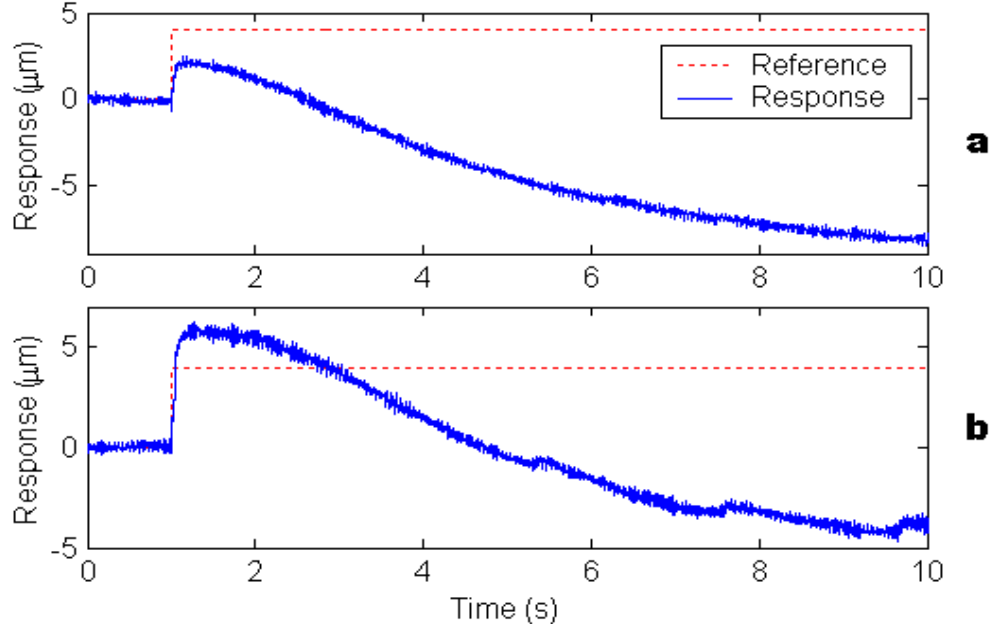


Figure 2.7: Clamped-clamped ionic polymer step responses.

while Figure 2.7b has an overshoot of 50% with a rise time of 60ms. One of the first things noticed when looking at the figure is the noisy data. This is much more of a problem when looking at such small deflections because ambient vibrations affect the polymer much more. Attempting to minimize this problem, the test fixture was placed on a separate table where the computer and amplifier would not interfere with measurement. Aside from this unpleasant effect, overshoot, slow relaxation, and steady-state error govern the step response. Relaxation times are of the same order as those of the cantilever ionic polymer, as the relative overshoots are diminished. The biggest difference between the two configuration's responses is the relative decay point. In the cantilever actuator, the response sometimes decayed to a positive value between zero and the reference and sometimes it would go 100% to 200% the step value in the negative direction. However, the clamped-clamped case went negative each of the eight times tested, reaching up to 200% the reference step.

Before beginning the discussion of the sinusoidal responses, a table has been included to summarize the step response results for the different actuator designs. Table 2.1 shows the response characteristics described above, and makes it easier to see their progression as the actuators were changed from single-layer to 2-stack packaged to 4-stack. The clamped-clamped results have also been included. Showing representative data, the table reports results from Figure 2.4a, Figure 2.6b, Figure 2.5b, and Figure 2.7b.

Table 2.1: Step Response Characteristics for Cantilevered Ionic Polymer Actuators.

Response Characteristic	Units	Single Layer (CF)	2-Stack, Packaged	4-Stack	Single Layer (CC)
Overshoot	%	470	100	none	50
Rise Time	ms	6	14	300	60
Settling Time	s	>10	>10	>10	>10

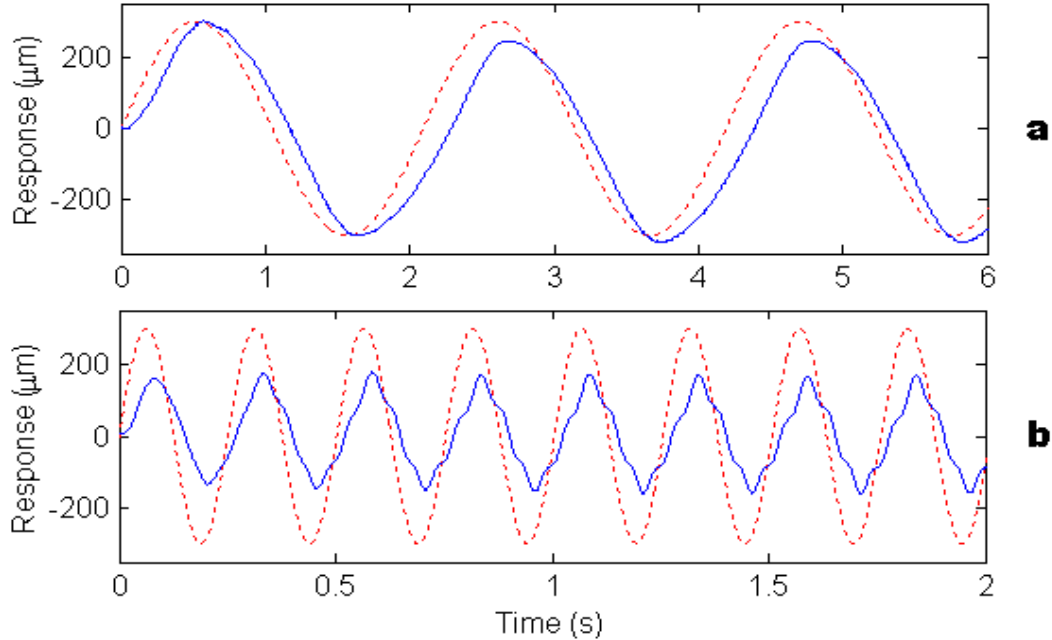


Figure 2.8: Cantilevered ionic polymer responses to sinusoidal input of 300 microns at 0.5Hz (a) and 4Hz (b). Note that the time scales are different.

By completing the discussion of various step responses for ionic polymer actuators, the time response to a sinusoidal input remains for this section. This topic will be described next.

2.1.3 Sinusoidal Displacement Results

The response of ionic polymers to time varying reference inputs will be illustrated here. For these results, both the cantilever and clamped-clamped configurations were tested, again aiming the laser at the point of greatest deflection. In the discussion of the sinusoidal results, only single actuators will be presented, starting first with the cantilever, followed by the clamped-clamped condition.

Table 2.2: Sinusoidal Time Response Characteristics for Ionic Polymer Actuators.

Response Characteristic	Units	Clamped-Free Ionic Polymer		Clamped-Clamped Ionic Polymer	
Frequency	Hz	0.5	4	0.16	3
Input Amplitude	μm	300	300	2	2
Output Amplitude	μm	300	180	400	1.6
Phase Lag	degrees	12	30	30	50

Using a reference input with an amplitude of 300 microns and varying the input frequency gives the results shown in Figure 2.8. The figure shows the response for both a low frequency (*a*) of about 0.5Hz (3rad/s) and a higher frequency (*b*) of near 4Hz (25rad/s). Each plot in the figure shows a small phase lag, 12 degrees for Figure 2.8a and 30 degrees for Figure 2.8b, but that does not seem to be the worst response characteristic. Figure 2.8a displays a positive quadratic-like response on the positive slope side of each cycle and a negative quadratic-like response on the negative slope side of each cycle. Some drift is also apparent in the response after the first cycle, as evidenced by the peak values. This lower frequency does seem to be in the polymer’s bandwidth though, because the amplitude of the input and output match. Figure 2.8b continues with the unfavorable characteristics, but it goes a little further. There are other harmonics being excited in this response, but the dominant frequency appears to be that of the input. Amplitude attenuation is also seen to be around 60%, which indicates that 4Hz is outside of the open-loop bandwidth for this cantilevered actuator.

The clamped-clamped polymer responds somewhat similar to the cantilever. As was the case in the step response of a clamped-clamped polymer, noisy data is again prevalent, but the responses show that tracking can be achieved to a certain degree. Figure 2.9a shows a phase lag of 30 degrees when the output actually amplifies the input signal by nearly 400%. This is a lower frequency input of about 0.16Hz (1rad/s). Figure 2.9b increases the frequency to 3Hz (19rad/s), where a phase lag of 50 degrees is present and the amplitude begins to be attenuated. In this case the output amplitude is 80% of the input. This provides evidence that the frequency is approaching the clamped-clamped polymer’s bandwidth. Like the cantilever, at low frequencies, there is only one output frequency, but as the frequency increases, other harmonics are being excited.

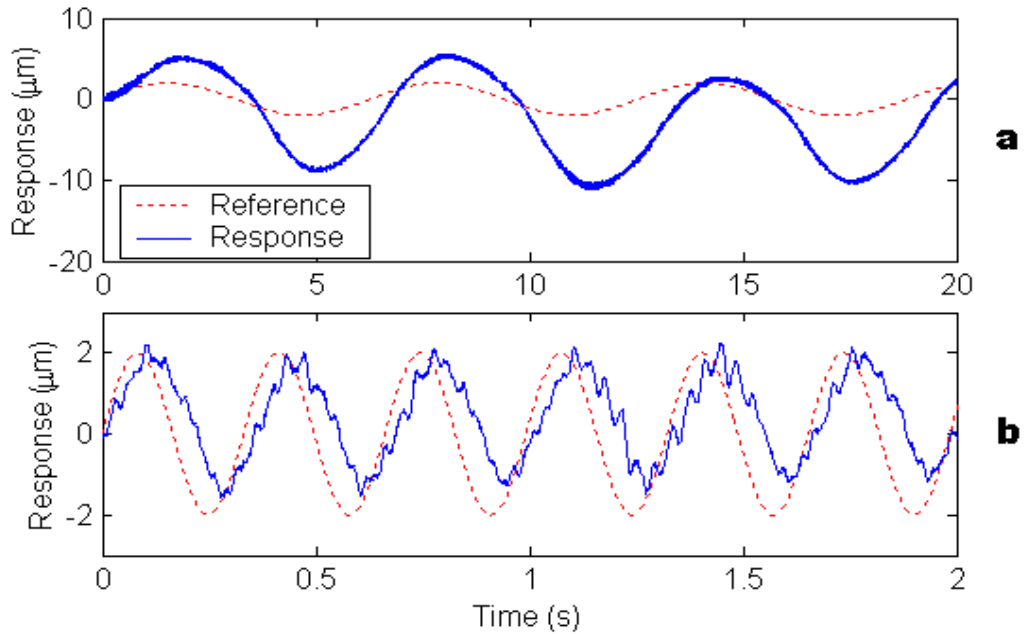


Figure 2.9: Clamped-clamped sinusoidal time response for a 2 micron wave at 0.16Hz (a) and 3Hz (b).

As was done at the end of the step response section, Table 2.2 has been included to give a synopsis of the results. It includes results for all the sinusoidal responses shown, for both cantilever and clamped-clamped configurations, in the categories of frequency, input amplitude, output amplitude, and phase lag. Common to both testing configurations is how the increase in frequency decreases the output amplitude and increases the phase lag. This is analogous to a linear system.

Finishing up the time response section of the dynamics of ionic polymers actuators, the next section will discuss frequency response characteristics.

2.2 Frequency Response

Changing analysis domains from time to frequency, this section will present some preliminary results for how ionic polymers will respond to sinusoidal inputs. A frequency response function, or transfer function, is a plot with amplitude and phase information for how a system responds to sinusoidal inputs. This method of analysis is valid only for linear systems, which ionic polymers clearly are not. However, under brief periods of time, using transfer functions for controller design has yielded successful results (Mallavarapu and Leo, 2001). Also, readers interested in dynamic system analysis tend to be more familiar with frequency

response plots. Therefore, this method will be used to gain insight into the behavior of ionic polymers. This section will present some of the fundamental concepts regarding the dynamic response characteristics of ionic polymers. A much more comprehensive investigation using frequency response will be provided in Chapter 3. First, the experimental setup will be discussed, and then the results will follow.

2.2.1 Test Setup

Much of the laboratory equipment used for the frequency response testing is the same as that used for the time response measurements. The major difference is that, in place of the dSPACE, a Tektronix 2630 Fourier Analyzer was used to create the input signal to the polymer and to collect the output motion of the polymer from the Polytec laser vibrometer. The same test fixture shown in Figure 2.3 was also used to hold the polymer. Because of the similarities in equipment, a figure will not be included in this section. Figure 2.1 can be referred to, substituting the Tektronix for the dSPACE.

Getting more into the data collection process, Table 2.3 has been included. The values in the table are typical values used for some of the specific analysis settings. Sometimes they were altered based on initial results of coherence or data collection time, where a trial and error approach was then applied. The aim was for 0.25Hz resolution for the cantilever tests, which had lower resonant frequencies, and 1Hz resolution for clamped-clamped tests, where the frequencies were much higher. A uniform window was used on the data because the input to the polymer was a signal composed solely of random content with a regulated root-mean-square (rms) value. Random content was used as the actuation signal because it is thought to include all frequencies in the band. A chirp signal is often used for dynamic analysis of structures, but for these polymers, more coherent data resulted from a random content signal than for a chirp.

2.2.2 Transfer Function Results

Results of frequency response characteristics of ionic polymers in this section are representative. The next chapter will give a more in-depth analysis, while this chapter is meant simply to acquaint the reader with the material. The first two results to be shown are the result of the equipment described above, while the third results from the test setup to be described in Chapter 3. That result was presented here for continuity of concepts and will

Table 2.3: Data Collection Settings for Frequency Response Testing.

Setting	Cantilever	Clamped-Clamped
Baseband (Hz)	50	500
Sample Size	1024	1024
Averages	5	5
Input Signal	Random Content	Random Content
Window	Uniform	Uniform

be elaborated on in assessing the dehydration effect.

The first frequency response characteristic to be discussed is qualitatively consistent with beam theory, so some well known equations will be used to help with the explanation. This characteristic is how the natural frequency of a beam changes with length. The natural frequency of a system can be determined from knowing the mass and stiffness by the relation given in the equation

$$\omega_n = \sqrt{\frac{k}{m}} = \sqrt{\frac{3EI}{mL^3}} \quad (2.1)$$

where k is the stiffness, m is the mass, E is the elastic modulus, I is the moment of inertia, L is the beam length, and ω_n is the natural frequency in radians per second (Inman, 2001). To get the natural frequency in Hertz, which was used in this work, the following relation must be used

$$f_n = \frac{\omega_n}{2\pi} \quad (2.2)$$

In Equation 2.1, the first quantity is still in terms of the generic stiffness and mass of a system, while the second quantity substitutes in the stiffness parameters for transverse vibration, or bending. To illustrate how the natural frequency decreases as length increases, the denominator holds the necessary information. Clearly, increasing the length of a beam will also increase the mass, but the length term increases in a cubic fashion, whereas the mass term only increases linearly. For example, if a beam's length were doubled, the mass

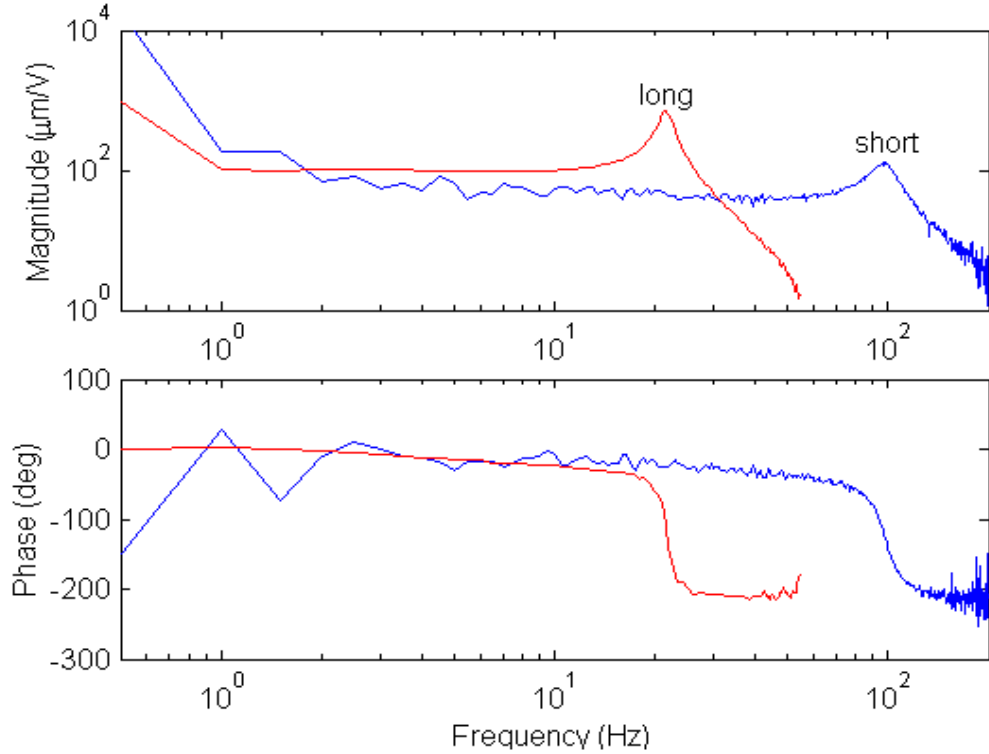


Figure 2.10: Natural frequency comparison of ionic polymer benders. The short polymer is (8 x 5 x 0.2)mm and the long polymer is (24 x 5 x 0.2)mm.

would also be doubled, increasing the mass term by a factor of 2. However, the length term in Equation 2.1 would increase by a factor of 8, four times as much as the mass term. Together these factors are compounded and the denominator would increase, making the result of the equation a smaller number by a factor of 4. This explanation is made, of course, assuming that the beam is uniform with E and I constant along the length.

This concept is shown for two ionic polymer cantilevers of different length in Figure 2.10. In the figure the “short” polymer is 8mm long and the “long” polymer is 24mm long. Both actuators are 5mm wide and 0.2mm thick. The decrease in frequency with increasing length is not quantitatively consistent with the theory of a uniform beam, but it is satisfied qualitatively. While beam theory states that this length increase should result in a factor of 9 decrease in natural frequency, the ionic polymer’s natural frequency only decreases by a factor of 5. From what has been said about ionic polymer actuators, it is obvious that they cannot be modeled as uniform beams, but the comparison will still be made since many readers are familiar with beam theory.

Not saying that ionic polymers should match with uniform beam theory, but it may

be worthwhile to comment on a possible source of error. This lies in the clamps of the test fixture. Since the ionic polymers experimented with are small and very lightweight, it was not thought that much force need be applied to hold the end of the polymer in a clamped condition. For this reason, rubber bands were used on the fixture clamps to provide the clamping force. These may introduce inconsistencies from one side to the other for the clamped-clamped configuration, and may not give a true clamped condition in either of the configurations. Also, as the frequencies increase, it is more likely that this improper clamped condition would become more of a problem, as the polymer is being excited faster.

A general remark to be made about the frequency response of ionic polymers is their phase lag at low frequency. A simple spring-mass system, for example, does not have any phase lag until it goes through the resonance, where a -180 degree shift occurs. Ionic polymers, on the other hand, exhibit a phase lag throughout the low frequency region that causes their shift to reach lower than -180 degrees. This effect will be seen as more transfer function results are shown. Some modeling work has been done to identify a model that accounts for the phase lag. Newbury (2002) has been able to predict this lag in an equivalent electrical circuit model with experimentally determined material properties.

It has been stated several times before that the response of an ionic polymer varies as the material begins to dehydrate. Many factors affect the dehydration rate and this is not the place for that discussion, so these results show this effect in a general sense. Following suit, the first results are for a cantilever, and are given in Figure 2.11a. The polymer that produced these results was a relatively long polymer, as is implied by the low natural frequencies. The reason that cantilevered polymers around 20mm or more are considered long is that by increasing the length, you soon reach a point where the polymer cannot support its own weight and it folds over. To illustrate this effect, think of holding a piece of paper at one end and notice how it will fold over to one side.

Returning to Figure 2.11a, in a matter of 10 minutes of continuous actuation, the natural frequency shifts from about 21Hz to 25Hz, or by a factor of nearly 20%. During this frequency shift, the magnitude stays relatively constant around $750\mu\text{m}/\text{V}$. There is also a phase lag of 25 degrees leading up to the point where the phase shift occurs. This increase in frequency can be related back to Equation 2.1, too. Thinking in terms of mass and stiffness, as the polymer dehydrates, it loses mass, resulting in a higher frequency as long as the stiffness at least remains constant. However, it is thought that as the polymer

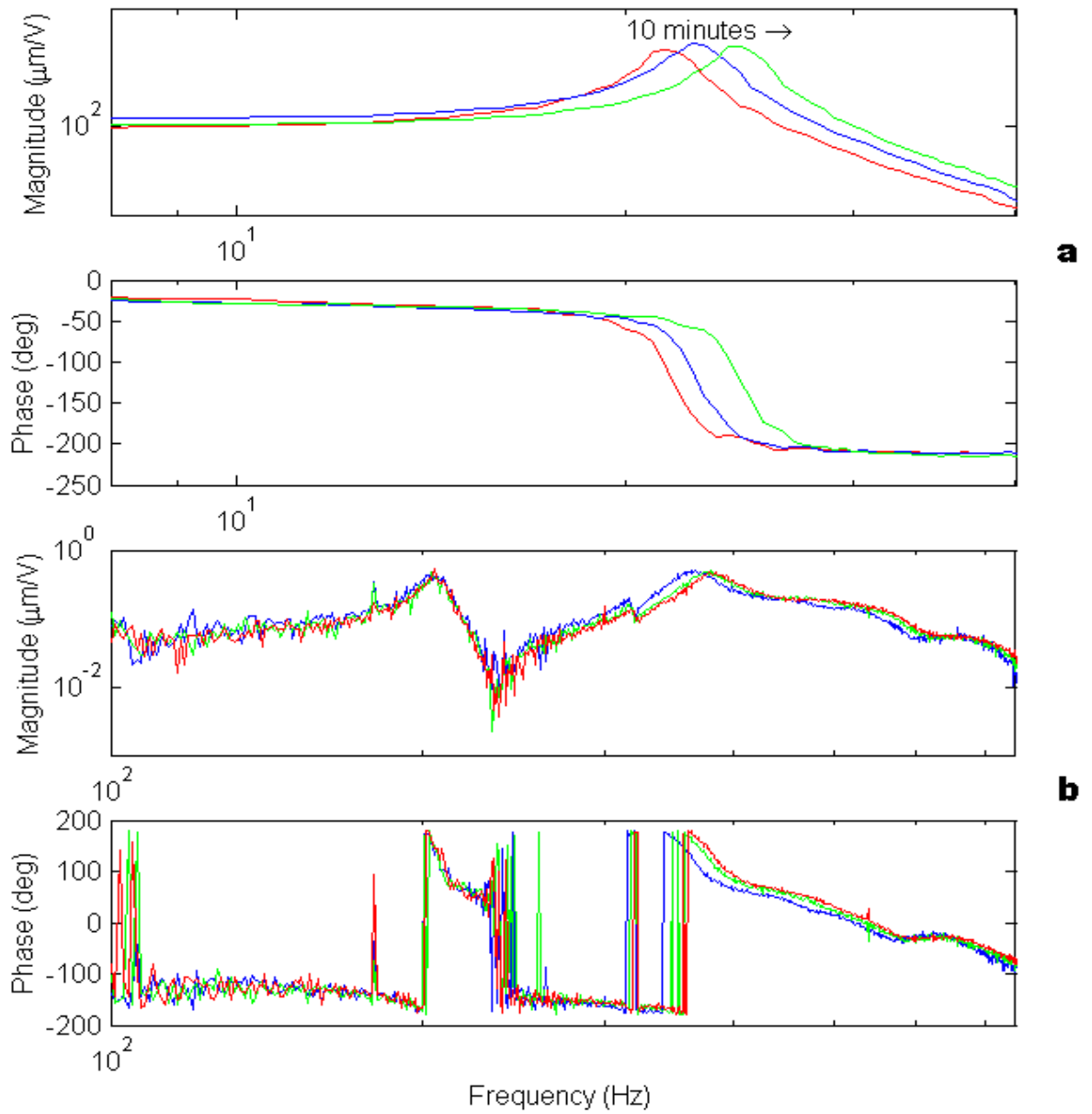


Figure 2.11: Cantilever (*a*) and clamped-clamped (*b*) frequency response functions shifting with time.

dehydrates, it also stiffens, which increases the natural frequency even more.

One surprising feature shown in this figure is the amount of damping, which was thought would not be so much in air. The damping comes out of the width of the resonant peaks. A very lightly damped system has sharp, narrow peaks, while a heavily damped system has dull, wide peaks. Those in Figure 2.11a seem to fall near the middle of the range. When comparing this response to a linear system, the first bending mode of the ionic polymer resembles a second-order system because of the resonant peak and 180 degree phase shift.

Shifting configurations to clamped-clamped gives Figure 2.11b. This figure is quite a bit more involved than the simple cantilever case. There are more modes present in the zoomed area. By experimentation, the first peak (205Hz) was determined to be some ambient frequency being picked up by the analyzer because it did not shift with time and sometimes it was not displayed in the data. The first bending mode was found to be around 360Hz for this particular polymer. This frequency is shown to shift from 365Hz to 385Hz (5%) in the time period. It should be noted that environmental conditions were not the same for each of the tests shown in the figure. Similar to the cantilever, the magnitude remains fairly constant, this time around $0.5\mu\text{m}/\text{V}$ during the frequency shift. Regarding the phase lag, the clamped-clamped configuration starts out just over 100 degrees before the shifts from resonances and anti-resonances occur.

Another point that can be commented on is the frequency increase going from one configuration to another. Using the equations for single-span beams, this boundary condition can be compared to uniform, Euler-Bernoulli beam theory (Blevins, 1979). The equation that can be used is based on beam properties and dimensions, which were kept the same for both the cantilever and clamped-clamped tests. This equation has the form

$$f_i = \frac{\lambda_i^2}{2\pi L^2} \left(\frac{EI}{m} \right)^{1/2} ; \quad i = 1, 2, 3, \dots \quad (2.3)$$

where λ_i is dependent on boundary conditions and f_i is the natural frequency in Hertz. By examining Equation 2.3, it can be seen that it is advantageous to use polymers of the same dimensions for each test configuration. This makes the length and moment of inertia the same, and it can be assumed that the elastic modulus and mass are equivalent

Table 2.4: Weighted Natural Frequencies for Clamped-Free and Clamped-Clamped Beams.

Mode Number	Clamped-Free	Clamped-Clamped
1	1.87510407	4.73004074
2	4.69409113	7.85320462
3	7.85475744	10.9956079

when comparing the natural frequencies at the beginning of the test, before dehydration begins. The frequencies for different configurations are then left to the values of λ_i . The i denotes the mode number of a particular natural frequency, with the first mode being under investigation in this study. Table 2.4 lists the first couple λ values for the cantilever and clamped-clamped boundary conditions, as given in Inman (2001).

Using the values in Table 2.4 for mode 1, a comparison can be made of the frequency ratio in going from clamped-free to clamped-clamped conditions. In collecting several frequency response functions for both the configurations, the cantilever gave the more repeatable resonant frequency of about 27Hz. In the clamped-clamped condition, there was more spread in the natural frequency, so a representative value was chosen to be 250Hz. In the calculations that follow, the frequency ratios of clamped-clamped to clamped-free are determined for an ionic polymer 20mm in length and a theoretical beam.

$$\frac{f_{CC}}{f_{CF}} = \frac{250\text{Hz}}{27\text{Hz}} = 9.3$$

$$\frac{f_{CCt}}{f_{CFt}} = \frac{\lambda_{1CC}^2}{\lambda_{1CF}^2} = \frac{4.73004074^2}{1.87510407^2} = 6.4$$

In the calculations, the subscripts CF and CC refer to “Clamped-Free” and “Clamped-Clamped,” respectively, while the t denotes the theoretical values. The outcome of this comparison states that changing the boundary condition from clamped-free to clamped-clamped increases the natural frequency of the ionic polymer by 45% more than the theoretical calculation for a uniform beam. Some deviation was expected, however.

What can be concluded from the frequency response results of ionic polymers is that they share some qualitative behavior with an ideal, uniform beam, but there is not much

coherence between the two. The next section provides a summary of the topics discussed involving the dynamic response characteristics of ionic polymer actuators.

2.3 Summary

This section discussed the dynamic response of ionic polymers in both the time domain and the frequency domain. The time response for a step input was dominated by overshoot and slow relaxation to some non-starting position. Different actuator designs were briefly discussed, showing intuitive results based on their construction and the response of a single-layer actuator. Sinusoidal time responses gave some insight into the open-loop bandwidth of the actuator, as the amplitudes decreased with increasing frequency. Turning to the frequency domain, qualitative results were achieved in relation to Euler-Bernoulli beam theory. Namely, the resonant frequency decreases as length increases, and the natural frequency increases by switching configurations from clamped-free to clamped-clamped. The dehydration effect on the frequency response was also discussed, showing that it has a stiffening effect on the actuator by increasing the frequencies. One overriding theme in the dynamics of ionic polymers is their trouble with repeatability. Much of this can likely be attributed to their nonlinearity, keeping in mind that the response of nonlinear systems is highly dependent on initial conditions. Some of this will try to be addressed in the following chapter, which deals with effects on open-loop bandwidth.

Chapter 3

Effects on Open-Loop Bandwidth

With some knowledge of the dynamic response, this chapter will elaborate on the frequency response of ionic polymer actuators, keying in on the open-loop bandwidth. While the frequency shifting effect has been commented on in the literature, it is yet to be quantified. That is the goal of this chapter. The two types of effects to be discussed are related to material dehydration and applied tension. Each will be discussed in turn, followed by a chapter summary, and since the same test equipment was used to study each effect, it will be described first.

3.1 Test Setup

The work for both the humidity effects and tension effects on ionic polymers was performed at the Air Force Research Laboratory in Albuquerque, New Mexico, so some of the equipment is different than that used at Virginia Tech, as described in the preceding chapter. In order to investigate the dehydration of ionic polymers, it was necessary to construct a test chamber in which the humidity of the air could be regulated. This chamber was made with 3/8-inch thick plexi-glas and was 54 inches long, 27 inches wide, and 24 inches tall. The reason that such a large chamber was used to test such a small actuator was to ensure that there was enough air mass in the chamber to be controlled. There was a movable door on the top of the chamber through which the test specimen could be inserted. A 6-inch diameter hole was cut into the other end of the top for humidified air to enter the chamber. The moist air, supplied by a mist-free Lasko evaporative humidifier, model 1120, entered the chamber via a duct. This method was chosen over putting the humidifier directly inside the

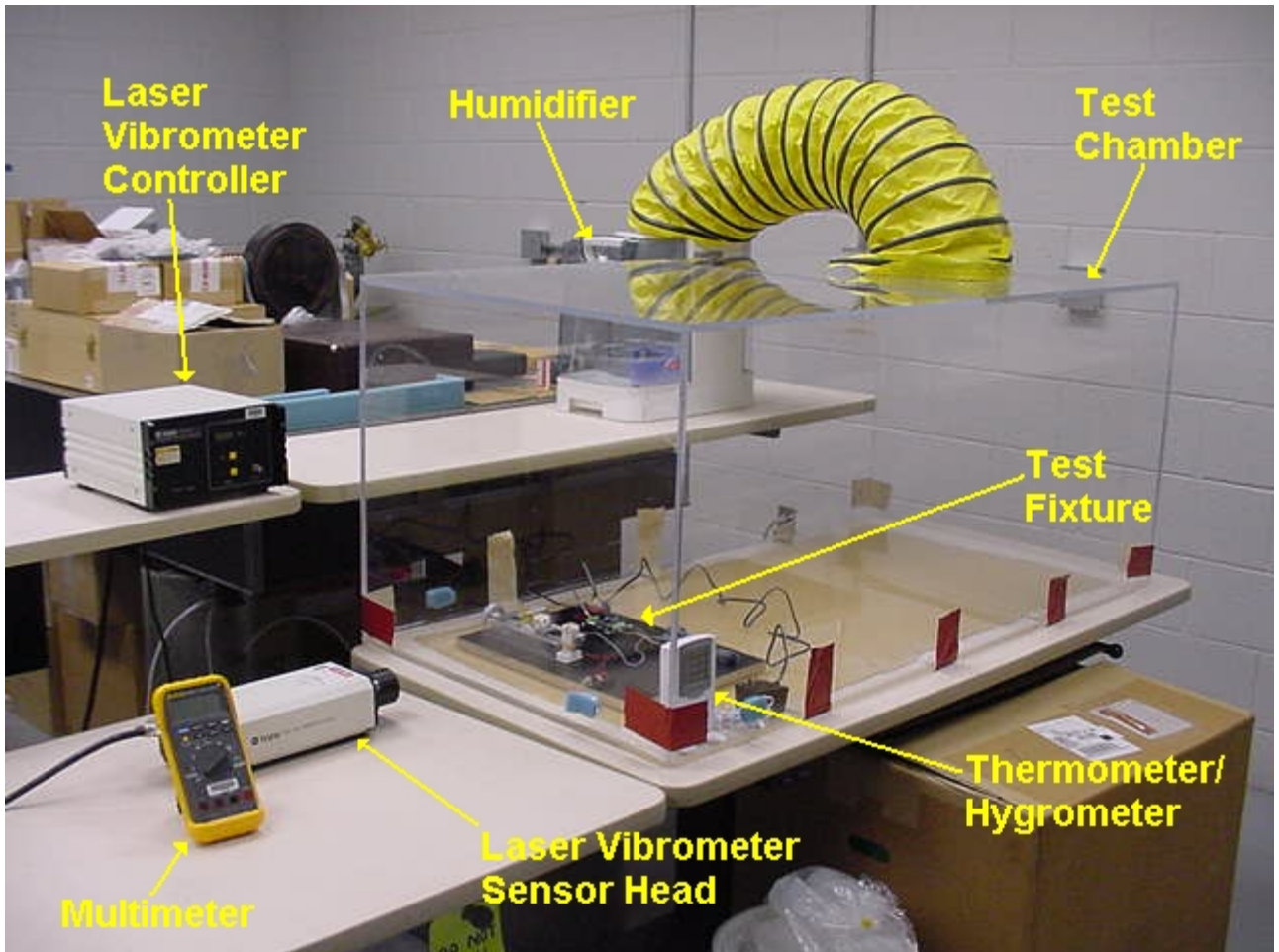


Figure 3.1: Test setup for controlled humidity experiments. Note that the signal analyzer is not included in the figure.

chamber because the vibration associated with the fan would likely interfere with the polymer's motion, giving poor results. The humidity level inside the chamber was monitored using a RadioShack thermometer/hygrometer (63-1032), which gave temperature readings as well. Small holes were also cut in three sides of the chamber in order to run wires and cables for the electrical powering of devices and data transfer.

The actuation voltage was supplied to the polymer by a Hewlett-Packard (HP) 35665A dynamic signal analyzer. Like the Tektronix, the HP signal analyzer had double duty, supplying the voltage in addition to collecting the signals for calculation of the transfer functions. The motion sensing was again performed by a laser vibrometer, but not the same model because of availability conflicts. This one was a Polytec OFV 353 Sensor Head and Polytec OFV 2601 Vibrometer Controller. The major difference between this laser and

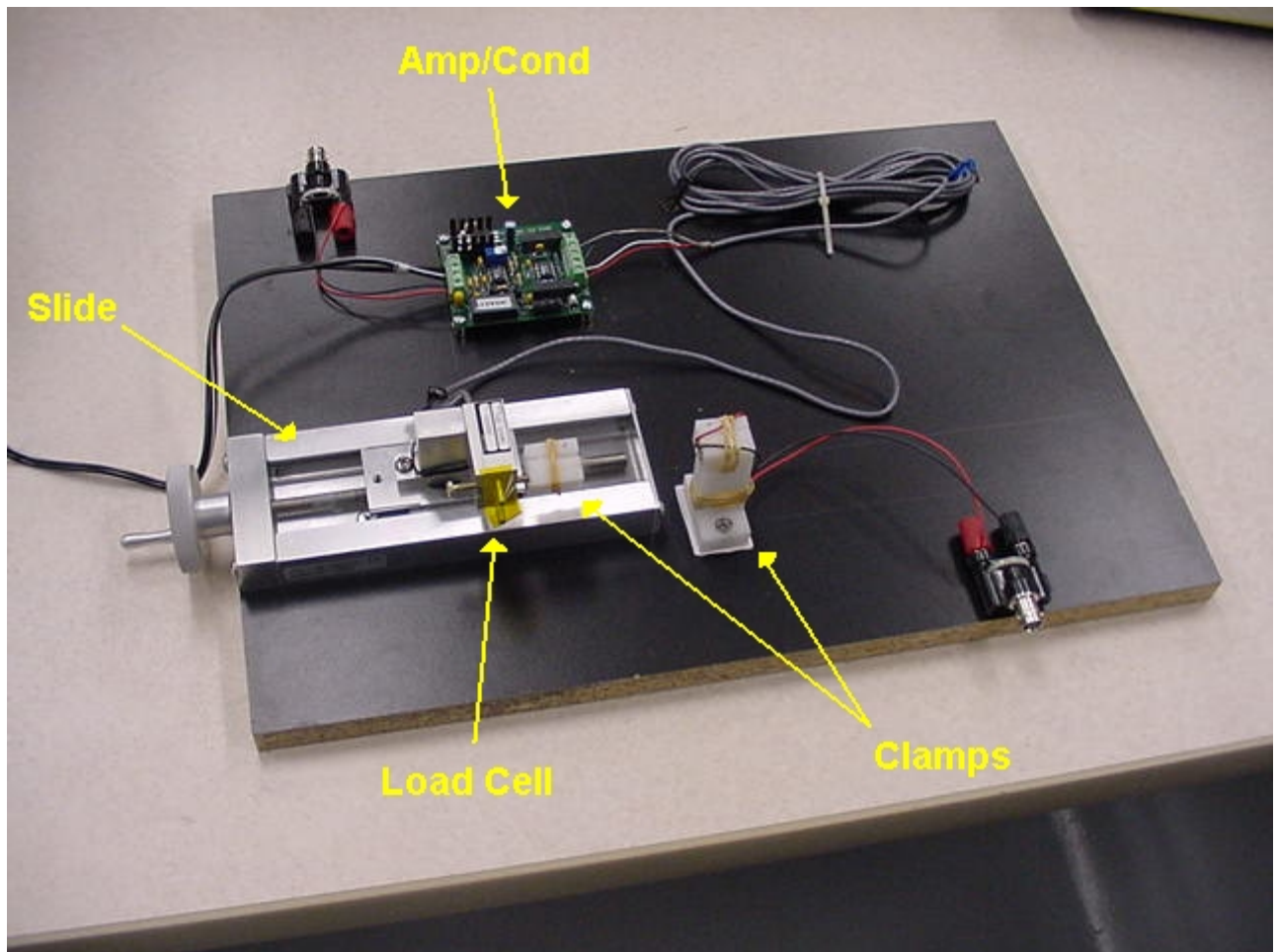


Figure 3.2: Close-up of the test fixture points out the pertinent devices used in the testing configurations.

that described in the last chapter is that this one measures velocity, not position. Once the transfer functions (mobility) were calculated by the signal analyzer, they then had to be integrated to get the corresponding position transfer function (receptance). After all the initial data collection, all post-processing was performed using Matlab 5.3 and Microsoft Excel software. Figure 3.1 shows a digital image of this laboratory equipment.

Taking a closer look at the test fixture, it can be seen that it has a strong resemblance to the one in Chapter 2. This fixture was made similar to the one at Virginia Tech because with that design working well, it seemed convenient to mimic it. Figure 3.2 shows an annotated picture of the fixture. The figure shows the two delrin clamps, one stationary and one movable on a Velmex, Inc. unislide. The electrodes were again made with gold foil. Attached to the movable clamp is a Transducer Techniques, Inc. load cell for tension

monitoring, which was observed through a Fluke 87/III digital multimeter. The figure also shows an “amp/cond,” which is an amplifier/conditioner required for the load cell. It is also from Transducer Techniques, Inc., model TMO-1.

To comment on some signal collection settings, it can be said that they are much the same as described in Chapter 2, only the HP replaces the Tektronix. A signal of random content actuated the polymer, with the rms level varied according to the testing configuration. Because the input was a random signal, a uniform window was used on the data since the measured output has equal importance throughout the time block. The basebands of frequency were increased from those before because the shifting effects were being studied over long periods of time, typically 30 to 40 minutes, capturing one transfer function every 4 minutes. Usually 5 averages comprised each transfer function. Also, the data blocks were most often set to collect 401 or 801 sample points.

This completes the review of the laboratory equipment used for the experimentation. The remainder of this chapter is organized to discuss the testing method used for each effect, prior to analyzing the results. Then results for a cantilever and clamped-clamped actuator will be presented for humidity effects, while only the clamped-clamped condition will be addressed for tensioning effects.

3.2 Humidity Effects

As shown in the frequency response section of the previous chapter, a dehydrating ionic polymer has a stiffening effect on the material. This stiffening causes the natural frequencies to shift in an increasing manner. Currently, most applications for ionic polymers deal with operation in wet environments where dehydration is not a factor. Testing in an open air environment cannot afford that luxury, however. This section will present results of the frequency shift caused by dehydration of an actuator in the clamped-clamped condition, as well as the cantilever. The aim of this section is to develop relationships for how the frequency response characteristics vary in time at constant humidity levels. The test setup and methods for each configuration will first be described, followed by the results.

3.2.1 Testing Method

The testing method is a little more involved when regulating the humidity. This is mainly due to the fact that the humidifier cannot be placed inside the test chamber. It has a humidity sensor on it, but being outside of the chamber, it senses only the ambient humidity. To make up for this, a sort of manual feedback was used. This was executed in the following way. When the hygrometer would fall below the testing humidity level, the humidifier would be turned on, raising the humidity level inside the chamber. In the event that it was left running for too long and the chamber humidity rose above the desired level, the top door of the chamber was opened, allowing the humidified air to escape to the less humid air in the room. It should also be noted that the humidifier was turned off while data collection was in progress to eliminate any possibility that the air entering the chamber would act as an external force on the ionic polymer.

Sliding the movable clamp to within reach of the polymer, the configuration was changed to clamped-clamped. For the humidity effects study, it was desired to have no tension applied on the polymer. However, as the polymer dehydrates, its dimensions tend to reduce like the material is shrinking, which causes tension in the material. This consequence was monitored and the movable clamp was adjusted so that the load cell was reset to zero before each test began.

A final remark to be said about the testing method for humidity effects has to do with the data collection process. It was previously mentioned that transfer functions were taken at 4-minute intervals for 30 to 40 minutes. There was no mathematical or physical reasoning behind these choices, but it was thought that 4 minutes would provide enough time to capture a transfer function and then allow the system parameters to change slightly before the next transfer function was taken. Also, using 4-minute intervals does not leave an overwhelming amount of data to sort through during analysis. There were 10 transfer functions taken for each test, simply because 10 is a round number and, at 4-minute intervals, this gives a total testing time of 36 minutes. Recall from the second chapter that the resonant frequency of a cantilevered ionic polymer shifted by 20% in only 10 minutes. For this reason, testing for 36 minutes was determined to be a sufficient amount of time to study frequency response changes.

With the testing method in order, the experiments were performed for a cantilevered

and clamped-clamped ionic polymer 20mm long. The results of these tests are given in the following sub-sections.

3.2.2 Cantilever Results

Before getting into the discussion of results, a comment needs to be made regarding the obtainable humidity levels in the test chamber. The humidifier proved to reach a maximum of only about 70% relative humidity inside the chamber, which is the onset of “wet” conditions, according to the hygrometer. Testing in a “wet” environment was meant to be one of the goals of this research, by comparing those results to results from conditions where the air is “comfortable” or “dry.” This unfortunate drawback of the apparatus severely limited the range over which testing could be conducted to only about 15%. This range started with the low point being the humidity of the ambient air each morning. In Albuquerque, this was usually around 55% for the month of July. Therefore, the available testing range was 55% to 70% relative humidity.

The first set of results to be shown have the input set to a 500mV-rms random content signal, which was used as the baseline for cantilever testing. In the data, the frequency shifting is based off the first natural frequency (bending mode), and the magnitude that occurs at that peak. Figure 3.3 represents the trend associated with frequency shifting due to material dehydration. Each curve in the figure has data points for a different humidity level, given in the legend. These results go with intuition, in that at lower humidity levels, the polymer dries out faster, causing a steeper slope in the frequency versus time curve. Conversely, at higher humidity levels in the chamber, the polymer takes longer to dehydrate, resulting in a more gradual frequency shift. An interesting thing to note about the trend seen is that it appears to be linear. It was thought that at some point in time, the frequencies would begin to level off and approach some final value, but this was not the case. It could also be that the time period was not long enough to witness this leveling off of the frequency curves.

A comment that should be made is that there is some variation in the starting frequency for each test. Ideally, this would be fairly constant as long as the dimensions, material properties, and initial conditions were identical for each transfer function. However, the initial frequency is seen to vary by $\pm 10\%$. In considering reasons for this deviation from a constant value, the dimensions come up as the steadiest testing parameter. This leaves

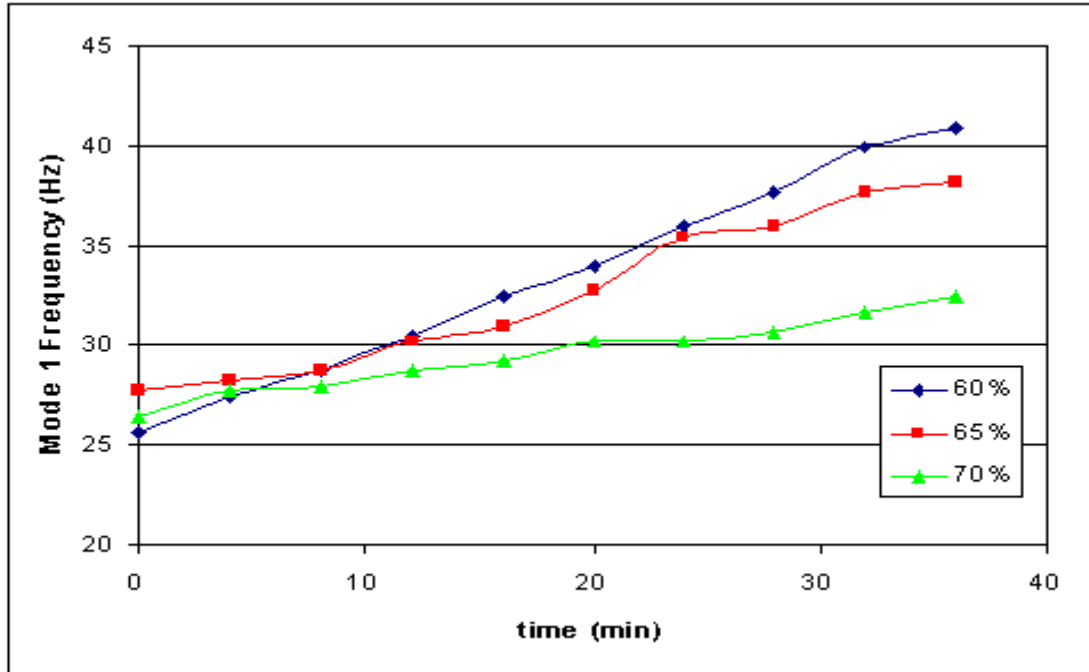


Figure 3.3: Natural frequency as a function of time and humidity for cantilever polymer.

material properties and initial conditions as the possible means of variation. With the nonlinearity of the material, it was thought that initial conditions should be kept as close to constant as possible. For this reason, there were multiple test specimens used, one after another. This would make adequate soaking time be available between tests for a particular specimen. Material properties are then left as the main culprit. Attempting to minimize this problem, the three specimens used were cut from the same larger sample of ionic polymer material, but experiments have shown that material properties do vary across the dimensions of a single fabricated sample. Therefore, according to this logic, the material property inconsistency is the main reason for different initial natural frequencies.

Turning attention now to the corresponding magnitudes, Figure 3.4 does not give as agreeable results as the frequency plot. There does not seem to be linear trend related to this data. However, there is an eventual downward, oscillatory motion, the consequence being that the magnitude at 36 minutes is less than that at the start of testing. Again, the initial reading has much deviation from a set starting point, spanning over a few hundreds, which will be attributed to material inconsistencies.

To address the possible situation that 36 minutes was not long enough for any leveling

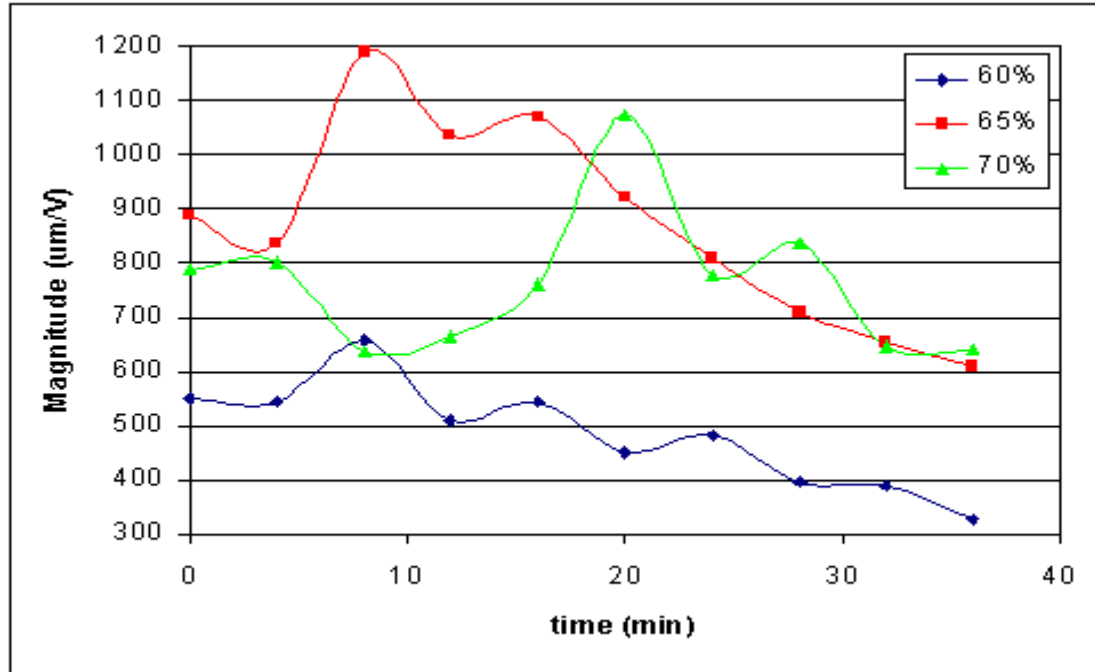


Figure 3.4: Cantilever peak magnitude as a function of time and humidity.

off to occur in the frequency plots, another series of tests was run, this time increasing the input rms value by 50% to 750mV. These tests were also run for 36 minutes, but because more power was being supplied to the polymer, it would heat up quicker, dehydrating at an increased rate. Performing these experiments verified this assumption, and the results are shown in Figure 3.5. In this group of tests, only two humidity levels were used, one high and one low, leaving the middle open for interpolation. Like Figure 3.3, the transfer functions taken at higher humidity resulted in a slower frequency shift, and vice versa.

The magnitude plots for the increased input show a more favorable pattern. Figure 3.6 shows that the magnitude has a much more discernable decaying trend than when 500mV-rms was used as the input. The starting point for the data shown at each humidity level is also much closer to being the same, but this point may not necessarily be due to increasing the input voltage. It could be the repeatability issues that happened to give coherent data in these particular tests. A strange aspect of this plot is the magnitude at the end of testing. Seeing how the frequency shifted less under higher humidity, it would be thought that the same would hold true for the magnitude, but the figure shows the contrary. This could be attributed to the repeatability issues or the material inconsistencies, but regardless of where the magnitude ends for each humidity level, it is obvious that the

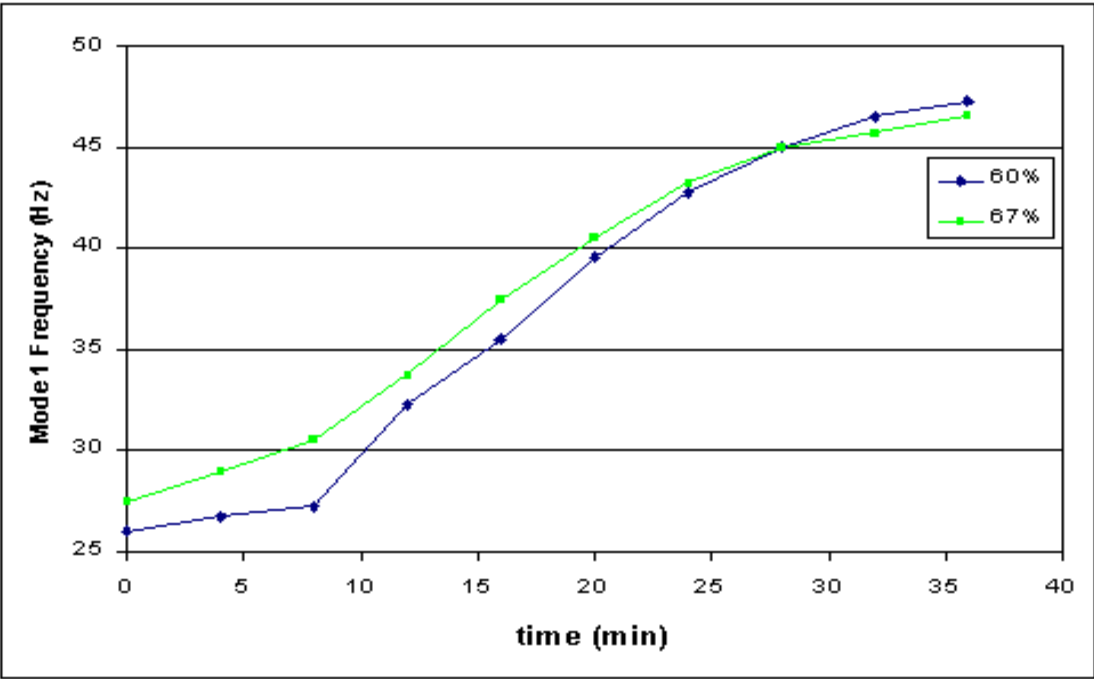


Figure 3.5: Cantilever natural frequency shift with increased input voltage.

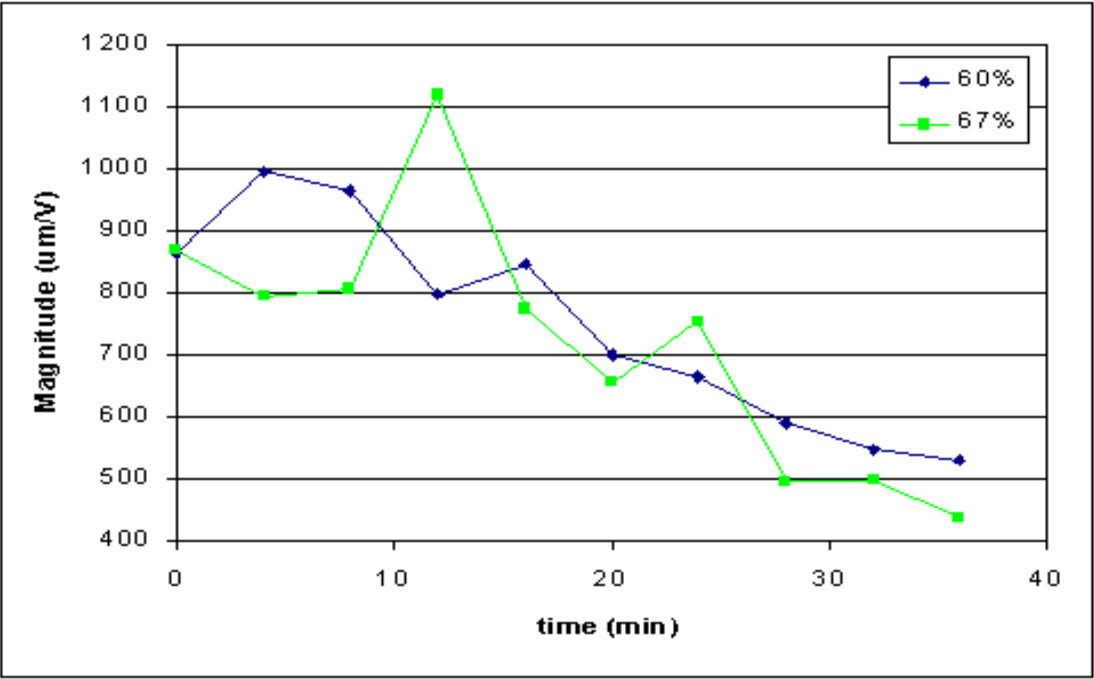


Figure 3.6: Magnitude plots of cantilever for increased input.

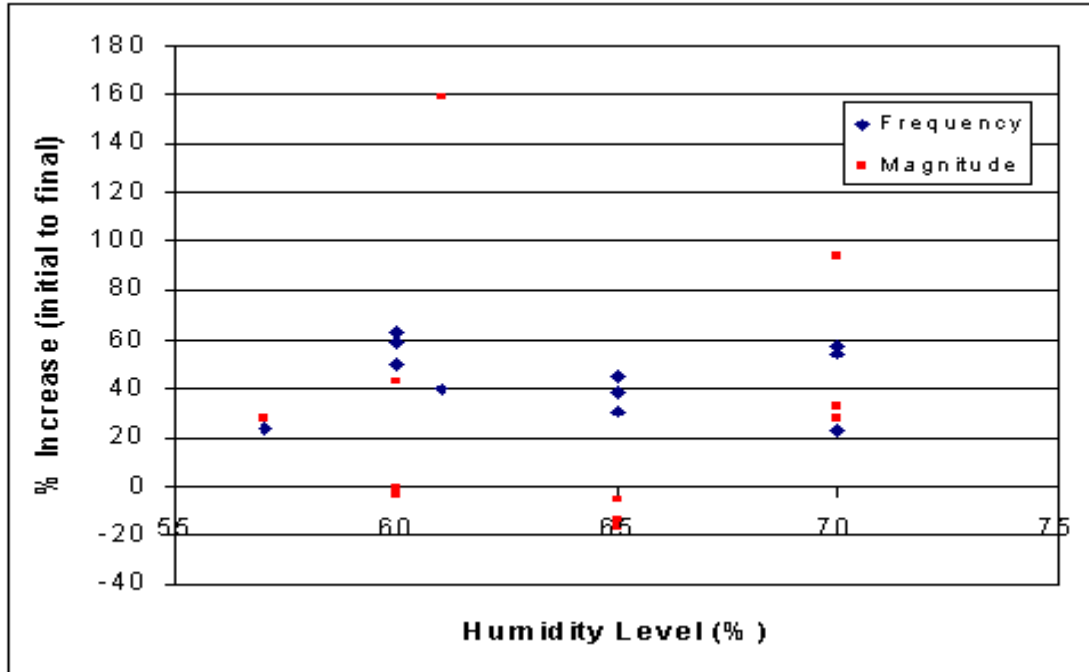


Figure 3.7: Percent difference plots comparing initial to final values for frequency and magnitude at each humidity level.

trend is decreasing as the polymer dehydrates.

On the topic of repeatability issues with ionic polymer actuators, a plot was made comparing the percent difference of frequency and magnitude values in going from the initial to the final value for all the transfer functions taken. It is organized as a percent difference versus humidity level plot. The results shown in Figure 3.7 are more of a “where did it start, and where did it end” comparison, not paying any attention to the path taken by the peak frequency or magnitude. What the figure shows is that, except for a few outliers, the frequency shifts are grouped together and the shift decreases as the relative humidity increases. This is what the data presented earlier in the chapter showed. The magnitude, for the most part, follows the expected outcome, shifting in the opposite direction. What is interesting is that the magnitude and frequency do not shift the same relative amount. Instead, the frequency usually shifts much more than the magnitude. It should also be noted that the data shown is for the results when the polymer was actuated with a 500mV-rms random signal.

Completing the presentation of results for a cantilevered ionic polymer, leaves the clamped-clamped configuration results. This is next and is followed by a discussion that

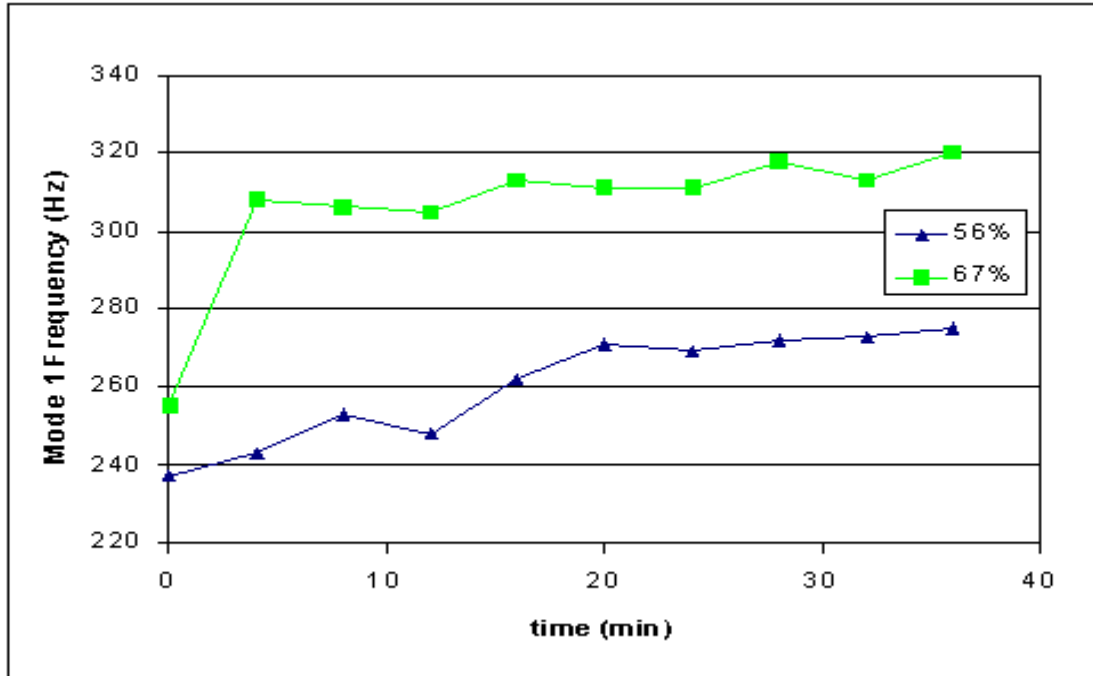


Figure 3.8: Clamped-clamped frequency shift as a function of time and humidity.

finishes the section of humidity effects on ionic polymers.

3.2.3 Clamped-Clamped Results

The clamped-clamped configuration, as noted before, increases the natural frequencies by a factor of about 9, and these results will show how the humidity levels affect the dehydrating polymer's frequency response. As for the cantilever, the bending mode was tracked for frequency and magnitude of the resonant peak, with the baseline input of 500mV-rms. Since the basic trend established from the cantilever results was that higher humidity shifted the frequencies less, only results from the maximum and minimum humidity levels will be presented. The first frequency results are given in Figure 3.8.

In the figure, the starting frequency for both data sets shown is near 250Hz, which shows the factor of 9 increase from the cantilever configuration. Immediately noticed in the data is the large frequency jump in the first four minutes of the 67% humidity data. It is unclear what may have caused this to happen, but the data from 4 to 36 minutes shows what was expected. This expected result, based off the cantilever tests, is for the frequency shifting to follow a linear increase, which is exhibited in the plot. Different from

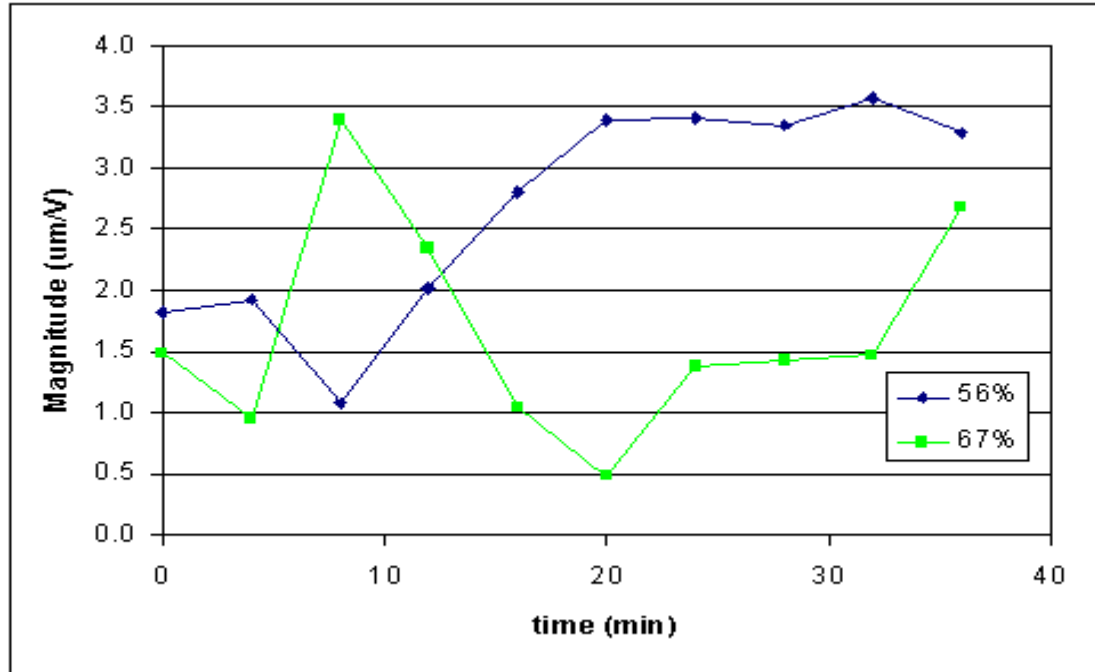


Figure 3.9: Magnitude results for clamped-clamped polymer actuator.

the cantilever data is the two humidity levels in the plot. On this particular day of testing, the humidity fell below 60% for long enough to get results, broadening the humidity testing range slightly. Discounting the large initial jump at 67% humidity, the frequency increases more gradually at higher humidity, than for lower humidity. This was also seen for the cantilever.

The magnitude for the clamped-clamped condition brings about some interesting results, differing from the cantilever results. Figure 3.9 displays the data. Unlike the cantilever, the clamped-clamped results do not show a downward sloping progression of magnitude as the polymer dehydrates. In fact, the results have no discernable trend, other than being non-decreasing. The values are much smaller than those seen for the cantilever, but this was expected because clamping the free end of the cantilever drastically reduces the amount of motion. This reduction happens to be two orders of magnitude in this case. There is also not much to be said of the shifting that occurs at different humidity levels because it is difficult to classify the behavior seen.

With contradicting results between the two test configurations, the input to the polymer was increased to 1.0V-rms to search for more coherent results. First, the frequency results are presented in Figure 3.10. Using a linear curve fit, the frequency data here is

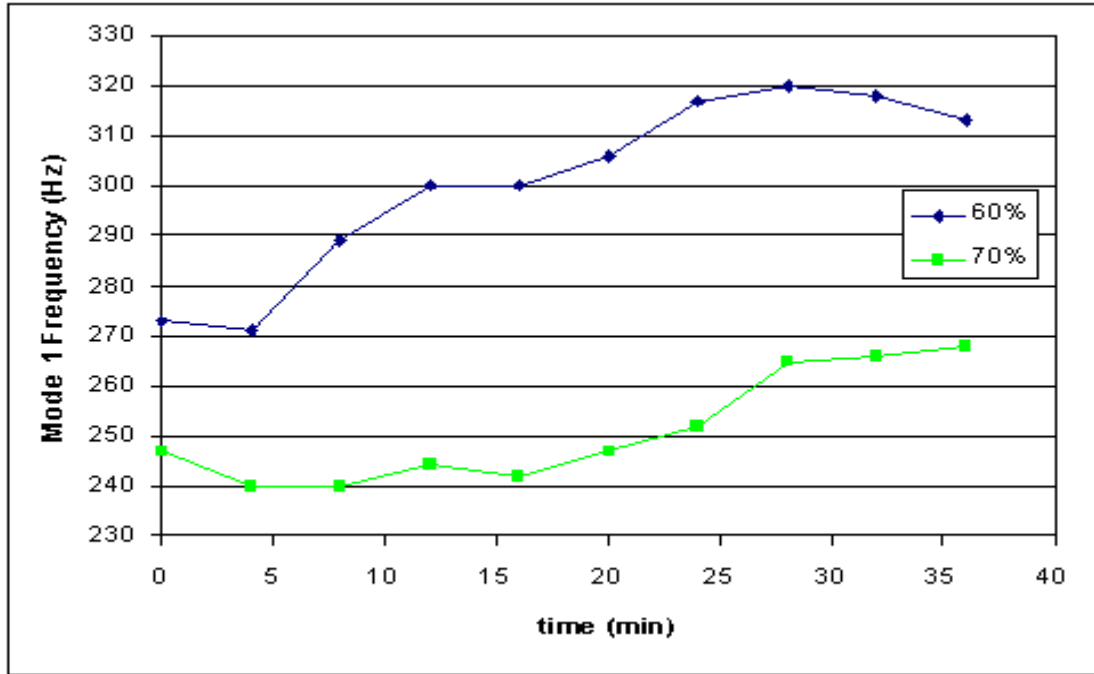


Figure 3.10: Clamped-clamped frequency shift for an increased input.

increasing at nearly double the rate of that in Figure 3.8. A linear curve fit may not be the best choice of fitting this data, however. It should be sufficient at 70% humidity, but the 60% humidity data has a rounding off effect beginning about 25 minutes into the test. The starting frequencies, at first glance, appear to be far apart, but because they are so much higher than the starting cantilever frequency, they still fall within the $\pm 10\%$, mentioned earlier.

Switching emphasis now to the magnitude results for increased input to the clamped-clamped polymer gives more unexpected results. They are shown in Figure 3.11. One of the first things noticed is that the increased input does not have an effect on the output magnitude. The values still lie below $4\mu\text{m}/\text{V}$. Regarding any trend associated with this data, non-decreasing, almost constant, can be deduced. Again, there is not much to be said of the humidity effect on the magnitude. This is contrary to what was expected from the cantilever results, but may be due to the limited motion of the clamped-clamped configuration, where it is not moving enough initially to be reduced.

The last plot to be shown for the clamped-clamped ionic polymer is the percent difference plot, like that shown for the cantilever. This plot gives data points for both the magnitude and the frequency for all the tests taken with an input of 1.0V-rms. For the

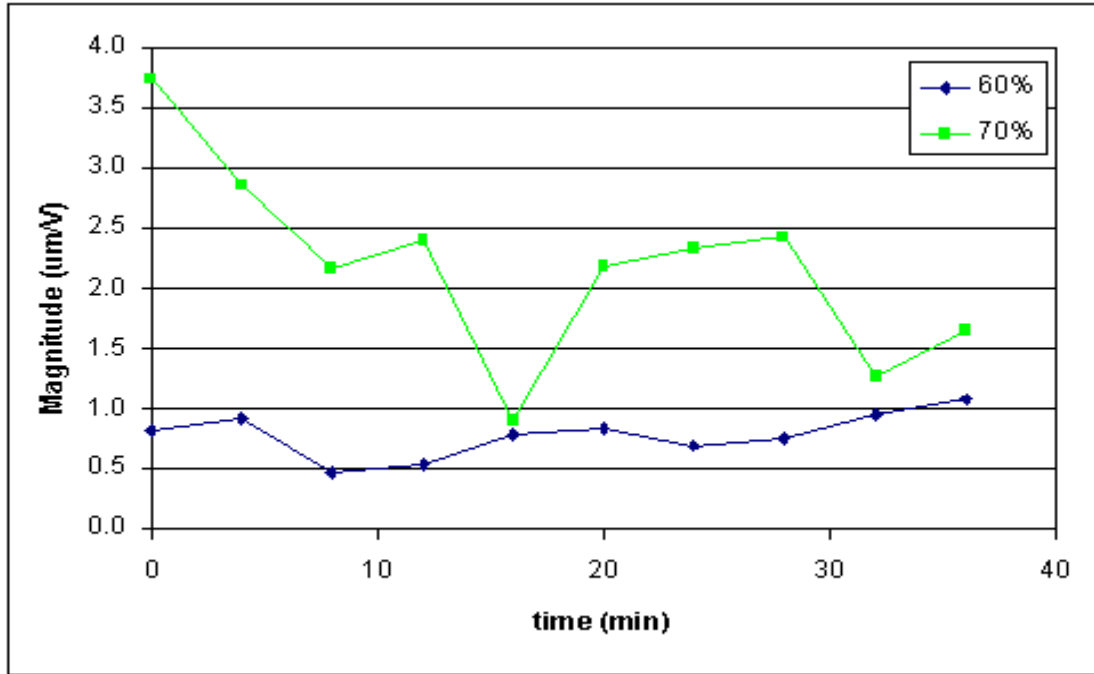


Figure 3.11: Clamped-clamped magnitude shift for an increased input.

cantilever, the percent difference plot was shown for the baseline input, but since the trends are similar for the clamped-clamped configuration, the higher input was chosen. The data in the plot reflects the increase or decrease in the frequency and magnitude values as the polymer dries out, looking only at the initial and final values. Figure 3.12 has this data. As humidity increases, the magnitude data displays more variation, while the frequency values tend to remain close together. This is strange because intuition gained from previous results says that the expected outcome would be that frequency increases are higher at lower humidity levels, whereas magnitude increases are lower. This figure shows that the frequency changes are nearly constant across humidity levels, while magnitude changes increase. For the magnitude, this result provides more evidence for the nondiscernable trends seen in the data.

Having presented the results for the humidity effects on ionic polymer actuators, a discussion follows. This discussion will wrap up the humidity effects section, leading into the effects of tension on a clamped-clamped ionic polymer.

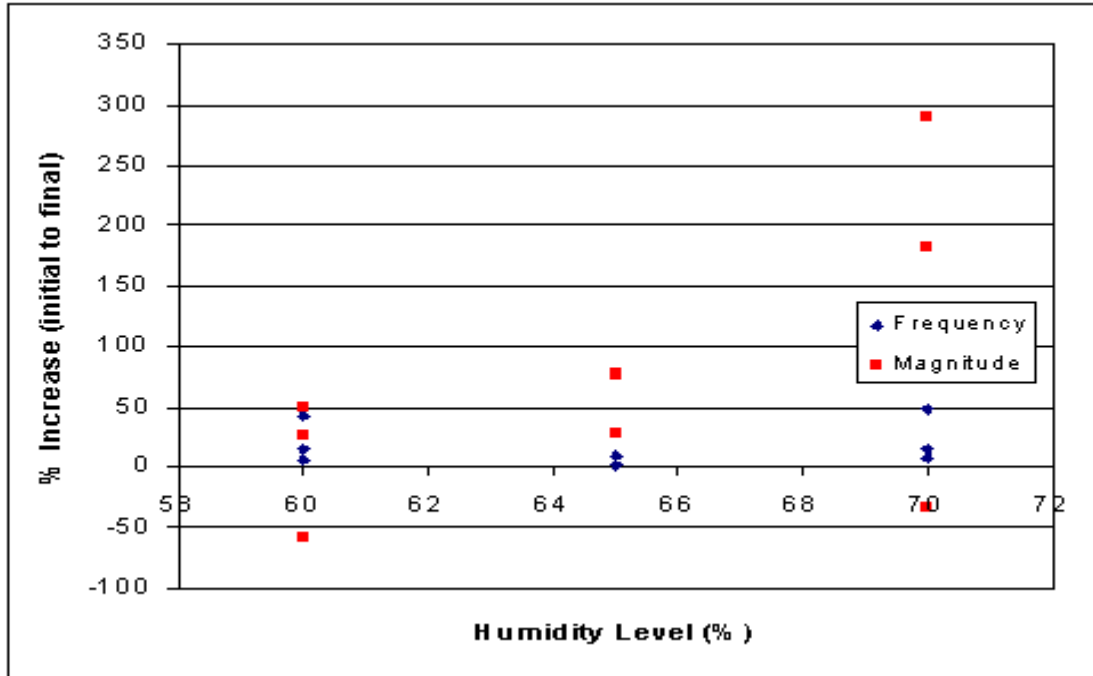


Figure 3.12: Percent difference for the clamped-clamped ionic polymer.

3.2.4 Discussion

To aid in the discussion of the humidity effects on ionic polymers, a table has been made including data from all the transfer functions taken. As noted previously, the data shown in this section so far was representative data. With the number of transfer functions taken in this investigation of humidity effects, including it all would likely be overwhelming. Table 3.1 has data for both the cantilevered and clamped-clamped boundary conditions, presented as averages for each humidity level. Plots of all the humidity data taken have been included in Appendix A. Because of the discrepancies in the magnitude data between configuration, the table only presents frequency shifting data. The initial frequency reported for each case is the average of all data taken in that configuration, at the given input voltage. This was done because the humidity level should have no effect on the starting frequency of each test, assuming that the initial hydration state of the material was kept constant. The precautions taken for this measure were previously described.

The table has some interesting results. First off, as the input increased, the average initial frequency increases 3% to 4% for each 50% increase in voltage. This means that the starting natural frequency may be dependent on the actuation voltage to the polymer, which may cause difficulty later. In all the cases shown, except for the 750mV-rms cantilevered

Table 3.1: Summary of Data for Humidity Effects on the Natural Frequency of Ionic Polymers.

Parameter	Units	Clamped-Free Ionic Polymer					Clamped-Clamped Ionic Polymer			
		500			750		500		1000	
Input	mV-rms									
Humidity	%	60	65	70	60	67	60	70	56	67
Frequency (0min)	Hz	26.5	26.5	26.5	27.4	27.4	247	247	268	268
Linear Slope	Hz/min	0.415	0.318	0.305	0.433	0.476	2.80	1.99	2.05	1.16

polymer, the linear slope decreases as the humidity increases. Recalling from Figure 3.5, a linear slope is a very poor approximation for the data because it levels off as time increases. The data was included with a linear slope to look for any broad statements that could be made about the results. The trend makes sense because with more moisture in the air, the water from the polymer will not evaporate as fast, causing less frequency shift. In the case for the 500mV-rms cantilever, sets of tests at three humidity levels were run, and the data shows that from 60% to 65% there is a much greater change than between 65% and 70%. This is where the limitation of the humidifier really affected this study. Whether the slope continues to decrease by smaller and smaller amounts as the air enters the “wet” conditions would be very interesting to see, but this will have to wait for a more sophisticated test setup. Because testing was only performed at two humidity levels for the other test cases, any possible recurrence of this effect cannot be seen.

One last point to be made about the frequency data has to do with the slopes for different humidity levels. In the 500mV-rms data for both configurations, the relative decrease in slope for increasing humidity from 60% to 70% is about 27%. This hints that the frequency shift is related more to the humidity of the environment than it is to the testing configuration of the polymer. This same comparison cannot be made for the increased inputs because the linear fit for the cantilevered data was not very representative. However, it can be noted that for doubling the input of the clamped-clamped case, a humidity increase of 10% results in a near doubling of the relative frequency decrease.

To comment on the magnitude, it can be concluded that for the cantilever, a downward, oscillatory shift occurs in peak value, but it is not correlated to the humidity level of the test chamber. The clamped-clamped polymer acts much differently than the cantilever,

in that it displays no downward trend at all. It acts in much the opposite fashion, not necessarily increasing, but definitely not decreasing. This has been referred to as a non-decreasing trend in this research. The input for both testing conditions also does not seem to affect the peak magnitude.

Since this chapter has to do with the bandwidth of these ionic polymer materials, it may be worth mentioning something about that now. These comments, along with those in the tension effects section, have to do with the open-loop bandwidth of the actuators. Typically, the bandwidth of a system is determined by a frequency just below the cross-over frequency. The cross-over frequency is the frequency at which the magnitude plot has a value of 1 (0dB). With the magnitude being a ratio of output to input, this implies that they are equal in amplitude. The bandwidth is most often referred to as the point where the magnitude is 0.707 (-3dB). The significance of this point is related to energy, where a magnitude of this value indicates a half power reduction. This means that the output is much less than the input and the polymer will have a difficult time tracking the input.

For ionic polymers, the cantilevered configuration does not gain much open-loop bandwidth as the frequency increases because while the frequency becomes higher, the magnitude is decreasing. The clamped-clamped ionic polymer, on the other hand, is able to gain open-loop bandwidth because of the non-decreasing trend in the magnitude plots. Given that increasing frequencies result in a non-decreasing magnitude, the bandwidth will increase as the polymer loses hydration.

This discussion concludes this section on the effects of humidity on ionic polymers. Next up is the discussion of the effects tension has on the bandwidth of the actuators.

3.3 Tension Effects

Contrary to the purpose of the previous section, when studying the tension effects on a clamped-clamped ionic polymer, the humidity level was held constant and the tension levels were varied. Also unlike the humidity effects study, this section deals only with the clamped-clamped configuration because it is difficult to apply a tensile load to an actuator with one end free. Incidentally, the test fixture, as designed, does not have the capability. This section will first discuss the testing method used, followed by the results for the tension effects on the frequency response of ionic polymers.

3.3.1 Testing Method

Similar to the tension rezeroing before each test explained in the humidity effects section, when actually applying a tension to the material, it too had to be regulated. This involved adjusting the movable clamp to reset the tension to the desired load. One adverse effect that came about as the tension increased was that the tension level was not very stable. As soon as the resetting was completed, the tension would start changing again. Ideally, a controller would have been implemented to correct this problem. However, due to time considerations, this was not an option. To account for this instability, a type of manual feedback was again used, keeping the tension close to the desired value while data was being collected.

The humidity level chosen for these experiments was 65% because that was the most stable humidity attained and the ambient air often reached this level of humidity. Testing at the relative humidity of the air in the room also made it easier to proceed with the experiments because that variable was eliminated from contention. It was assumed, too, that the effects tension had on the polymer at one humidity setting would be similar at other humidities.

Also to keep things consistent from test to test, the same 4-minute interval testing for 36 minutes was used initially, but as more tests were conducted, the length of time over which transfer functions were captured was increased. This was done to look for any roll off in the data, like that seen in the humidity effects section for increased inputs to the cantilever. Additionally, the baseline input was raised to 1.0V-rms for these experiments. Otherwise, the techniques used in testing the tension effects were the same as those used for testing the humidity effects, so to avoid redundancy, that is all that will be said here of the testing method. The results of this study will be given next.

3.3.2 Tensioning Results

The load cell used in the tension testing was rated at 100 grams because ionic polymer have demonstrated their low force characteristic. The data presented here will follow a similar format to how the humidity effects were presented, in that the frequency effects will be shown first and the tension effects on magnitude second, with Appendix B showing plots of all the data. In the data taken, results for five different tension levels are given, starting at

Table 3.2: Force Conversion Values for Load Cell Outputs.

Voltage (mV)	0	200	400	600	800
Force (mN)	0	24.6	49.2	73.8	98.4
Stress (kPa)	0	24.6	49.2	73.8	98.4

no tension, taking steps of 200mV up to 800mV. Certainly milli-Volts are not a unit of force, but the multimeter reading from the load cell is proportional to force. The proportionality of load cell output to force is

$$F_T = 123\vartheta \quad (3.1)$$

where F_T is the applied tensile load in milli-Newtons, and ϑ is the load cell output in Volts. With this relation being specified, it is worthwhile to show the representative forces imparted on the polymer, given the load cell voltages. Table 3.2 presents these conversions. In the table, both measured force and the corresponding stress are given, using the nominal cross-section dimensions of 5mm wide and 0.2mm thick. Taking a first look at the force and stress values, it appears that they may be in error, but with the cross-section dimensions and unit conversions, the forces only get multiplied by factors of 10, which do not affect the digits. For ease of reference when analyzing the data, each 200mV increase in tension can be thought of as about a 25mN increase in the applied force.

Before getting into the results, a remark will be made about what is expected. This comment, like in the dynamic response discussion, is based off a uniform beam with an applied tension. When a load applies tension to the beam, the natural frequencies increase, and conversely, when the load is compressive, the natural frequencies decrease. For certain boundary conditions, exact solutions can be found for the increase of the frequencies, but the clamped-clamped condition has only an approximate solution (Blevins, 1979). The ratio of natural frequency increase uses the clamped-clamped frequency with no applied load as the reference value, and it can be calculated by

$$\frac{f_{i,F \neq 0}}{f_{i,F=0}} = \left(1 + \frac{F_T}{|F_b|} \frac{\lambda_1^2}{\lambda_i^2} \right)^{1/2} ; \quad i = 1, 2, 3, \dots \quad (3.2)$$

where F_b is the buckling load for the beam. The buckling load for a beam is dependent on dimensions, elastic modulus, and boundary conditions. For the clamped-clamped configuration, the buckling load has the form

$$F_b = \frac{4\pi^2 EI}{L^2} \quad (3.3)$$

Unlike the dynamic response discussion, where all material properties cancelled out of the relations, to be able to compare these relations with a beam, a material has to be selected with similar properties. After searching for a candidate metal, none was found with proportional properties, so a fictitious material will be used with the same properties as the ionic polymer-metal composite. Using the same dimensions as the polymers tested, calculations were made to predict what the theoretical frequency increase would be, assuming that the polymer properties are constant, and that it can be modeled as a uniform beam. The predicted results for the starting natural frequency under various loads will be given in Table 3.3 after the plot is shown. In the table, the percent increase column is based on the initial frequency when no load is applied to the beam. These percentages indicate that the frequency shift starts out high, but then decreases slightly as the load continues to increase.

With this in mind, the frequency shift caused by tensioning the polymer can be addressed. Figure 3.13 shows the results. Looking at the starting frequencies, it appears that there is a large initial jump, followed by smaller jumps as the tension increases. There are two cases that happen to start at the same frequency, one of which was disregarded in making the previous statement. Table 3.3 compares these values with those calculated for the theoretical beam with properties and dimensions identical to an ionic polymer. There is significant discrepancy in the frequency and percent increase values listed. The experimental frequencies are much higher than the theoretical frequencies, while the percent increase is much greater for the theoretical case than for the experimental results. Though some qualitative results are similar, the quantities involved are in disagreement. This may be another sign that modeling ionic polymers as uniform beams does not give satisfactory results.

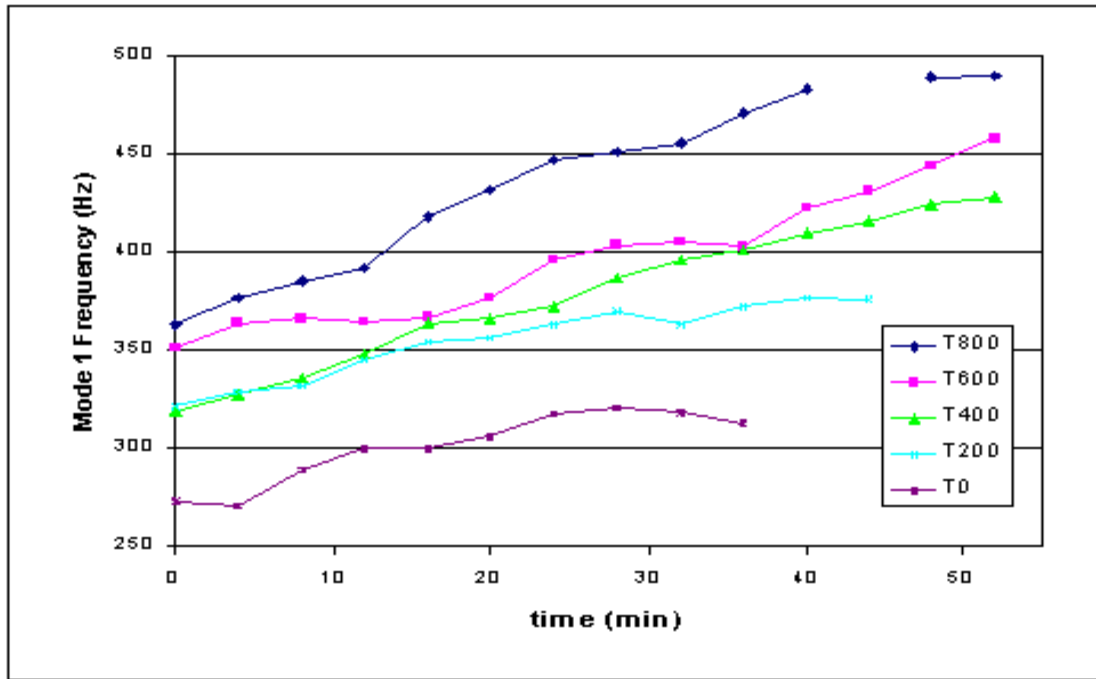


Figure 3.13: Tensioned ionic polymer frequency shift as a function of time and humidity.

Table 3.3: Natural Frequency Comparison of a Clamped-Clamped Uniform Beam with Polymer Properties to an Ionic Polymer.

Tensile Load		Theoretical		Experimental	
(mV)	(mN)	Frequency (Hz)	Increase (%)	Frequency (Hz)	Increase (%)
0	0	81.3	-	273	-
200	24.6	129	58.7	321	17.6
400	49.2	164	101	319	16.8
600	73.8	193	137	351	28.6
800	98.4	217	167	363	33.0

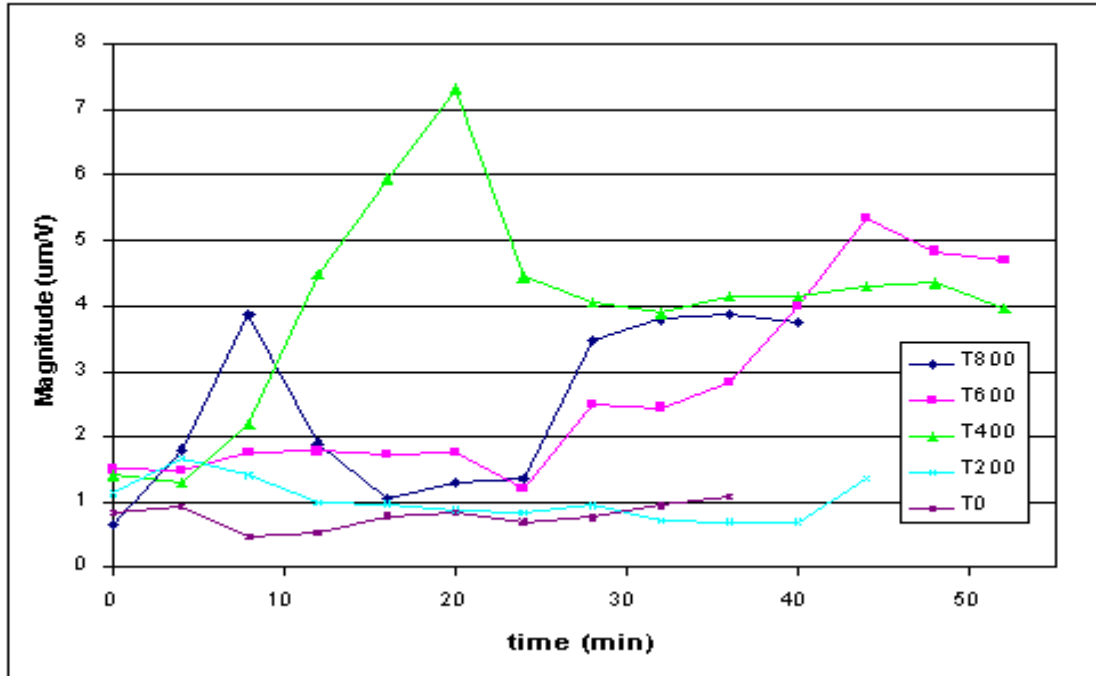


Figure 3.14: Tensioned magnitude results of clamped-clamped ionic polymer.

Similar to the humidity results, the slopes for each tension are approximately linear. A type of ripple effect does appear in most of the frequency shift curves, in that the curve appears to be approaching a final value, only to jump up again and approach another constant. This effect can be seen to repeat in each of the curves. It also appears that there is not much change in the slope of the frequency shift as the tension increases. However, upon further inspection, the linear fit slope doubles from 0mV tension to 800mV tension. The same does not hold true in between, as there is not a consistent increase.

The magnitude plots put more faith in the clamped-clamped results shown in the humidity effects section. Again, there is no discernable trend, other than non-decreasing. Some of the results shown in the last section did have a final point below the starting point, but when tensioned, none are below. If anything other than nearly constant, the final value is higher than the initial value. This is a very interesting and counter-intuitive result, which may prove to be helpful in micro-manipulation applications. Strangely, the data does not even show any correlation between tension levels and magnitude. These results can be found in Figure 3.14.

Transfer functions for a polymer suffering from dehydration and no applied tension were shown in the dynamic response chapter, but none for a tensioned polymer have been

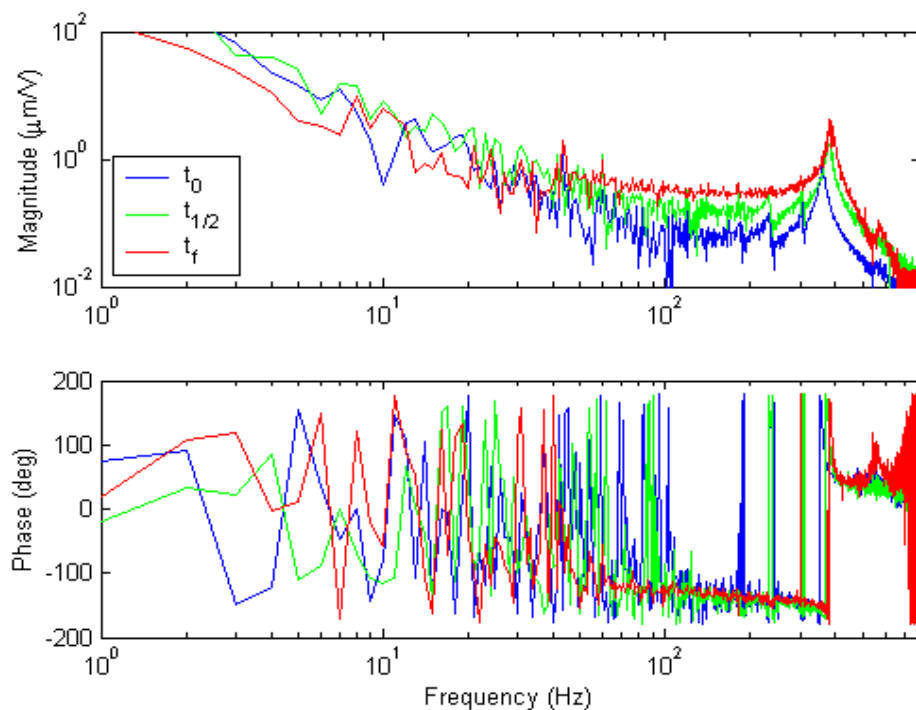


Figure 3.15: Transfer functions of clamped-clamped polymer with 800mV tension.

shown yet. Figure 3.15 displays three transfer functions taken with 800mV tension. Unlike those of Chapter 2, these span the entire test period of 52 minutes. The t_0 , $t_{1/2}$, and t_f show results taken at the start of testing, half way through the duration, and the final test, respectively. The frequency is seen to increase in time, as does the magnitude, which follows from the results presented earlier in this section. Another interesting note that can be made is how the other modes present in the initial transfer function do not appear in the final transfer function. This says that as the polymer dehydrates, the less prominent modes are greatly reduced. Tension also has the effect of removing non-dominant modes, as evidenced by comparing the clamped-clamped frequency response shown in Figure 2.11b with the plot here.

It has been mentioned before that low frequency response characteristics are important for certain shape control applications, like those for advanced optical systems in space. Since the low frequency motion present in such a system would cause tension in the membrane transducer, it is of interest to look more closely at low frequency of a tensioned polymer to see what is happening near DC magnitudes. To get good coherence in this

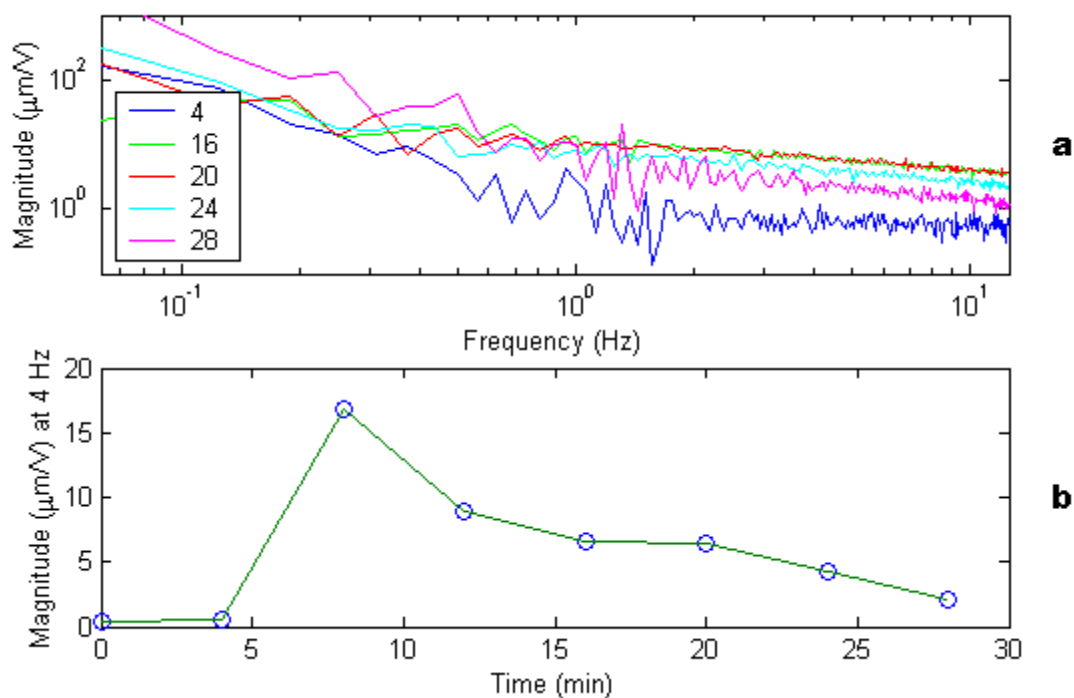


Figure 3.16: Low frequency magnitude plots for 600mV tension (a) pointing out magnitude values at 4Hz (b).

low frequency range, the baseband was reduced to 12.5Hz prior to collecting data. A test was then run capturing the transfer function in the usual manner, allowing the polymer to dehydrate. The tension used in this test was 600mV (73.8mN). Some of the data had good coherence down to sub-Hertz frequencies, but not enough to make a sound judgement on the effects. In looking back at the plots, it was discovered that five different transfer functions had good coherence as low as 4Hz. Those results are shown in Figure 3.16a with the minute of data capture given in the legend. Figure 3.16b highlights the magnitude values at 4Hz. While all the points fall in the given range, the only data that can be trusted are the points corresponding to the times given in (a). The data shows that after an initial increase, the low frequency magnitude then decays slightly.

Completing the presentation of results for the effects that tension has on a clamped-clamped ionic polymer, a discussion follows, with an emphasis on how the open-loop bandwidth is affected.

3.3.3 Discussion

Like the previous section, a discussion of bandwidth will also end this section. The same idea can be repeated here about the non-decreasing trend in magnitude as the frequency increases, but this time the evidence is supported even more. Some of the transfer functions, while dehydrating, actually shifted up when tension was applied. This was seen in Figure 3.15, and would result in increasing the open-loop bandwidth. This upward shifting trend is very favorable for increasing the bandwidth because, as discussed with the dynamic response, dehydration of the material has a stiffening effect. Now with an applied load, the natural frequencies are being increased by another source that can be related to increased stiffness in the polymer.

The consequence of increasing stiffness on the magnitude plot is decreasing magnitude. This can be illustrated by considering a simple transfer function, like that for a spring-mass system:

$$G(s) = \frac{1}{s^2 + \left(\frac{k}{m}\right)^2} = \frac{1}{s^2 + a} \quad (3.4)$$

The mass and stiffness are the only parameters that affect this system. By assuming that the mass is constant, increasing the stiffness will give a larger value of a . Calculating the DC gain of the system as the stiffness increases will give insight into how the magnitude is affected. The DC gain can be calculated as

$$\text{DC Gain} = \lim_{s \rightarrow 0} G(s) = \lim_{s \rightarrow 0} \frac{1}{s^2 + a} = \frac{1}{a} \quad (3.5)$$

Upon inspection, it is seen that as a increases, the result of Equation 3.5 gets smaller. Hence, it can be said that the magnitude will decrease. This means that while the natural frequencies are increasing, the downward shifting magnitude from the increased stiffness and the upward shifting magnitude from the tensioned polymer are counteracting each other. The result, if the effects are equal, will be that the magnitude will remain as it is. When the downward effect is larger, the bandwidth will be decreased, and conversely, the bandwidth will increase when the upward shift is greater.

Although not related to bandwidth, nothing has been stated about the damping for tension effects. Damping was commented on earlier when it was observed that there seemed to be more than expected for an air environment. This was because of the width of the resonant peak. As evidenced in Figure 3.15, tensioning the polymer results in a much narrower and sharper peak, indicating that there is less damping. Accordingly, this suggests that applying tension to a clamped-clamped ionic polymer reduces the damping.

This ends the discussion of tension effects on ionic polymer actuators. A review of both humidity and tension effects is given next in the summary section.

3.4 Summary

This chapter has presented results for two effects on ionic polymers, those due to dehydration and applied tension. The analysis was based on frequency response functions captured experimentally. Both the cantilever and clamped-clamped configurations were tested to assess humidity effects, while only the clamped-clamped condition was used to examine the tension effects. The outcome of the humidity investigation was that the natural frequencies increase in a nearly linear fashion for each configuration, with a steeper slope for lower humidity levels. The peak magnitudes decrease in an oscillatory manner for the cantilever, but no trend was evident for the clamped-clamped polymer. The tension effects showed that the natural frequencies increased with applied force, whereas the magnitudes progressed non-decreasingly. All the effects were studied as functions of time, as the polymer dehydrated.

As was discussed in the dynamic response chapter, some qualitative comparisons can be made to the theory of a uniform beam, but the quantitative aspects had much disagreement. The general statement that can be concluded for a clamped-clamped ionic polymer is that the open-loop bandwidth will increase as the material dehydrates and as more external tension is applied. The cantilever configuration has characteristics opposite to this, since the magnitude decreases as the frequency increases. This effect is not encouraging in terms of improving the open-loop bandwidth. The next chapter will discuss control techniques used for ionic polymer actuators and extend their bandwidth characterization to the closed-loop system.

Chapter 4

Control Techniques

With the open-loop bandwidth effects being discussed, this chapter will use different types of feedback to close the loop and improve the response characteristics of the ionic polymer actuators. In addition to improving the response characteristics, the closed-loop bandwidth will also be discussed. The chapter is organized into four sections, three of which discuss different control techniques, and one giving a summary at the end. The first method presented is based on previous work that was used as a starting place for the results to follow in the succeeding sections. It deals with an optimal state-space control method called the linear quadratic regulator. Following the previous results, new research will be presented from proportional-integral control and adaptive control. In each of these two sections, model development and simulations are discussed before experimental results are presented. Then, the chapter will be concluded with a summary of the results.

4.1 State-Space Control

This section will present the control design approach taken to apply a state-space controller to a short cantilevered ionic polymer actuator. Since it is a presentation of previous results, the descriptions may be somewhat brief, leaving more to be explained in the new research sections. The work here is the result of that done by Mallavarapu (2001). This section will first go into the method used and the basics of this state-space control approach, and then the results will be shown.

4.1.1 Method and Design Basics

The basis for the modeling technique used by Mallavarapu was initially developed by Kanno et al. (1994), but modified slightly to incorporate resonant modes. The model proposed by Kanno et al. was made for a short polymer that did not exhibit any resonance phenomena, as is seen for longer actuators. Mallavarapu's work extended the use of this empirical model to an ionic polymer of arbitrary length. A linear combination of dynamic response terms was used to approximate the step response, and in transfer function form is given as

$$G(s) = \frac{Y(s)}{U(s)} = \frac{a}{s + \alpha} + \frac{b}{s + \beta} + \dots + \frac{K_{r1}\omega_{n1}^2}{s^2 + 2\zeta_1\omega_{n1}s + \omega_{n1}^2} + \frac{K_{r2}\omega_{n2}^2}{s^2 + 2\zeta_2\omega_{n2}s + \omega_{n2}^2} + \dots \quad (4.1)$$

where α, β, \dots are time constants, a, b, \dots are step response coefficients, $\omega_{n,i}$ are natural frequencies, ζ_i are damping ratios, and $K_{r,i}$ are resonant response coefficients. The optimal model parameters were determined using a nonlinear least squares technique, minimizing the error between the experimental data and the simulated model, while matching the steady-state displacement. Then, by conducting a study of the necessary number of model terms, it was discovered that using three real pole terms and one resonance term adequately fit the model to the experimental step response. The ideal model parameters were finally found using a cost function analysis for a series of step responses.

With the model form in order, the controller design was ready to be conceived. So far, the system model has been based off the transfer function form of a series of step responses. But as the section title dictates, state-space control is used on the polymer. In order to take advantage of state-space control techniques, the transfer function of the system had to be rewritten in a canonical state representation. As with the transfer function model, the states of the state-space model have no physical interpretation because the model was developed from empirical data. However, representing the dynamics this way relates the time constants in the model to the states. The general form of a linear time-invariant state-space system has the form

$$\begin{aligned} \dot{x}(t) &= Ax(t) + Bu(t) \\ y(t) &= Cx(t) + Du(t) \end{aligned} \quad (4.2)$$

where $x(t)$ is the state vector, $u(t)$ is the input vector, $y(t)$ is the output vector, A is the state matrix, B is the input matrix, C is the output matrix, and D is the direct transmission matrix. In this case, the tip displacement of the polymer is the output and the applied voltage is the input. It should also be noted that in transforming the transfer function model to state-space form, the matrices are functions of the model parameters.

Taking the new form of the model, the design of the controller could now be carried out. The type of control chosen was linear quadratic regulator (LQR), which is a type of optimal full-state feedback control. It involves calculating the optimal gains by minimizing the cost function

$$V = \int_0^{\infty} [x(t)^T Q x(t) + u(t)^T R u(t)] dt \quad (4.3)$$

where Q is the state weighting matrix and R is the control weighting matrix. The two weighting matrices are defined as

$$Q = qC^T C \quad R = rI \quad (4.4)$$

where q and r are scalar constants chosen to influence the relative weighting of the states and inputs, and I is the identity matrix. This equation can be simplified further to depend on only one design variable because all that is important in the cost function is the relative size of q and r . Pulling an r out of the integral leaves this q/r parameter on the states, where it can be varied to affect the states and controls differently. Studies are usually conducted to determine the best value of this single design parameter.

It was noted before that the ionic polymer system under consideration is an output feedback system, meaning that the only signal available for feedback is the tip displacement. For a system of this type, an observer is usually designed to provide full-state feedback. The observer estimates the states of the system and can be used to calculate the gains for full-state feedback. The observer is designed using the state error, the difference between the

actual states and observer states, in the differential equation and the gain matrix K , used to determine the speed of convergence. Once the observer is designed, full-state feedback can be applied to it, giving the gains G to be used with the system. The control also contained a feedforward gain matrix G_r to eliminate steady-state error. In calculating the values in this matrix, a new matrix E must be calculated that is conveniently equivalent to the state matrix A for a step input. This allows the feedforward gains to be computed using Equation 4.5.

$$G_r = [C(A - BG)^{-1}B]^{-1}C(A - BG)^{-1}E \quad (4.5)$$

This new system made up of the original system and the observer can be written in closed-loop form as

$$\begin{aligned} \begin{Bmatrix} \dot{x}(t) \\ \dot{\hat{x}}(t) \end{Bmatrix} &= \begin{bmatrix} A & -BG \\ KC & A - KC - BG \end{bmatrix} \begin{Bmatrix} x(t) \\ \hat{x}(t) \end{Bmatrix} + \begin{bmatrix} BG - BG_r \\ BG - BG_r \end{bmatrix} \{r(t)\} \\ y(t) &= [C \quad 0] \begin{Bmatrix} x(t) \\ \hat{x}(t) \end{Bmatrix} + 0\{r(t)\} \end{aligned} \quad (4.6)$$

where $\hat{x}(t)$ is the observer state vector and $r(t)$ is the reference input vector. A more detailed account of this design process is presented in Friedland (1986). This closed-loop system model was then used for simulations with varying q/r values to find the desired response characteristics and check for stability. After this was accomplished, experiments could be performed.

4.1.2 Previous Results

Experiments showed that some of the response characteristics did improve, as was predicted in the simulations. The greatest improvement came in the overshoot, where the open-loop's 500% was reduced to only 30%. There still remains a slow relaxation to steady-state (greater than 20 seconds) and steady-state error, despite the efforts made in the controller design to

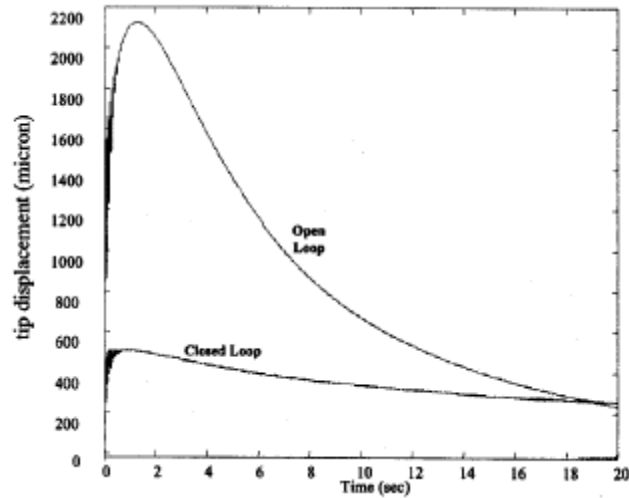


Figure 4.1: LQR control results using a linear observer-estimator.

reduce or eliminate these factors. Figure 4.1 shows the results for one control experiment run on the cantilevered ionic polymer.

By examining these experimental results, it can be seen that more improvement needs to be made in the controlled response for the ionic polymer actuator. While the overshoot was greatly reduced, the settling time remains a major problem, as does the steady-state error. Typically, the type of control used when the tracking of a system needs to be improved is integral control. Consequently, this happens to be the subject of the next section.

4.2 Proportional-Integral Control

In order to improve the tracking capability of ionic polymer actuators, proportional-integral control was the next technique used. Integral control is often times used to improve the low frequency response of a system, such as steady-state error for a step input. Normally, the drawback of integral control is increased settling time. This section will discuss the modeling and simulation results for a cantilevered ionic polymer actuator and the experimental results, showing how the controlled response has been improved even more.

4.2.1 Modeling and Simulations

For the sake of completeness, a brief introduction to integral control will be provided. Theoretical integral control, in the time domain, has the form

$$u(t) = \frac{K}{T_I} \int_{t_0}^t e(\eta) d\eta \quad (4.7)$$

where $e(t)$ is the error between the reference input and the system output, T_I is the integral time, and η is a dummy variable of integration. As in the previous section, K is the gain. The integral time is a measure of the speed of response because its inverse determines the breakpoint of the compensator. The advantage of using integral control is the infinite gain at zero frequency, but the disadvantage comes in the phase plot of the frequency response. The phase is shifted down 90 degrees, which can cause stability problems with the closed-loop system. Another aspect of integral control, due to the control signal's dependence on past values of the error, is its ability to produce a control signal even when the error goes to zero. This is evident from the limits of integration in Equation 4.7, where t_0 is the initial time and t is the present time. Additionally, the theoretical form of proportional control, as the name implies, is

$$u(t) = Ke(t) \quad (4.8)$$

with the gain acting like a dial that can be turned up or down, depending on the desired response. The combination of these two types of control is simply their sum.

With that being said, the modeling will now be discussed. The model used for simulation purposes of integral control is similar to that used by Mallavarapu (2001). Since it has been shown that the length of the cantilevered ionic polymer actuator affects its frequency response, the model developed has identical dimensions to the one of the previous work (7 x 5 x 0.2)mm. This way the adverse effects of resonance phenomena will be removed. A model of this form was best approximated using the state-space equations

$$\dot{x}(t) = \begin{bmatrix} -\alpha & 0 & 0 \\ 0 & -\beta & 0 \\ 0 & 0 & -\gamma \end{bmatrix} x(t) + \begin{bmatrix} a \\ b \\ c \end{bmatrix} u(t) \quad (4.9)$$

$$y(t) = [1 \ 1 \ 1]x(t) + [0]u(t)$$

where the model parameters are the same as those discussed in the previous section. Through a set of five experiments, Mallavarapu used an optimization routine and cost function analysis to determine values for the A and B matrices. For the model developed in this study, each parameter was averaged over the five data sets, and the averaged parameter values were used in the model. Table 4.1 shows these averaged values.

Once the parameter values were determined, the system model could be implemented with full-state feedback of the fictitious states. However, prior to attempting full-state feedback, which assumes that all states can be measured, it is necessary that the controllability of the system be checked. Whether or not the system is controllable will determine if the closed-loop poles can be arbitrarily placed anywhere in the s -plane. A system is said to be controllable if and only if the matrix P has full rank (Friedland, 1986). For this ionic polymer model, P can be calculated as

$$P = [B \ AB \ A^2B \ A^3B] \quad (4.10)$$

Table 4.1: Averaged Parameter Values used for State-Space Model with Integral Control.

Parameter	Averaged Value
α	0.3036
β	61.276
γ	112.91
a	-0.4592
b	560.97
c	-701.87

and the rank is defined as the number of linearly independent rows or columns, which in this case is 4, meaning that P has full rank and is controllable.

At this point, there is still one more addition to the system equations that must be made. This addition is required to incorporate integral control and reference tracking to the design (Friedland, 1986). The formulation for this has the form

$$\begin{Bmatrix} \dot{x}_I(t) \\ \dot{x}(t) \end{Bmatrix} = \begin{bmatrix} 0 & C \\ 0 & A \end{bmatrix} \begin{Bmatrix} x_I(t) \\ x(t) \end{Bmatrix} + \begin{bmatrix} 0 \\ B \end{bmatrix} u(t) + \begin{bmatrix} -1 \\ 0 \end{bmatrix} r(t) \quad (4.11)$$

where $x_I(t)$ is the integral term, and $r(t)$ is the reference input. With this set of augmented system equations, full-state feedback can now be applied. This is done by substituting Equation 4.12 into the system equations:

$$u(t) = -[G_I \quad G_O] \begin{Bmatrix} x_I(t) \\ x(t) \end{Bmatrix} \quad (4.12)$$

where G_I is the integral gain and G_O is the gain vector for the original states. Combining terms, this substitution gives the closed-loop system equations as

$$\begin{Bmatrix} \dot{x}_I(t) \\ \dot{x}(t) \end{Bmatrix} = \begin{bmatrix} 0 & C \\ -BG_I & A - BG_O \end{bmatrix} \begin{Bmatrix} x_I(t) \\ x(t) \end{Bmatrix} + \begin{bmatrix} -1 \\ 0 \end{bmatrix} r(t) \quad (4.13)$$

Also, since nothing has been said yet of the output equations for the ionic polymer actuator. These are given in Equation 4.14 as

$$y(t) = \begin{bmatrix} 0 & 1 & 1 & 1 \\ G_I & G_{O1} & G_{O2} & G_{O3} \end{bmatrix} \begin{Bmatrix} x_I(t) \\ x(t) \end{Bmatrix} \quad (4.14)$$

Together, Equations 4.13 and 4.14 make up the state-space model for this polymer. With this model established, pole placement can now be used to determine a set of gains,

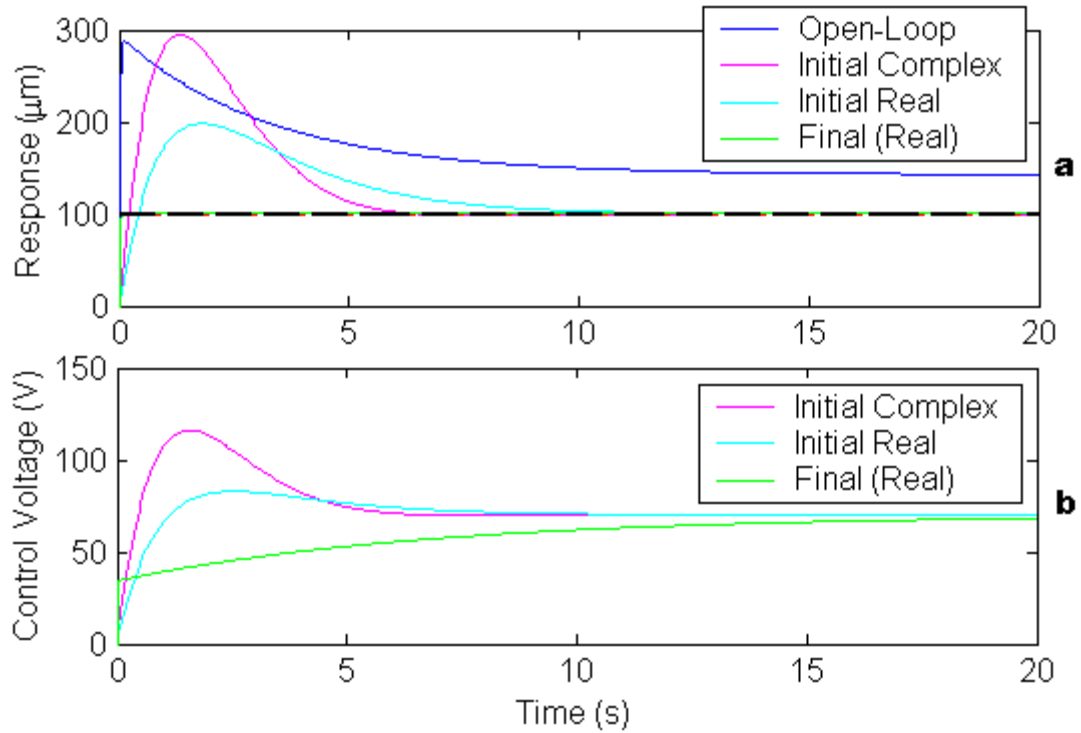


Figure 4.2: Full-state feedback integral control simulation results (a) and associated control voltage (b).

and thus the system response. To assist in this usually arduous, iterative process, the Matlab function `PLACE.M` was used. The pole placement procedure begins with an initial guess, which was taken to be the open-loop poles, plus an additional pole placed between the two closest to the origin. The additional pole was needed to account for the integral term. By moving the poles around, it was discovered that the steady-state error was eliminated from the start. This left the overshoot and settling time to be improved. Using all real poles, the settling time could be greatly reduced, but at the cost of greatly increasing the overshoot. On the other hand, using a pair of complex conjugate poles reduced the settling, while at least keeping the overshoot what it was to begin with.

After several different trial locations were chosen, what came to be discovered was that real poles offer the best response characteristics. Figure 4.2 displays the results for the initial guesses with both complex and real poles, as well as the final locations on the real axis. As expected, using integral control eliminated the steady-state error, but the initial guess locations left a poor transient response. In looking at the two initial guess responses, it appears that using a pair of complex conjugate poles with two real poles gives a better

Table 4.2: Results from Pole Placement Iterations using Integral Control.

Design Parameter	Open-Loop	Closed-Loop (Initial Complex)	Closed-Loop (Initial Real)	Closed-Loop (Final-Real)
Pole Locations	-	$-(120,80,8 \pm 0.5i)$	$-(120,60,1,0.5)$	$-(610,200,100,0.15)$
Gains	-	2.9,14,0.08,0.02	1.2,5.0,0.0004,0.02	603,15,8.2,5.5
Steady-State Error (μm)	43	0	0	0
Overshoot (%)	190	195	100	<1
Settling Time (s)	∞	5.8	11	0.06
Rise Time (ms)	23	170	320	40

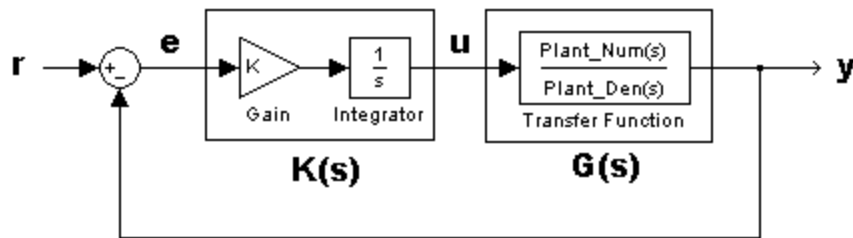


Figure 4.3: Block diagram model of integral control.

settling time, but more overshoot, while using all real poles gives less overshoot and a longer settling time. This indicates that a trade-off may exist between overshoot and settling time. However, by examining the poles and zeros of the open-loop system, a low frequency zero (0.02Hz) was found, which is uncharacteristic for comparable smart materials. By moving the poles around, the only way the overshoot could be eliminated was by cancelling this low frequency zero with a low frequency pole. Then the other poles were placed out at higher frequencies to enable a fast response, which came to be the final (real) pole locations. It should also be noted in the figure that the control voltage is unexpectedly high, which may lead to problems during implementation. Table 4.2 has been included to compare the response characteristics shown in Figure 4.2.

With the tracking improved using a model-based full-state feedback design, it became interesting to consider another, easier to apply, approach to using integral control. In this approach, the state-space equations were transformed back to transfer function form, and the feedback applied was just an integrator and a gain. A schematic of this method is shown in Figure 4.3. This is the more classical type of integral control with a proportional gain.

In the figure, $K(s)$ is the transfer function of the controller and $G(s)$ is the plant transfer function. The signals r , e , u , and y are the reference input, error, control, and output, respectively. Typically, the lower-case notation is reserved for functions of time with the time-dependence left out, but this mixing of domains is common in control system block diagrams.

To perform analysis of this control system, the closed-loop transfer function needs to be written. This can be done directly from the signals and blocks in Figure 4.3. The first thing that needs to be done is combining the open-loop transfer function $G(s)$ with the controller transfer function $K(s)$. In the Laplace domain, this is simply $K(s)G(s)$. This has put the system in the simplest form of a unity feedback (negative) system, where $K(s)G(s)$ is referred to as the loop transfer function.

Looking now at the signals in the system, note that u has been removed. Using Laplace representation of the signals for proper equation development, the following is seen:

$$E(s) = R(s) - Y(s) \quad (4.15)$$

Now with the output $Y(s)$ being a linear combination of the error signal and the loop transfer function, the error can be described as

$$E(s) = \frac{Y(s)}{K(s)G(s)} \quad (4.16)$$

Substituting this result back into Equation 4.15 and multiplying through by $K(s)G(s)$ gives

$$\{K(s)G(s)\}R(s) - \{K(s)G(s)\}Y(s) = Y(s) \quad (4.17)$$

Now by rearranging and grouping terms, Equation 4.17 becomes

$$\{K(s)G(s)\}R(s) = (1 + \{K(s)G(s)\})Y(s) \quad (4.18)$$

Recalling that a transfer function is the relationship between two signals, the input-output relationship of the closed-loop system is

$$\frac{Y(s)}{R(s)} = \frac{K(s)G(s)}{1 + K(s)G(s)} \quad (4.19)$$

This closed-loop transfer function holds for any general type of linear control system where the controller can be represented as $K(s)$. One of the particulars for integral control is the pole at zero frequency. While helping the steady-state error of the system by increasing the low frequency gain, this pole also has the detriment of shifting the phase down 90 degrees and a poor transient response.

Testing the performance of this control, simulations were run. This new model gave results very comparable to those obtained using the full-state feedback approach. Figure 4.4 shows the results. In this figure, the cantilevered polymer has an overshoot of 9%, a settling time of 200 milli-seconds, a rise time of 60 milli-seconds, and zero steady-state error. Obviously, this shows a much better capability for ionic polymers to be able to track a reference input. A gain of 6.5 is used in the figure.

There is also a great advantage in implementation when applying integral control this way. That is, no system model needs to be developed or analyzed, and the controller does not really need to be “designed.” A block diagram of the feedback system can be created in Simulink and taken directly to the laboratory for experimentation. All that will have to be changed is the polymer block, which will be replaced with the dSPACE input and output. This leaves one gain value to be adjusted, just like a knob, to attain the desired response. The test setup is explained next, followed by the results of actual implementation and the effects on closed-loop bandwidth.

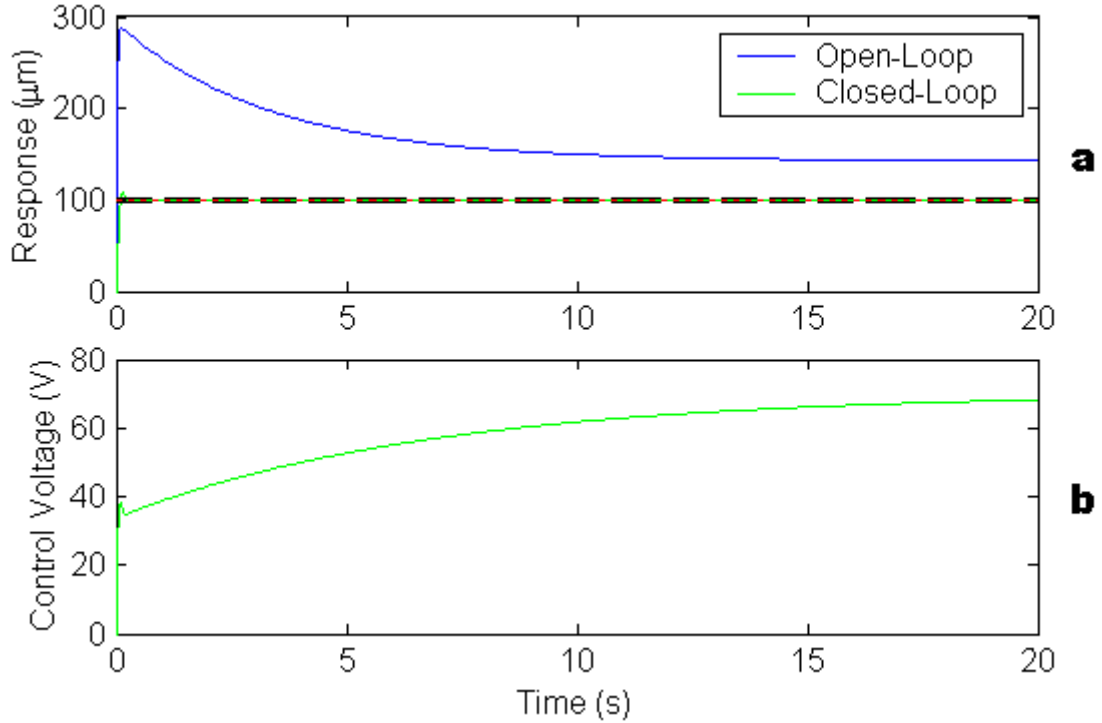


Figure 4.4: Simulation results for integral control in transfer function form (a) and control voltage (b).

4.2.2 Test Setup

The ease of implementation in using a transfer function for the integral control significantly reduces the amount of computer time required by eliminating the calculations necessary for feeding back all the states. This strictly output feedback system simply integrates the error signal and produces the control signal that is the input to the polymer. A schematic of the test setup is given in Figure 4.5. This figure is nearly identical to Figure 2.1, but since control is being applied, the polymer output and control input signals are labeled.

As before, the laser vibrometer measures the small tip displacement of the cantilevered ionic polymer, which is the output signal y of the closed-loop system. This is fed into the dSPACE where the error signal is formed. Then the error signal is integrated and multiplied by the gain to produce the control signal u , which becomes the new input to the polymer. This procedure is repeated realtime at the sampling rate of the system, and the polymer's motion is controlled.

Knowing that the integral control scheme can easily be applied, both the cantilever and clamped-clamped configurations were tested. As described previously, clamping both

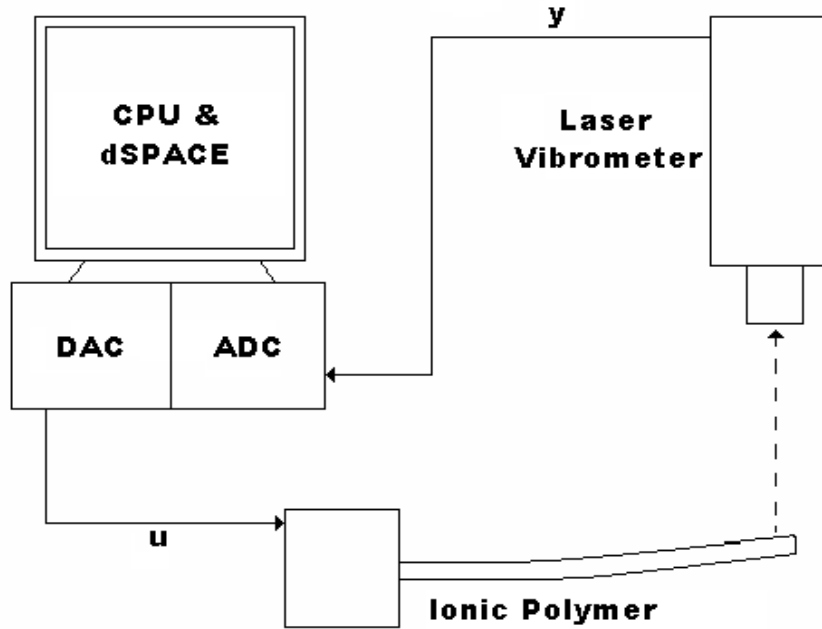


Figure 4.5: Schematic of the control experiment setup.

ends greatly increases the natural frequencies, while significantly reducing the displacement. Therefore, reference inputs for the clamped-clamped control experiments were values two orders of magnitude below those for cantilever tests. Another interesting outcome of the control experiments was that the effectiveness of the control depended on the sampling rate. For the cantilevered polymer, 2kHz was used with no problems, but when the other end was clamped, the control did not work so well. However, by increasing the sampling rate to 10kHz, the integral control proved effective on the clamped-clamped actuator. This can be related to digital control of linear systems, where the sampling rate can be approximated as a linear function of natural frequency (Franklin et al., 1998). From this justification, since the clamped-clamped polymer's natural frequency is an order of magnitude greater than the cantilever's, increasing the sampling frequency by order of magnitude makes sense.

Pertaining to the block diagram of the system, an additional block had to be placed right before the input to the polymer. The block used was a saturation block. The reason this "safety" block had to be used was to prevent possible damage to the polymer. Ionic polymers have a certain voltage level that they respond well to, but over which electrolysis will occur. When this happens, the polymer makes a sizzling sound and curls to one side.

Depending on the extent that the material has suffered from high voltage, it is possible that it will become unresponsive. To prevent this from happening during the control experiments, the saturation level was set to ± 3 Volts. There is a possibility that this will limit the performance of the control system, but the precaution is necessary for the life of the actuator. It should also be noted that this was not a factor in the open-loop tests because the step size and laser vibrometer range were adjusted with this potential problem in mind.

In the last chapter, the effects on open-loop bandwidth were discussed as the polymer dehydrated and was tensioned. Regarding the humidity and dehydration of the polymers for these control experiments, testing was only performed immediately following the rehydration of the actuator. This was done because, with the knowledge gained in Chapter 3, the effects could be inferred. As far as tension is concerned, the same is true. The control experiments were performed with no applied tensile load. That being said, the results follow for both of the configurations, as well as some multi-layer actuator results. The multi-layer actuators were only tested in the cantilever configuration, however.

4.2.3 Single-Layer Step Response

The step results for both a cantilevered and a clamped-clamped actuator will be presented here. Following the discussion presented in the previous chapter, the cantilever results will be shown first and the clamped-clamped results second. The presentation of results will cover the response characteristics discussed in the dynamic response chapter, with the addition of control effort and gain. The control effort or control voltage is the voltage necessary to correct the present error in the system. It is calculated using the gain and the integrator. The gain, as stated before, is like a knob that can be adjusted up or down depending on how the system is responding and what needs to be improved. Typically, increasing the gain will shorten the rise time, but increase the overshoot and possibly the settling time, while decreasing the gain will give less overshoot at the expense of response time. These trends are what was seen in the experiments.

The first plot of results can be seen in Figure 4.6. Figure 4.6a shows the open-loop step response, which is how the response looked prior to adding control. The controlled response is then shown in Figure 4.6b. Clearly, the use of integral control significantly improves the tracking of the ionic polymer to a reference step input. Some overshoot still remains in the response, but it has been reduced from 470% to only 30%. Steady-state

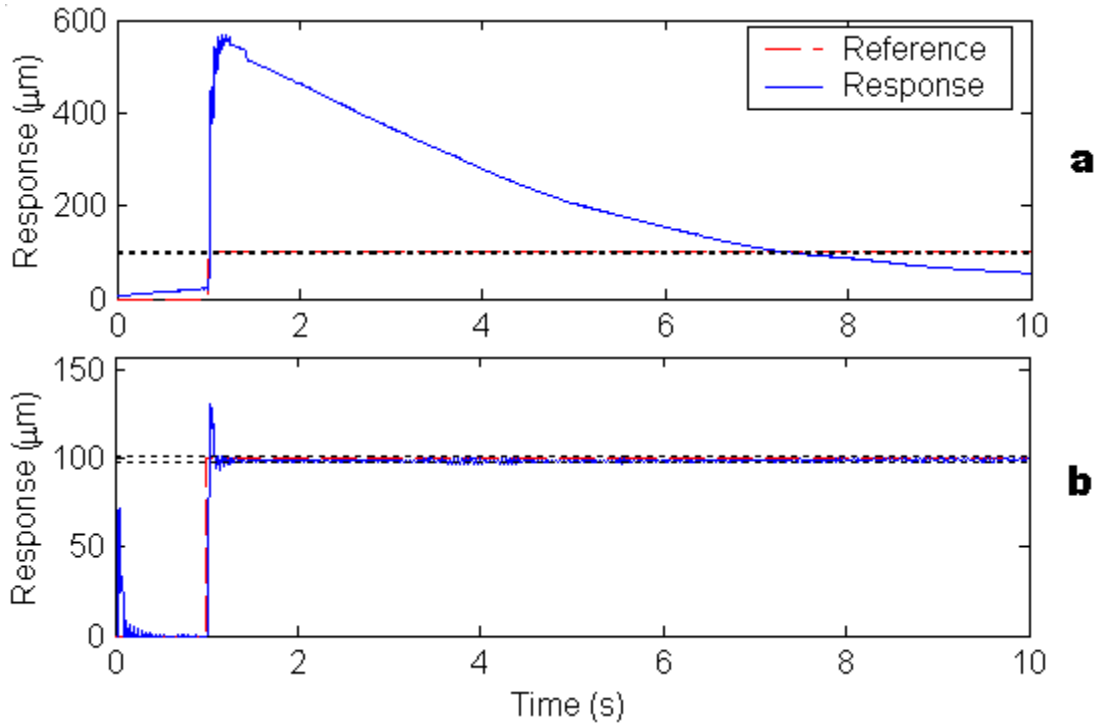


Figure 4.6: Open-loop step response (a) of cantilevered ionic polymer compared to result using integral control with a gain of 16 (b).

error, on the other hand, has been eliminated, as was expected from using integral control. In terms of response time, the rise time suffered a 10 milli-second decrease, but the polymer settled to within $\pm 2\%$ in only 300 milli-seconds. Through trial and error, the best gain was found to be 16, resulting in a control effort of less than 2.4 Volts throughout the testing period.

By recalling what the simulated response of Figure 4.4 looked like, it is found to have a strong resemblance to the experimental results. This indicates that the model developed from a series of step responses is an accurate way to empirically model the cantilevered ionic polymer, at least in the short-term, before any effects from dehydration begin to take over.

Fixing the free end and reducing the step size, integral control was tested on the clamped-clamped ionic polymer actuator. This was done with no prior simulation runs because the control system in transfer function form was so easily applied. The results are presented by Figure 4.7. Like in the cantilevered results, (a) shows the response before control and (b) shows the effects of the integrator and the gain. Again, some overshoot is present but it has been reduced by more than 10%. The rise time is 40 milli-seconds,

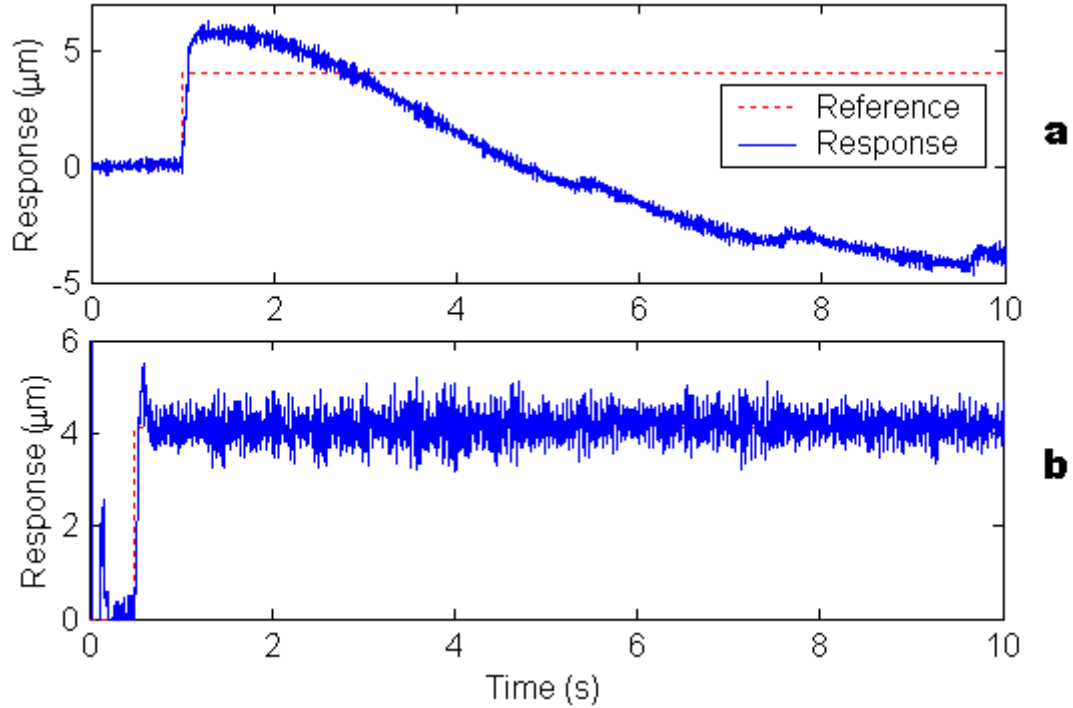


Figure 4.7: Open-loop step response (a) of a clamped-clamped ionic polymer compared to result using integral control with a gain of 20 (b).

while the settling time is around 600ms. Because of the noisy data, the settling time was determined by seeing how long the polymer took to reach ± 0.8 microns. This value was chosen because the response stays in this range for most of the time block. The best gain found for the clamped-clamped polymer was 20, with the control voltage never exceeding 1.0 Volt.

Out of curiosity, the length of time that the polymer could hold a desired position was studied. This was carried out by simply extending the time period over which the input was applied. The results in Figure 4.8 show that a cantilevered actuator is able to hold the input position for 30 seconds. The figure also includes a plot of the control voltage as a function of time instead of the open-loop response. Since the two previous figures contained open-loop responses with the controlled response, it was unnecessary to include another. The control voltage shown is characteristic of what the curve typically looked like in all the control experiments so far. The gain used in this extended time period was 15, and the control effort was kept below 1.8 Volts. The polymer stays within $\pm 2\%$ of the reference input nearly the entire time. However, at the end of 30 seconds, the cantilever begins to move farther from the input. This is likely due to dehydration from the extended time

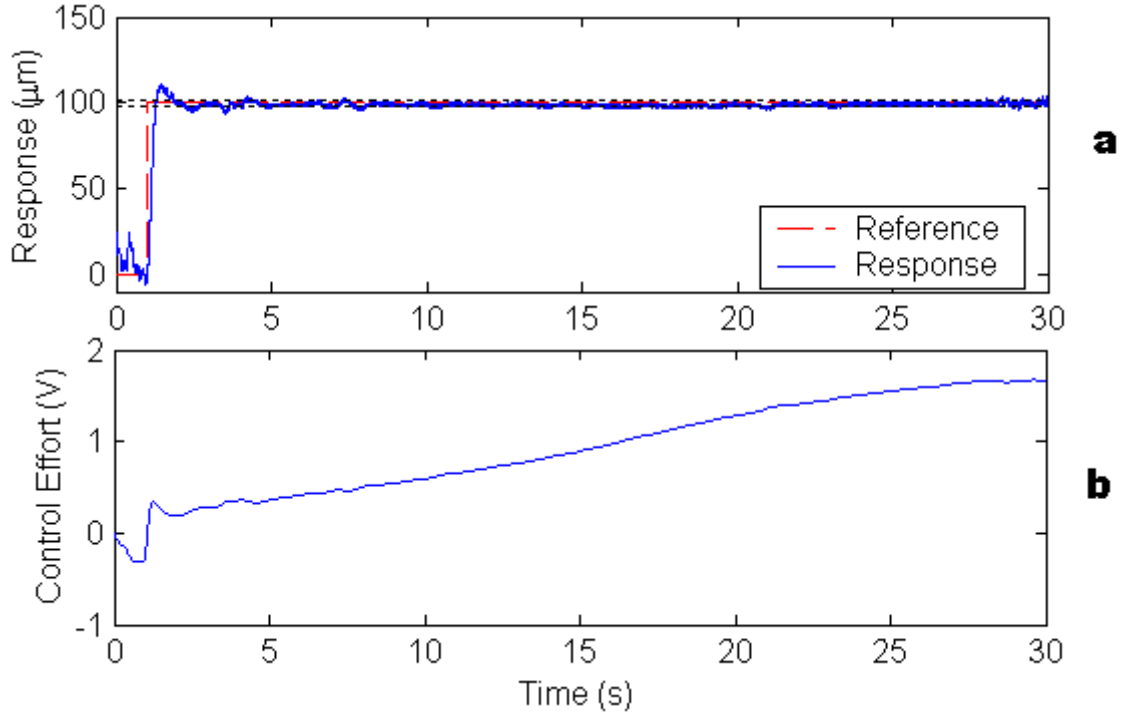


Figure 4.8: Cantilevered polymer displaying its position holding capability (a) and corresponding control voltage (b).

period that the voltage is applied.

To summarize the results of integral control on single-layer ionic polymers, a table was constructed. Table 4.3 displays the values for the response characteristics discussed for the cantilever and clamped-clamped configurations. Both the open-loop characteristics and the closed-loop performance are shown in the table. For the open-loop columns, the control voltage and gain entries are left blank since they do not apply to the uncontrolled system.

A final comment to be made about the single-layer cantilevers is how the control voltage remained relatively low. The saturation block caused no problems in the performance of the system, reaching a maximum value of only 2.3 Volts. Having completed the discussion of these results, the single-layer polymers will be continued in the following subsection, where the sinusoidal response is shown.

4.2.4 Single-Layer Sinusoidal Response

Sinusoidal responses, as discussed in the dynamic response chapter, offer insight into the bandwidth of the actuators. Here, the cantilever and clamped-clamped conditions were examined to see the effects of integral control on single-layer actuators. Unlike the step

Table 4.3: Summary of Integral Control Results for Single-Layer Ionic Polymers under a Step Input.

Response Characteristic	Cantilever		Clamped-Clamped	
	Open-Loop	Closed-Loop	Open-Loop	Closed-Loop
Overshoot (%)	470	30	50	37
Settling Time (s)	>10	0.3	>10	0.6
Rise Time (ms)	70	16	60	40
Steady-State Error (%)	>50	~0	120	±20
Control Voltage (V)	-	<2.4	-	<1.0
Gain	-	16	-	20

responses above, the sinusoidal control results do not present the open-loop response. The results from two different frequencies are shown rather than the open-loop because this would present a more detailed account of the effects as the bandwidth is approached. For consistency, each testing configuration has the same input amplitude and gain, while the frequency is changed.

The first results are those for the cantilever configuration. Figure 4.9 shows these results. As it can be seen, the response in Figure 4.9a is able to track the frequency with only a small amplitude attenuation. The input is a $25\mu\text{m}$ sine wave at 5Hz. With a gain of 30, the control voltage stays under 2.5 Volts. The output amplitude does show a 20% reduction and a 20 degree phase lag. Keeping the gain and input amplitude the same, the frequency was increased to 15Hz giving the results shown in Figure 4.9b. At this frequency, the output amplitude has a 40% attenuation, and the phase lag is increased to 60 degrees. This figure shows some drift also, which could be attributed to the dehydration of the polymer. It was not thought that dehydration would cause a problem over such a short test period though, so some other factors may be behind this effect. Also, the overall control effort does not top 1.0 Volt. This says that although the response suffers slightly at the higher frequency, the required voltage is lower.

Turning now to the clamped-clamped polymer, integral control was applied with a gain of 8 to a $2\mu\text{m}$ sine wave. The two frequencies used in this condition were 2Hz and 6Hz. Figure 4.10a shows that the output is actually amplified by 20% in the controlled system, while the phase lag present is 35 degrees. Additionally, the control voltage never increases beyond 1.0 Volt. Figure 4.10b shows that increasing the frequency by a factor of three also increases the phase lag by a factor of three, while causing a 30% attenuation in the output

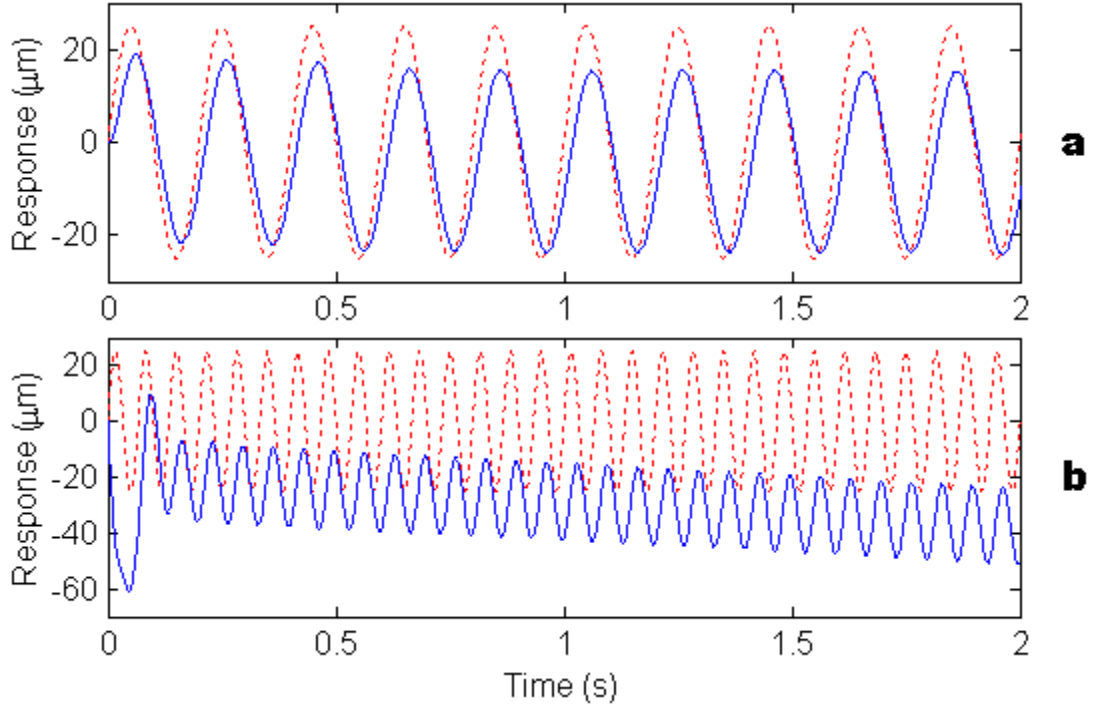


Figure 4.9: Integral control of cantilevered polymer used to track sinusoidal inputs. The $25\mu\text{m}$ input wave is at 5Hz (a) and 15Hz (b).

amplitude. This higher frequency also doubles the control effort, but it does not exceed 2.0 Volts. Only being able to reach 6Hz before the amplitude begins to be significantly reduced is a strange result because, from the configuration change, it was thought that the bandwidth for the clamped-clamped polymer would be higher than for the cantilever. The ratio of frequency increase used is the same for the cantilever and clamped-clamped, but the values for the cantilever are still higher. There is also a poor transient response present at the higher frequency that reaches a level nearly triple the input. Also common to both the responses is how other harmonics are being excited. It is not such a problem at 2Hz, but when the frequency is increased to 6Hz, the other harmonics begin to have larger amplitudes and affect the tracking in a more adverse manner.

A summary of these results is given in Table 4.4. While similar to Table 4.3, sinusoidal responses are not characterized using the same terminology, so different response characteristics are used. Those referred to are the same as those discussed with the figures. Also, there are two columns for each configuration, headed by the frequencies of the input.

Again, the control input did not come to within 0.5 Volts of the saturation limit, which is a good sign. This means that the gain could be increased more, as long as the re-

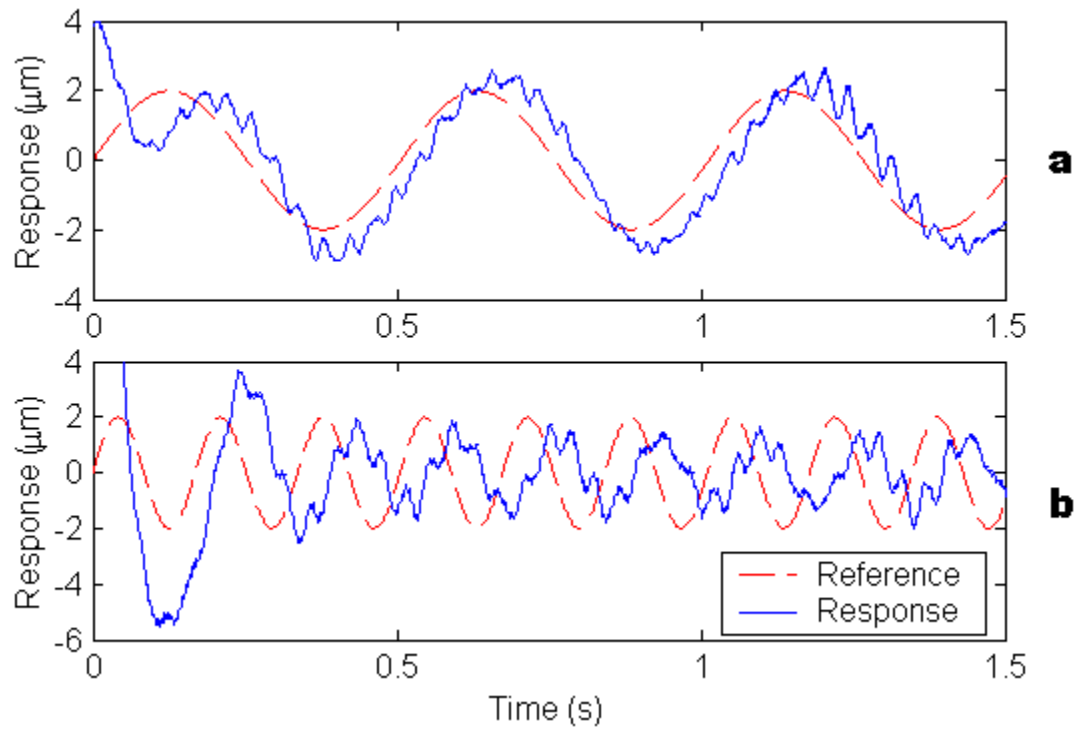


Figure 4.10: Clamped-clamped polymer tracking a $2\mu\text{m}$ sine wave at 2Hz (a) and 6Hz (b).

Table 4.4: Summary of Integral Control Results for Single-Layer Ionic Polymers under a Sinusoidal Input.

Response Characteristic	Cantilever		Clamped-Clamped	
	Low Freq	High Freq	Low Freq	High Freq
Frequency (Hz)	5	15	2	6
Input Amplitude (μm)	25	25	2	2
Output Amplitude (μm)	20	15	2.4	1.4
Phase Lag (degrees)	20	60	35	105
Control Voltage (V)	<2.5	<1.0	<1.0	<2.0
Gain	30	30	8	8

sponse did not suffer too many consequences. This will be done in the multi-layer sinusoidal responses, but first the multi-layer step responses will be discussed.

4.2.5 Multi-Layer Step Response

Two types of multi-layer actuators were experimented with. As discussed in Chapter 2, a packaged stack of two ionic polymers and a stack of four, unpackaged, were used. The reason these were of interest to study is that the packaging would act as a layer of insulation against dehydration, and the stacking would increase the attainable force of the actuator. The first results to be discussed are for the packaged 2-stack actuator, and the unpackaged 4-stack will follow. It should also be noted that the results to be presented here are only for the cantilever configuration.

Similar to the single-layer step results, the open-loop response is included in the figure with the controlled response. Figure 4.11a shows the uncontrolled step response for the packaged 2-stack actuator. The overshoot, though much less than the single-layer, is 90%. The rise time is at 23ms, while the settling time is off the plot. Steady-state error, like for the single-layer, is also present, reaching over 10%. This is not as much of a factor in this response as it was for the single-layer, but it is desired that this be eliminated. This is achieved using integral control, and is shown in Figure 4.11b. The controlled step response looks very similar to that for a single-layer actuator with an overshoot of 26%, settling time of 270 milli-seconds, and zero steady-state error. The two main differences in response characteristics are the increased rise time of 30 milli-seconds and the decreased control voltage of less than 1.0 Volt. The increased rise time can be attributed to the increased inertia of the system, since there are two polymers, a packaging material, and a layer of insulation between the two polymers. This control also used a gain of 30 to achieved the results depicted in the figure.

By removing the packaging material and adding two more ionic polymers in parallel, an actuator composed of four ionic polymer cantilevers can be constructed. The open-loop step response displayed in Figure 4.12a shows that no overshoot is present and that the steady-state is well below the reference input, only reaching 84% of it. Applying integral control results in the response given in Figure 4.12b. Although the peak response is reflected about the reference from -60% without control to 60% with control, the steady-state error is eliminated and the settling time is just below 0.5 seconds. The rise time was also reduced

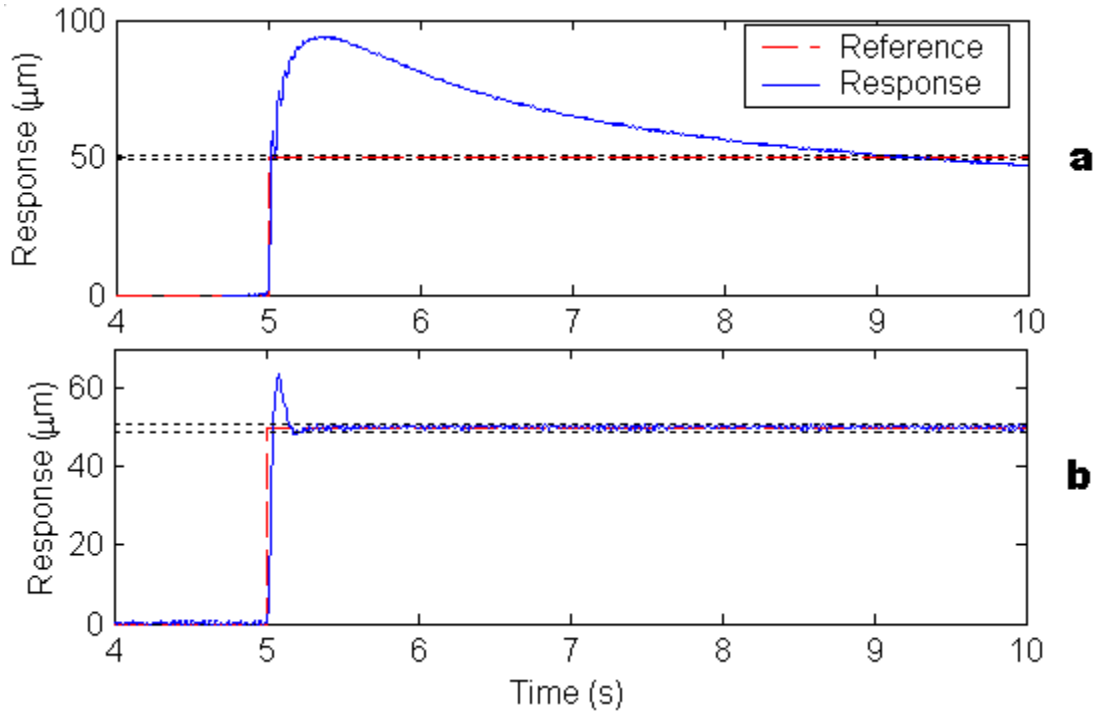


Figure 4.11: Packaged stack of two ionic polymer cantilevers open-loop response (a) compared to result using integral control (b).

by an order of magnitude, down to 40 milli-seconds. Keeping the gain the same as for the packaged 2-stack actuator, the control voltage remained underneath the 1.2 Volt level.

To keep up with summarizing the control results, Table 4.5 has been included. It has results for each of the two actuators described in this subsection, showing both the open-loop and the closed-loop response characteristics. This way, the improvement on the tracking made by the control scheme can be seen in numeric form, as opposed to visually in the figures. Interesting to note is how the rise time was not affected very much by controlling the packaged 2-stack actuator. It was thought that a result more like that seen in the 4-stack actuator would be seen, but instead the rise time increased when the actuator was being controlled.

Also, keeping on with mentioning the maximum control effort, the saturation level was not even reached half way. The 4-stack actuator required 200 milli-Volts more than the packaged 2-stack actuator to achieve the reference tracking, but the maximum voltage needed was less than 1.2V. Finishing the discussion of the multi-layer step responses, their sinusoidal responses are up next.

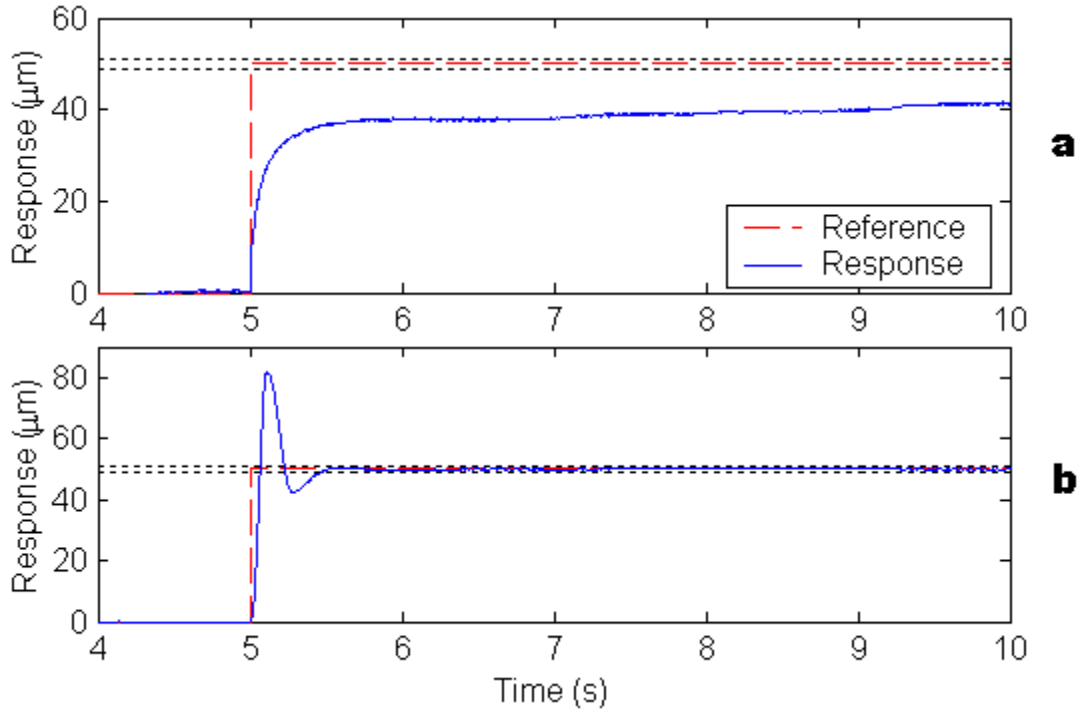


Figure 4.12: Stack of four ionic polymer cantilevers open-loop response (a) and result using integral control (b).

Table 4.5: Summary of Integral Control Results for Multi-Layer Ionic Polymers under a Step Input.

Response Characteristic	Packaged Stack of 2		Stack of 4	
	Open-Loop	Closed-Loop	Open-Loop	Closed-Loop
Overshoot (%)	90	26	none	64
Settling Time (s)	>10	0.27	>10	0.47
Rise Time (ms)	23	30	300	40
Steady-State Error (%)	20	~0	16	~0
Control Voltage (V)	-	<1.0	-	<1.2
Gain	-	30	-	30

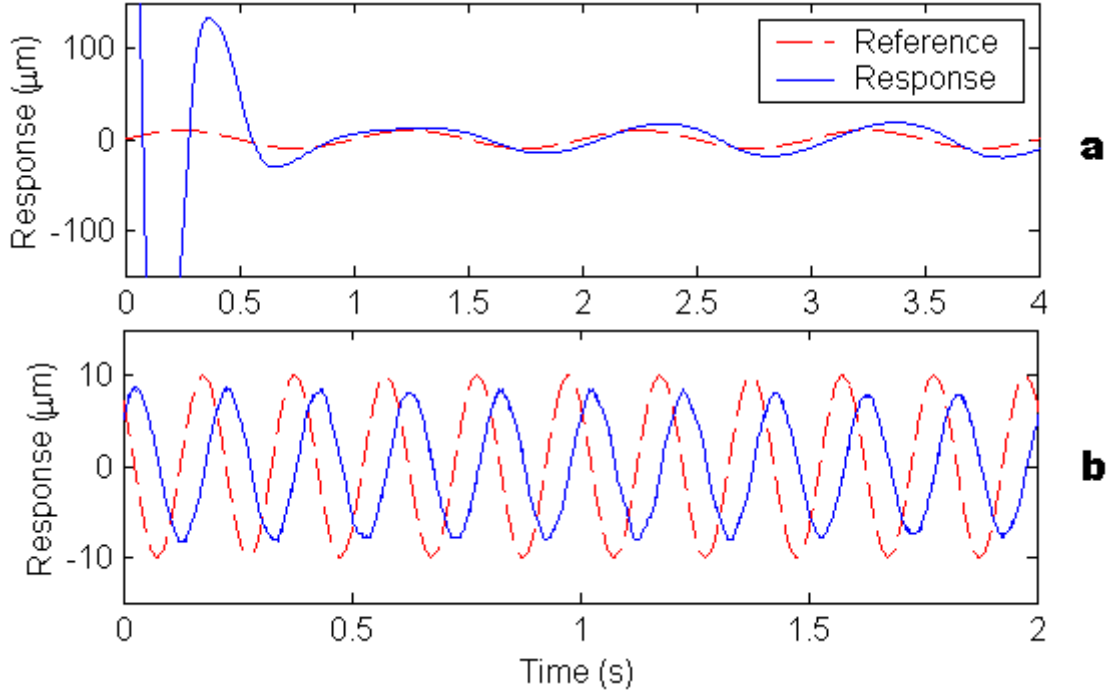


Figure 4.13: Sinusoidal tracking of packaged 2-stack actuator with integral control for a $10\mu\text{m}$ wave at 1Hz (a) and 5Hz (b).

4.2.6 Multi-Layer Sinusoidal Response

As in the multi-layer step responses, the sinusoidal responses only pertain to cantilevered actuators. The control experiments performed were done in a similar fashion to those of the single-layer actuators. That is, a single input amplitude was used for all the tests, while the frequency of the sine wave was increased. Unlike before, the gains were varied from one test to another to see what would happen. This was done because, as previously stated, the gain could likely be increased because the control voltages have been much lower than the saturation limit. Increasing the gain does change the system, however. This makes correlating one test to another more difficult, but the experiments were conducted to show its effects.

A packaged stack of two ionic polymer cantilevers is the first set of results shown. Figure 4.13a has the low frequency results. Here, the $10\mu\text{m}$ sine wave has a frequency of 1Hz and the gain is set to 5. The output shows that the amplitude is doubled, while the polymer is able to keep up with the frequency. There is a transient present in this response as well, but it decays after one cycle is completed. The phase lag for this system is 45 degrees. As has been the case in the results thus far, the control effort stays under 1.9

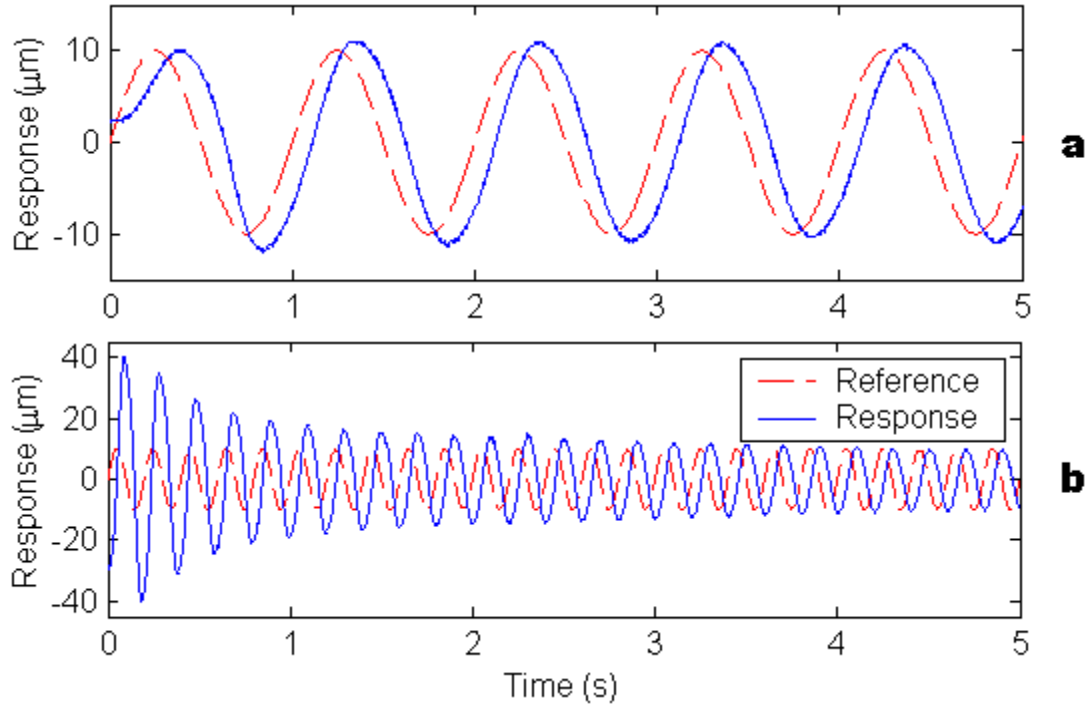


Figure 4.14: Sinusoidal tracking of 4-stack cantilevered actuator using integral control for a $10\mu\text{m}$ wave at 1Hz (a) and 5Hz (b).

Volts. By increasing the frequency to 5Hz and the gain to 50, Figure 4.13b indicates that no transient shows up in the response and that the amplitude is reduced by 20%, with a phase lag of 100 degrees. This increased gain also shows that the control effort does not exceed 950 milli-Volts. Again, it comes up that the increased gain actually reduces the maximum control voltage.

Moving on to the sinusoidal response for a 4-stack actuator, some similar results are seen. Figure 4.14a, with a gain of 20, shows almost a 10% amplification of the input signal's amplitude and a 35 degree phase lag. No transients are present in this response, however. Also, this $10\mu\text{m}$, 1Hz signal requires only 0.5V to perform as shown. Increasing the frequency again to 5Hz and the gain to 50, shows an unfavorable response. It can be seen in Figure 4.14b. A large decaying transient overshadows the steady-state response for more than 3 seconds, until it finally decays. Once steady-state has been reached, the output amplitude is 20% higher than the input amplitude and a phase lag of 90 degrees is seen. Although this response differs the most from the others, the control does not call for more than 900 milli-Volts.

One final table has also been put together, showing the numerical results of the

Table 4.6: Summary of Integral Control Results for Multi-Layer Ionic Polymers under a Sinusoidal Input.

Response Characteristic	Packaged Stack of 2		Stack of 4	
	Low Freq	High Freq	Low Freq	High Freq
Frequency (Hz)	1	5	1	5
Input Amplitude (μm)	10	10	10	10
Output Amplitude (μm)	20	12	11	10
Phase Lag (degrees)	45	100	35	90
Control Voltage (V)	<1.9	<0.95	<0.50	<0.90
Gain	5	50	20	50

response characteristics for multi-layer ionic polymer actuators. The control results are presented identically to the way they were for the sinusoidal response of single-layer actuators. And so the multi-layer sinusoidal results do not get left out, it should be mentioned that they, too, do not exceed, or even come near the saturation level set to protect the polymer material.

By completing the presentation of integral control results, a discussion will follow, bringing together some of the ideas and results developed herein. Closed-loop bandwidth will be the major topic discussed, using these control results as evidence.

4.2.7 Discussion

When discussing aspects other than general trends associated with the changing bandwidth, like that in Chapter 3, the definition will be used for characterization. Also for controls, the phase lag exhibited by ionic polymers will have more of an effect on the bandwidth because stability margins become a factor. This is especially true when using integral control, which introduces a -90 degree phase shift and is known for limiting the system bandwidth. The phase margin of a system is used as a stability measure and is defined as the amount that the phase exceeds -180 degrees when the magnitude is unity. Another quantity used to assess system stability is the gain margin. This is the factor by which the gain of the system is below 1 (0dB). For a system to be stable, its loop transfer function must have a positive phase margin and a gain margin greater than 1.

Before discussing the transfer functions for ionic polymers, a brief digression will be made about what is expected. Recall the form of the closed-loop transfer function in

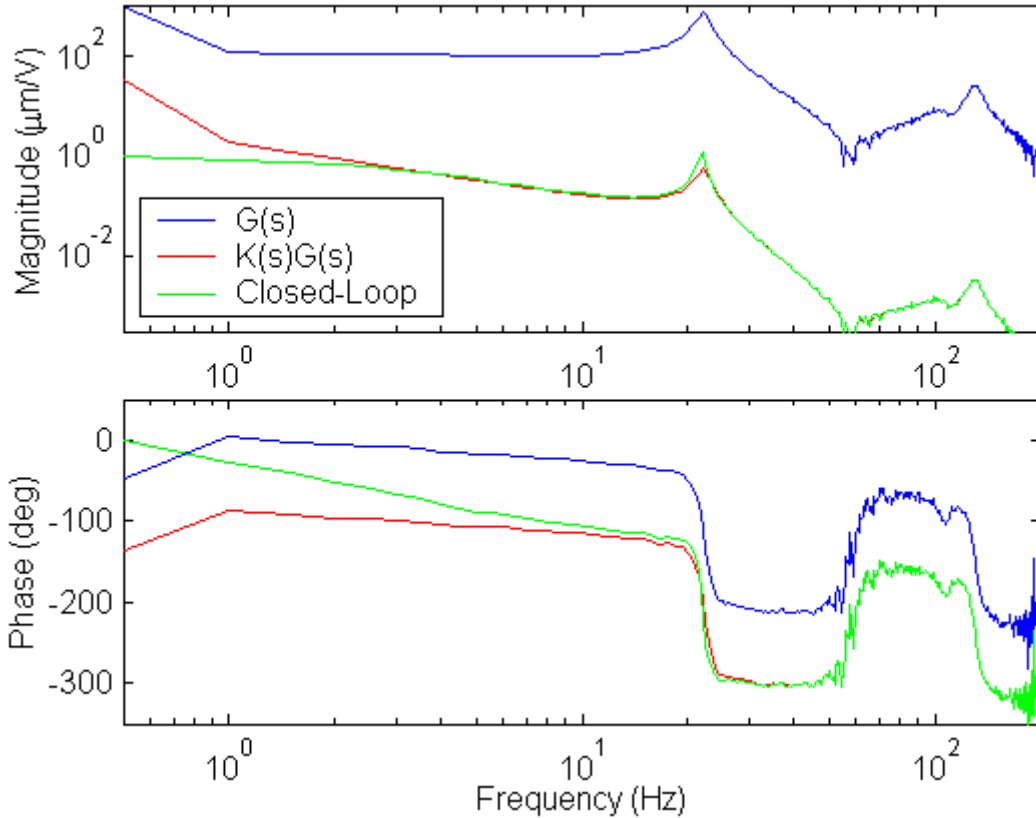


Figure 4.15: Transfer functions for cantilevered (20 x 5 x 0.2)mm ionic polymer actuator.

Equation 4.19. When the magnitudes of the loop transfer function are high, the closed-loop will be approximately 1. On the other hand, when the loop transfer function is relatively low, the closed-loop will be approximately equal to the loop transfer function. Therefore, due to the integrator, the low frequency magnitudes of the loop will be high, implying a near unity closed-loop response, while at high frequency, the loop and closed-loop transfer functions should match.

Both the loop and closed-loop transfer functions can be calculated using data from an open-loop transfer function $G(s)$. For integral control, each of the complex values of the open-loop frequency response function can be divided by each corresponding $j\omega$ value, giving the loop transfer function $K(s)G(s)$. Once this is calculated, the closed-loop transfer function can be computed using Equation 4.19. This procedure was carried out for a cantilevered actuator and a clamped-clamped actuator.

Figure 4.15 shows the frequency response functions for a cantilever. The expected results were obtained in the calculations, and except for the slight over-estimation of the

Table 4.7: Characteristic Cantilevered Frequency Response Values.

Response Value	Open-Loop		Loop		Closed-Loop	
	Low	Resonance	Low	Resonance	Low	Resonance
Frequency (Hz)	1	22	1	22	1	22
Magnitude ($\mu\text{m}/\text{V}$)	120	795	1.90	0.58	0.86	1.22
Phase Lag (degrees)	-5	100	85	190	25	205

resonant peak magnitude, the loop and closed-loop transfer functions match well from about 2Hz on. The phase lag of these materials and the control is also present in the figure, with matching phase between the loop and closed-loop transfer functions not occurring until after resonance at 25Hz. The closed-loop bandwidth of this (20 x 5 x 0.2)mm actuator, the frequency where the magnitude is 0.707 (-3dB), is 2.5Hz. This value is lower than expected, but using a linear analysis on a nonlinear material may introduce error into this calculation. Other important values to point out are the stability margins. The phase margin is 85 degrees at 1.8Hz, while the gain margin is approaching instability with a value of 1.01 at 22Hz. Some characteristics of this cantilevered actuator that may be of interest in certain applications are the low frequency response characteristics and those at resonance. Table 4.7 highlights the particular magnitude, phase, and frequency values where these occur.

In relating the predicted closed-loop response to the controlled sinusoidal response, Table 4.8 was created. This table draws attention to the poor agreement in values. Neither the magnitudes, nor the phase lags correspond well from one result to the next. The bandwidth also does not match because the sinusoidal results indicate that it falls between 5Hz and 15Hz, whereas the frequency response function predicted it would be below 5Hz. A possible reason for this discrepancy in analysis techniques is the repeatability issues associated with these materials. After presenting clamped-clamped results, more comments will be made to this end.

The clamped-clamped transfer functions have been put together in the same way as for the cantilever, and the results are given in Figure 4.16. It is again around 2Hz that the loop and closed-loop transfer functions nearly match in magnitude, but not until after 6Hz that the phase is approximately the same. The closed-loop bandwidth for the clamped-clamped (20 x 5 x 0.2)mm actuator is only 2.75Hz, which is surprisingly lower than

Table 4.8: Comparison of Controlled Cantilevered Response to Predicted Response.

Response Characteristic	Sinusoidal Results		FRF Prediction	
	<i>a</i>	<i>b</i>	<i>a</i>	<i>b</i>
Frequency (Hz)	5	15	5	15
Output/Input ($\mu\text{m}/\text{V}$)	0.80	0.60	0.35	0.15
Phase Lag (degrees)	20	60	85	105

expected. It should be noted that this result is with negligible tension. It was conceived from the results of Chapter 3 that the clamped-clamped polymer would have a much higher bandwidth due to the larger natural frequencies, but when looking at the magnitude plot in the figure, a first-order, or integrator, effect is noticed. What this means is that by clamping both ends of the polymer, the boundary restriction introduces somewhat of an integrator effect that reduces the attainable bandwidth.

Before continuing with the discussion of bandwidth for ionic polymers, a comment needs to be made about the plots of Figure 4.16. It is noticed that between 15Hz and 60Hz, a straight line is present. This is because in the original data plots, there was poor coherence in this range that was attributed to resonance effects of the test fixture. The reason it showed up in this plot and not any of the others is because at the time the transfer function was captured, the rubber band on the clamp had begun to stretch, making the clamp nearly ineffective. Therefore, a different clamping mechanism was used to apply the force, which gave differing results in this frequency range. Getting back to the data plots, this frequency range was simply removed and connected with a straight line, where it can be seen that not too much error has been introduced. It should also be noted that this transfer function was the final data set taken.

Repeating the process of emphasizing the low frequency and resonant response characteristics, Table 4.9 was made showing the values for the clamped-clamped actuator. Comparing these values to those for the cantilever, it is seen that the closed-loop, low frequency response is similar. Both of the magnitudes are near unity and the phase lag is 25 degrees. As before, the stability margins for this clamped-clamped polymer will also be pointed out. The phase margin is 100 degrees at a frequency of 2.1Hz, while the gain margin is 50 at 28Hz. These values shows that the clamped-clamped actuator as tested is well within the limits of system stability.

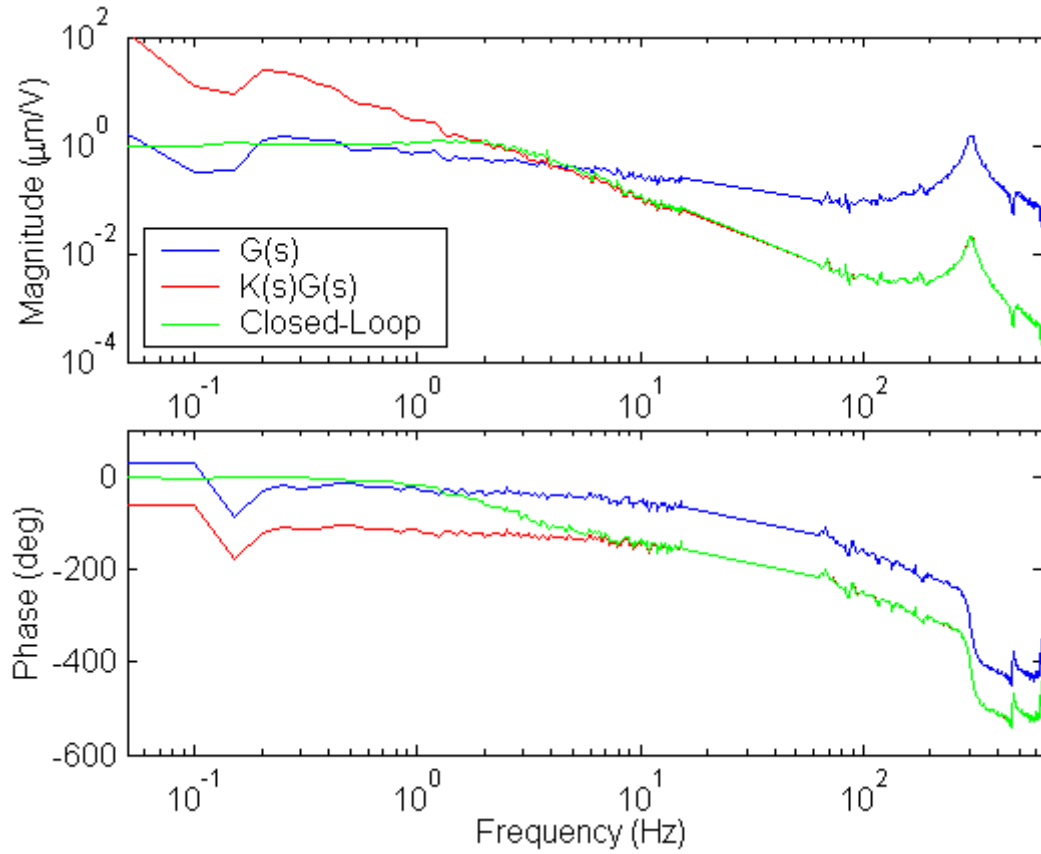


Figure 4.16: Transfer functions for clamped-clamped (20 x 5 x 0.2)mm ionic polymer actuator.

Table 4.9: Characteristic Clamped-Clamped Frequency Response Values.

Response Value	Open-Loop		Loop		Closed-Loop	
	Low	Resonance	Low	Resonance	Low	Resonance
Frequency (Hz)	1	300	1	300	1	300
Magnitude ($\mu\text{m/V}$)	0.76	1.05	2.40	0.016	1.12	0.016
Phase Lag (degrees)	25	340	120	410	25	410

Table 4.10: Comparison of Controlled Clamped-Clamped Response to Predicted Response.

Response Characteristic	Sinusoidal Results		FRF Prediction	
	<i>a</i>	<i>b</i>	<i>a</i>	<i>b</i>
Frequency (Hz)	2	6	2	6
Output/Input ($\mu\text{m}/\text{V}$)	1.20	0.70	1.05	0.20
Phase Lag (degrees)	35	105	75	120

These frequency response function results also show some disagreement with the closed-loop sinusoidal responses. Table 4.10 these results. At the frequency in the predicted bandwidth (2Hz), the magnitude values are reasonable in comparison, but the phase is off by more than a factor of 2. At a frequency outside the closed-loop bandwidth (6Hz), the magnitudes showed variation, while the phase was closer. These results also suggest that the bandwidth is between 2Hz and 6Hz, which follows from the predicted bandwidth of 2.75Hz.

In considering the predicted results versus the sinusoidal results for the ionic polymer in the cantilever and clamped-clamped configurations, there seemed to be more correlation for the clamped-clamped actuator. There is no obvious reason why one of the configurations would compare better between analysis methods, but it was thought that it would be worthwhile to bring that point out.

There is one more characteristic related to the speed of response that has not been brought up yet is the rise time. This is a time response characteristic that can be estimated with frequency response data. Using the design relation from Franklin et al. (1994), the rise time of a second-order system can be approximated as a function of the natural frequency in the form

$$t_r = \frac{1.8}{\omega_n} = \frac{1.8}{2\pi f_n} \quad (4.20)$$

However, this equation is only accurate for second-order systems with no zeros, which is not the case for the ionic polymers. This means that some error or discrepancy is expected when comparing the calculated values to the experimental values.

For the cantilever case, the rise time for the “best” closed-loop response was 16ms,

while the clamped-clamped configuration had a slightly higher, 40ms rise time. Calculating an approximation of the rise time, gives

$$t_{r,CF} = \frac{1.8}{2\pi(22\text{Hz})} = 13\text{ms}$$

$$t_{r,CC} = \frac{1.8}{2\pi(300\text{Hz})} = 1\text{ms}$$

These calculations show that the rise time of the cantilever can be closely approximated using Equation 4.20, but the clamped-clamped approximation is far from accurately estimating the experimental rise time. This is most likely due to the integrator effect that is exhibited by the polymer when both ends are clamped.

Continuing with the speed of response is the system's bandwidth, which has been shown to increase only 0.25Hz from the cantilever to the clamped-clamped configurations and not reach over 2.75Hz for either closed-loop system. In analyzing the frequency response functions for the cantilever, it can be concluded that the limiting factor for bandwidth is the resonance. This conclusion is reached from the system resemblance of a second-order system and the close approximation of rise time using Equation 4.20, which is dependent on the resonant frequency. This implies that using shorter cantilevered actuators will result in higher bandwidth. Figure 4.17 confirms this implication showing that a (8 x 5 x 0.2)mm can achieve a closed-loop bandwidth of 10.5Hz. The bandwidth of the clamped-clamped condition is limited by the integrator effect that is introduced by clamping the free end of the cantilever. This effect basically doubles the negative slope of the magnitude plot from the integrator in the controller, causing the transfer function to reach 0.707 (-3dB) at a much lower frequency. One possible cause for this effect could be that restricting the free end of the cantilever alters the system dynamics in a way that a low frequency pole is introduced. However, since no clamped-clamped modeling has been performed, this statement is only speculation.

Another interesting result of the closed-loop bandwidth characterization is brought into light by examining the results in a table. Table 4.11 shows a summary of these results. Looking at the clamped-free case, and comparing the resonant frequency with the closed-loop bandwidth, it is noticed that the actuator's bandwidth is approximately 10%

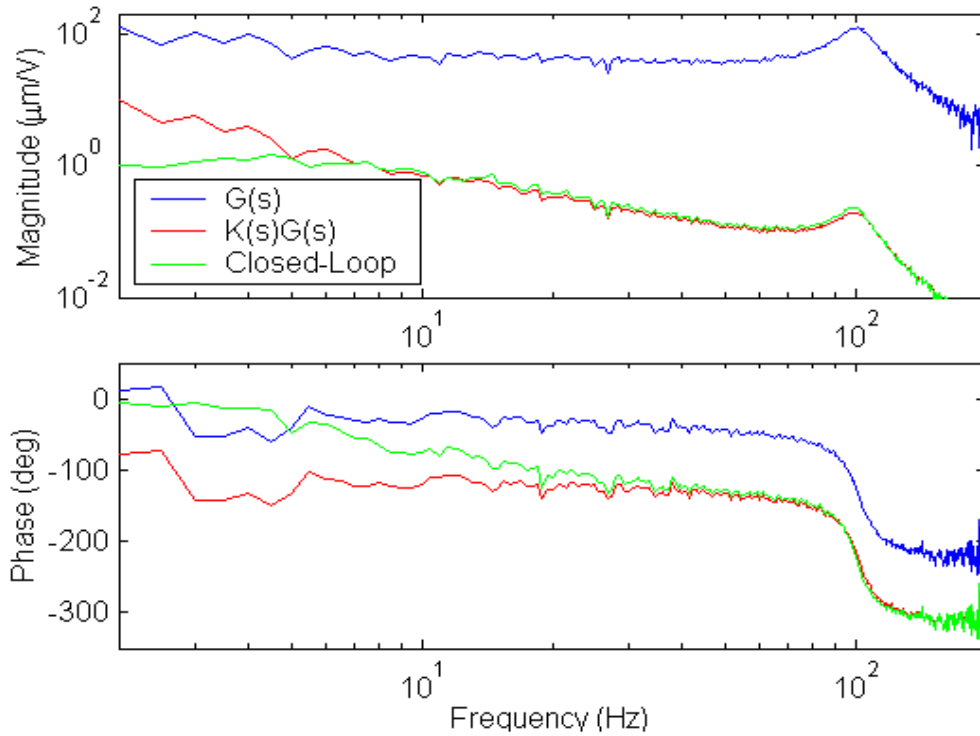


Figure 4.17: Transfer functions for “short” (8 x 5 x 0.2)mm cantilevered ionic polymer.

Table 4.11: Summary of Closed-Loop Bandwidth Characterization Results.

Characteristic	Clamped-Free		Clamped-Clamped
Length (mm)	8	20	20
Resonance (Hz)	100	22	300
Bandwidth (Hz)	10.5	2.50	2.75

of its resonant frequency. This relation is true, of course, only for this particular type of control scheme, but the result is very interesting, nonetheless. What this implies is that no calculations are required after the initial open-loop transfer function is captured because the bandwidth can be determined directly from resonant frequency, with only a small margin of error.

One final comment about the result discrepancies will now be made. It was stated previously that a possible reason for the disagreement is the repeatability issues that have been noticed with these polymers throughout the numerous tests discussed. While some of the blame can be taken by the inconsistencies from test to test, it certainly is not reasonable to think that they are all accountable. For this reason, the problem regimes will be brought

up. Classical control theory is based on linear systems, whereas ionic polymers make up nonlinear systems. It was thought for the short term that linearity could be approximated in the material and some evidence was even shown that this could be true. However, the frequency response plots tell a different story. Therefore, material nonlinearity is assumed to be the main cause for the discrepancies with linear theory.

With integral control providing good time responses, but some discrepancies between frequency and time domain analyses, another control technique was applied to the ionic polymer actuators to see if better results could be obtained. Adaptive control is the subject of the next section.

4.3 Adaptive Control

Many dynamic systems can be improved through the use of feedback control. However, not all systems that can benefit from control have constant or easily identifiable parameters. Some systems even have time dependent parameters that can vary large amounts. This variation in parameters can make classical control algorithms, such as PID and lead-lag, unsuccessful. Systems with this characteristic were the motivation for developing adaptive control, which is a type of nonlinear feedback control. The basic idea of adaptive control is to estimate the uncertain plant parameters based on measurements of the system, and then use these estimates in updating the controller. This makes one of the main differences between adaptive (nonlinear) control and typical linear control be that the controller parameters are variable.

Ionic polymers have a need for adaptive control for a couple reasons. The most prominent is that there is no set model describing their dynamics. In addition to having unknown dynamics, it is also known that at least one parameter in an ionic polymer system varies with time, that being the material dehydration discussed earlier. Knowing that ionic polymers fit the profile of a system that could benefit from adaptive control, it became time to choose the algorithm to be used. There are several types of adaptive control schemes available, covering both direct and indirect methods. The two most common methods are model-reference adaptive control (MRAC) and self-tuning regulators (STR).

With the results from the previous section using an integrator and a gain, the polymer's tracking ability was discovered. Recalling the results from Figure 4.6, it was thought

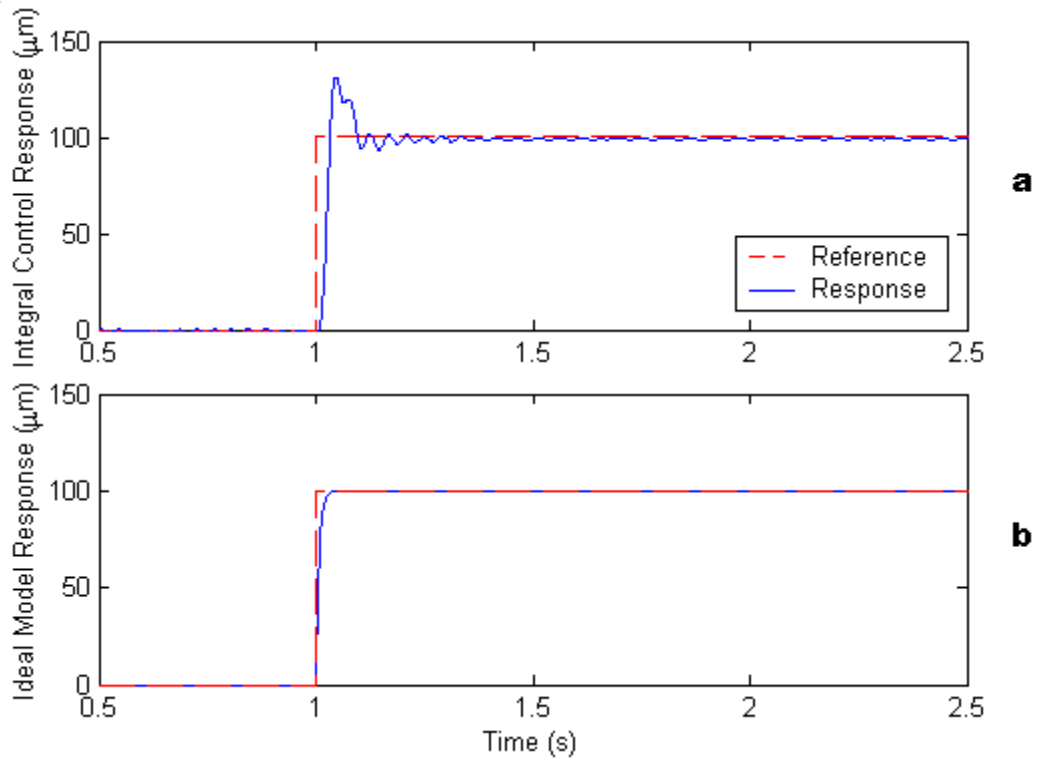


Figure 4.18: Integral control results (a) compared with a more ideal system model (b).

that this could potentially be an ideal model of the system for tracking purposes. Since the form of a system with a favorable response is known, the choice of adaptive control techniques to use was clear. The MRAC algorithm would be employed using a system with an ideal response as the reference model in the design.

This section will proceed according to the model-reference adaptive control design process. First the reference model will be selected, followed by the controller design and analysis. Once the system is designed, the controller will be implemented in a model control system, where simulations will be performed. After the simulations are in working order, the MRAC system will be taken to the laboratory for control experiments on a cantilevered ionic polymer actuator.

4.3.1 Reference Model Selection

With the form of the system shown in Figure 4.6 known, it is a potential candidate model. However, there does exist some overshoot that would not likely be present in a purely ideal system response. For this reason and the sake of simplicity, a model with no overshoot was

chosen. This model matches the response time characteristics of that in Figure 4.6b, but has an exponential increase to the reference step value rather than overshoot. This simple and ideal model should be a reasonable first try because experimental results confirm that the time characteristics are achievable, and this model has a relative-degree of one, as did the model developed by Mallavarapu (2001). Figure 4.18 compares the integral control results (a) to the more ideal model response (b) to be used in the design.

4.3.2 Controller Design and Analysis

Having determined a good form of a reference model, the MRAC design procedure can be applied. The design process to be discussed is outlined by Slotine and Li (1991). It begins with the model dynamics that have the form

$$\dot{y}_m(t) = A_m y_m(t) + B_m r(t) \quad (4.21)$$

where the subscript m denotes relation to the model and A_m is negative. The model can also be written as a transfer function as

$$M(s) = \frac{B_m}{s - A_m} \quad (4.22)$$

For the actual model being used, the value of A_m is -140 and the value of B_m is 140. These values were chosen to match the time characteristics of the integral control results using “guess and check” simulations in Matlab.

In a similar form to Equation 4.21, the plant dynamics may be written as

$$\dot{y}(t) = A_p y(t) + B_p u(t) \quad (4.23)$$

where the subscript p denotes reference to the plant. These are the unknown parameters. It should also be noted that the subscript has been left off the $y(t)$ term because it is the actual plant output.

With the basic idea behind MRAC to be getting the error between the actual system and the model to be zero, the control law

$$u(t) = \hat{A}_r(t)r(t) + \hat{A}_y(t)y(t) \quad (4.24)$$

can be chosen, where the “hat” denotes a variable parameter and the subscripts refer to the input or states. Substituting Equation 4.24 into 4.23 gives

$$\dot{y}(t) = \left(A_p + B_p \hat{A}_y(t) \right) y(t) + B_p \hat{A}_r(t)r(t) \quad (4.25)$$

where perfect model matching will occur when the variable parameters have the form

$$A_r^* = \frac{B_m}{B_p} \quad A_y^* = \frac{(A_m - A_p)}{B_p} \quad (4.26)$$

Now the need arises to look for an adaptation law to get the variable parameters to converge to the ideal parameters, denoted by the “*.” To do this, the tracking error must first be defined, since ideally this will become zero in some time. The error can be defined as

$$e(t) = y(t) - y_m(t) \quad (4.27)$$

Additionally, the parameter errors can be defined as

$$\tilde{A}(t) = \begin{bmatrix} \tilde{A}_r(t) \\ \tilde{A}_y(t) \end{bmatrix} = \begin{bmatrix} \hat{A}_r(t) - A_r^* \\ \hat{A}_y(t) - A_y^* \end{bmatrix} \quad (4.28)$$

The error dynamics can be found now by subtracting Equation 4.21 from 4.25, and adding and subtracting an $A_m y(t)$ term to the right side of the equation, giving

$$\dot{e}(t) = A_m e + (A_p - A_m + B_p \hat{A}_y) y + (B_p \hat{A}_r - B_m) r \quad (4.29)$$

where the time dependence has been left out to give the equation a more compact appearance. Equation 4.29 can be simplified further by substituting in the relations of Equation 4.28 and recalling the definitions of Equation 4.26, yielding

$$\dot{e}(t) = A_m e(t) + B_p \tilde{A}(t) v(t) \quad (4.30)$$

where $v(t) = [r \quad y]^T$. Equation 4.30 can be represented in terms of the system model transfer function, $M(s)$, by taking its Laplace transform

$$e(t) = \frac{1}{A_r^*} M(s) \tilde{A} v(t) \quad (4.31)$$

It should also be noted that in Equation 4.31, the representation uses both the time-domain and the Laplace-domain, which is often seen in adaptive control. Having reached a known form of the tracking error, it can be shown that choosing a certain form of adaptation law assures that the tracking error will converge to zero as time moves forward. These adaptation laws are

$$\dot{\hat{A}}_r = -\text{sgn}(B_p) \xi e r \quad (4.32)$$

$$\dot{\hat{A}}_y = -\text{sgn}(B_p) \xi e y$$

where ξ is the adaptation gain that is always a positive constant. The value of ξ is often found by a trial and error approach. It can also be noted that the adaptation equations are nonlinear from the multiplication of the error signal and the reference input or plant output. Having chosen a control law and the adaptation laws for the control of a cantilevered ionic polymer actuator, analysis of the controller can now be performed.

Stability of an adaptive control system is based on the boundedness of both the tracking error, $e(t)$, and the parameter errors, $\tilde{A}(t)$. In the design process discussion, it was stated that choosing the adaptation laws of Equation 4.33 produces an error that approaches zero as time increases. This can actually be shown through the use of Lyapunov analysis. By defining the positive definite Lyapunov function candidate

$$V(e, \tilde{A}) = \frac{1}{2}e^2 + \frac{1}{2\xi}|B_p|\tilde{A}^2 \quad (4.33)$$

the time rate of change can be checked to see if it is at least negative semi-definite. Differentiating with respect to time gives

$$\begin{aligned} \dot{V} &= e\dot{e} + \frac{1}{\xi}|B_p|\tilde{A}\dot{\tilde{A}} \\ &= e\left(A_m E + B_p \tilde{A}v\right) + \frac{|B_p|}{\xi}\tilde{A}(-\text{sgn}(B_p)\xi ev) \\ &= A_m e^2 \end{aligned} \quad (4.34)$$

Recalling from Equation 4.21 that A_m is negative means the result of Equation 4.35 is negative semi-definite. Now, using Barbalat's Lemma shows that this choice of Lyapunov function has asymptotic stability of the tracking and error parameters (Popov, 1973).

Having arrived at a formulation of an MRAC system and showed that the system is stable, the control system can now be implemented into a form to obtain experimental data of its performance.

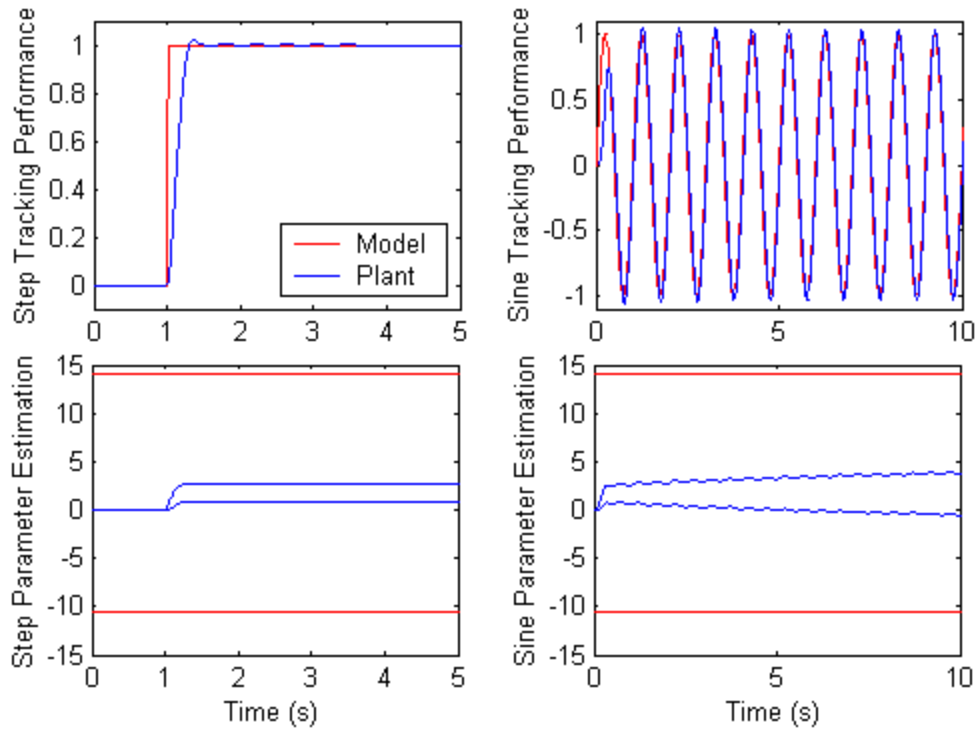


Figure 4.19: Simulation results of MRAC system given a reference step input (left) and a sinusoidal input (right). The adaptation gain in this example is 20.

4.3.3 MRAC Simulation

In implementing the model-reference adaptive control system, Simulink and Matlab were used. A block diagram of the system was constructed and tested using the ideal model as the plant. Once everything was in working order, different plant forms were tested to see how the adaptive system could perform. This was done because it is uncertain what the plant parameters of the model actually are. Everything from unstable constant parameter systems to time-varying parameter systems was tested to check the robustness of the control system. For every mock plant simulated, the control system was able to track both a constant reference input and a time-varying reference input. Knowing that the system was capable of tracking different reference inputs, the adaptation gain ξ was then adjusted to tweak the performance of the control system. The adaptation gain, having relatively small values, will make the adaptation of the system slow, with large transient tracking error. Conversely, relatively large values will result in very oscillatory adaptation parameters. As stated with the introduction of the adaptation gain, it is found by trial and error.

A typical system response for one of the plants simulated is shown in Figure 4.19. This figure has model and plant outputs, as well as the parameter estimation for both a step input and a sinusoidal input. The adaptation gain used in these simulations was 20. An interesting point to note about this adaptive control system is brought about by examining the parameter estimation plots. In red are the ideal model parameters, while the blue lines show the adaptation of plant parameters. In the step response, it can be seen that the tracking error goes to zero, but the parameter estimation does not converge, whereas for the sinusoidal case, the error eventually goes to zero and the parameters slowly converge. This non-convergence of parameters in the step response is because the adaptation algorithm only searches for parameters that make the tracking error zero, so if the error is driven to zero, the parameter estimation will cease, regardless of whether the parameters have converged or not. This can happen with simple inputs like a constant step. However, having a more complicated and time-varying input, as in the sinusoidal case, the parameters will continue to seek out the ideal parameter values because they are the only set that will give a true tracking error of zero.

With the simulations showing that the MRAC system can achieve zero tracking error, it became time to perform actual experiments with a cantilevered ionic polymer. This is the next topic of discussion.

4.3.4 Test Setup

The first step in moving from a continuous-time Simulink model to a model that can be used in an experiment with a digital signal processor is to convert the continuous states in the model to discrete states. This was done using a Tustin continuous-to-discrete transformation. Additionally, the plant was removed from the block diagram and replaced with digital-to-analog and analog-to-digital system blocks representing the signals being sent to the polymer actuator and the signal measuring the tip deflection of the polymer, respectively. A block diagram of this control system, along with one for the proportional-integral control, has been provided in Appendix C. The ControlDesk software, along with dSPACE, was used in this process. The dSPACE output the control signal to the polymer based on the displacement measurements from a laser vibrometer and calculations performed in the adaptive control system. A schematic of the test setup is identical to that in Figure 4.5, so it will be withheld here. The only difference is what is going on inside the CPU and

dSPACE.

4.3.5 Experimental Results

Now that the test setup is prepared and functioning properly, several data sets were taken showing the effect of the MRAC system to both a reference step and sinusoidal input. Various adaptation gains were experimented with, as well, in search of an ideal value. The results of the step response are presented first and the sinusoidal response is second, but prior to results, some general comments will be made about the testing.

Initially, the results were not turning out too well. Since the control experiments have been performed when the polymer was fully hydrated, it was thought that water motion on the actuator's surface could be skewing measurements. To overcome this possible problem, the area on the polymer that was reflecting the laser signal was dried off, giving as flat and dry a surface as possible to reflect. Then, when the polymer was rehydrated in between tests, deionized water was brushed over the polymer's entire surface except where the laser was reflecting.

Even with the extra precautions to get quality data, and thus quality control voltages sent to the polymer, the laser did not show great repeatability from one experiment to another. For this reason, several trial runs had to be taken with each set of test parameters, and then the data was sifted through in search of a quality set for analysis of the control system performance.

From the start of the experiments, it was noticed that the control voltage jumped between the maximum and minimum allowable values. These were the ± 3 Volts of the saturation block. This pegging of the control voltage means that the performance of the MRAC system has a limitation on the convergence of the error and parameter tracking in the control voltage. With the control voltage in the experiment at either extreme of 3.0V, this implies that the adaptation routine actually requires more power to achieve the desired performance. Despite this apparent limitation, some decent experimental results were obtained, mostly for the step tracking.

Figure 4.20 shows the results of a fairly clean data set, taken with an adaptation gain of 50. The tracking performance, parameter estimation, and control voltage are all shown. Because of the tracking loss with the laser, which was a common occurrence, the figure shows only a particular section of the data, after the initial step took place. The step value

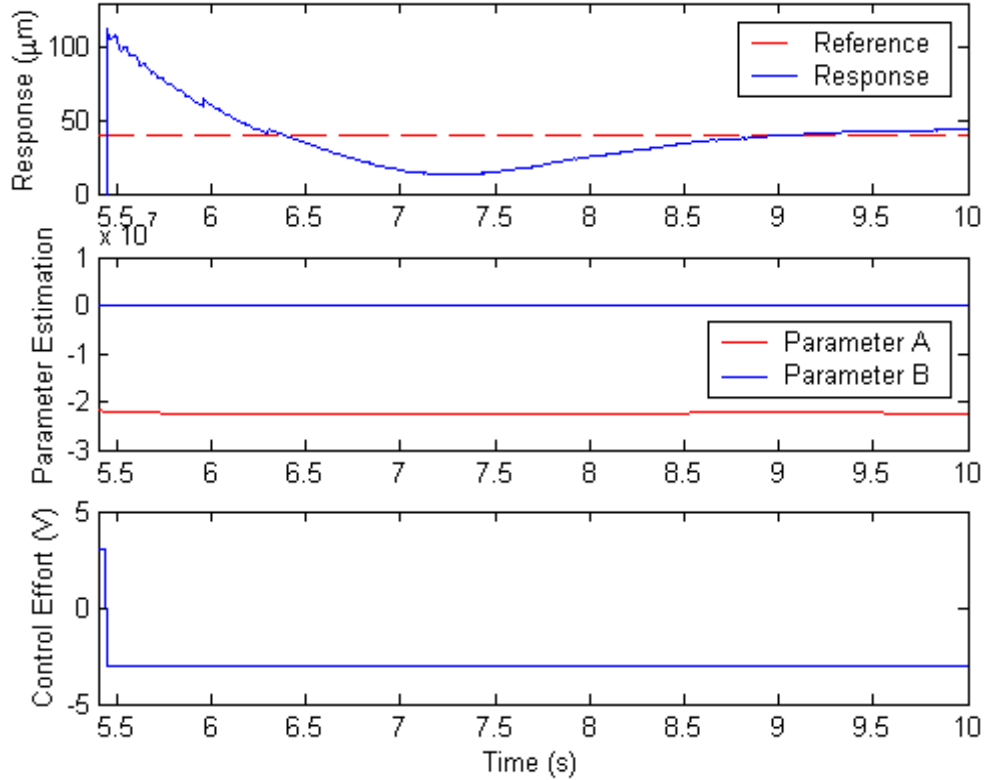


Figure 4.20: Step response with MRAC system using an adaptation gain of 50.

for this particular test was 40 microns. It can be seen that the control voltage is constant at -3.0V throughout the duration of the time shown. Also, the parameter estimates are relatively constant.

To show the effect of varying the adaptation gain, a series of experiments were performed using some higher values. Figure 4.21 shows the step response using an adaptation gain of 80. Recall that using higher values of ξ gives an oscillatory response, which is evident in the figure. Again, the control effort is at the maximum or minimum value throughout the response, but because of the oscillatory response this time, it appears to have entered a chattering mode. Looking back at Figure 4.20 and considering the adaptation gain used as relatively low, it also shows what was expected from a lower adaptation gain. That is, a slower response with large transient error.

Moving on to using a sinusoid as the reference input, the results were not nearly as good as those with a reference step input. The most likely reason for the poor results from the sinusoidal response is the limitation of the applied control voltage discussed before. This in mind, reference inputs with low frequencies were tried because it was thought that

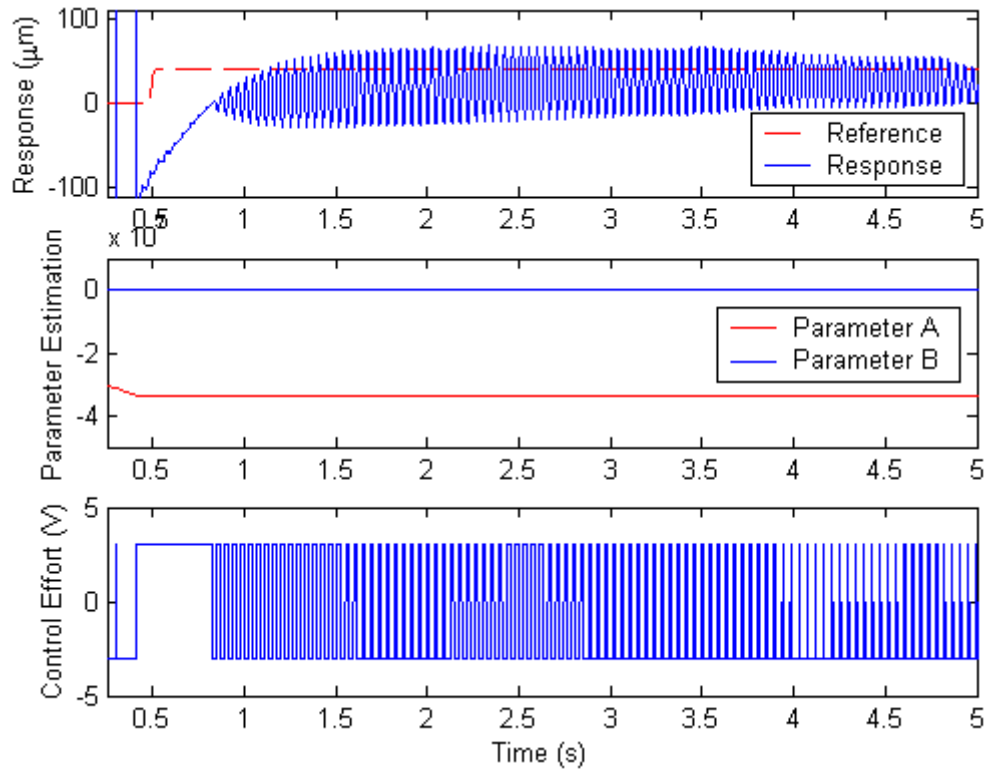


Figure 4.21: Step response with MRAC system using an adaptation gain of 80.

they would require the least amount of energy to actuate the polymer. The best result attained was a polymer output displacement of nearly the same amplitude as the input waveform ($20\mu\text{m}$), but at a much higher frequency. The frequency of the reference input was 0.3Hz , while the polymer was oscillating at 20Hz . These two frequencies vary by a factor of 67. Figure 4.22 shows these results, with an adaptation gain of 80 and chattering of the control voltage. One possible cause for this major discrepancy could be that some unmodeled dynamics are being excited. The likely reason that this is the main culprit is that the reference model used in the MRAC system was relative simple. Also, the ionic polymer could be exhibiting waveform nonlinearities that have been seen when the material is subjected to large electric fields. This could be relevant here because the control voltage was at the maximum amplitude allowed by the system.

Overall, the model-reference adaptive control system functioned unsuccessfully. However, for the step input it did a reasonable job of at least illustrating the effects of changing the adaptation gain, with some achieved level of tracking. The sinusoidal response, on the other hand, did not give favorable results at all. A summary of this chapter will follow as the final control technique is brought to a close.

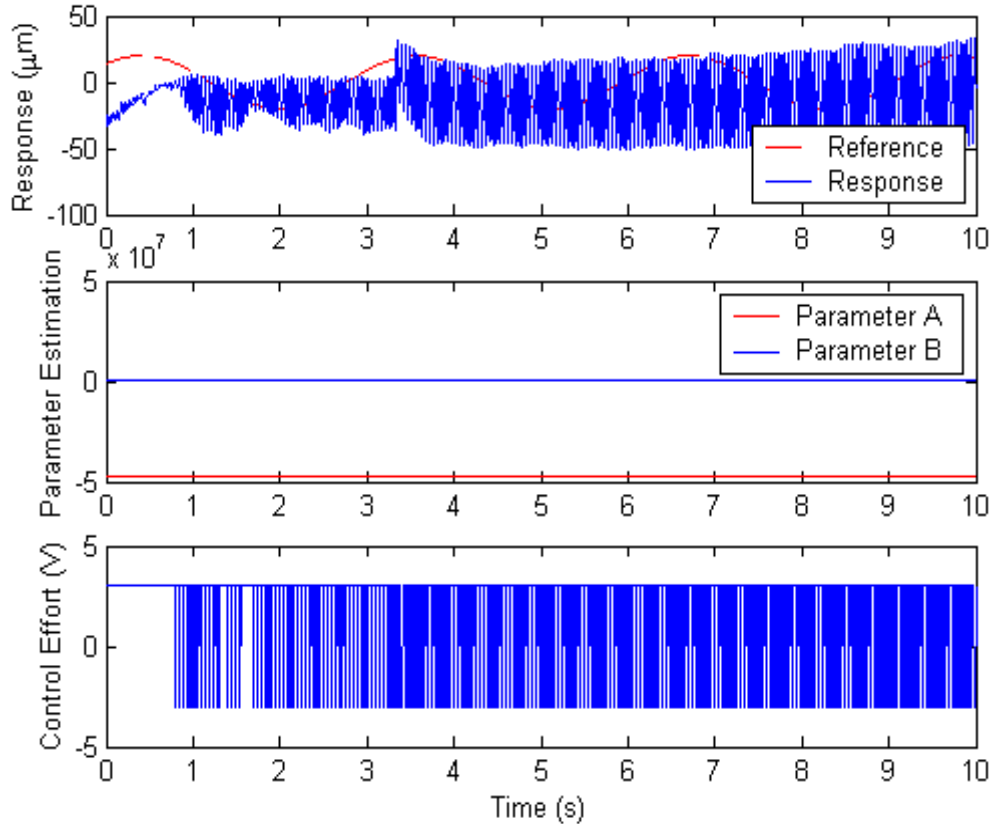


Figure 4.22: MRAC system results for a sinusoidal input.

4.4 Summary

Control techniques for ionic polymer actuators were discussed in this chapter in both equation development form, as well as experimental implementation. The first technique discussed was a linear quadratic regulator design, created from an empirical model based off a series of step responses. This full-state feedback design reduced the overshoot, but left settling time and steady-state error to be improved further. The states used for feedback were also not physical states of the polymer because they were the result of empirical data fitting. Applying integral control showed that the tracking capability could be greatly improved, resulting in a fast response, quick settling time, minimal overshoot, and no steady-state error. Another advantage to this technique is that a model need not be developed. Simply implementing an integrator and a gain in the feedback loop gave good results, where the gain was adjusted by trial and error. Trying to improve the response even further, model-reference adaptive control was applied. The reference used was a simple model with the same response time characteristics as the integral control result, but with no overshoot.

Despite encouraging simulation results, experiments showed that the polymer's low voltage tolerance limited its performance. The most likely reason was that the reference model used did not accurately represent the actual polymer.

The closed-loop bandwidth was also discussed. The cantilever actuator was shown to have a closed-loop bandwidth of 2.5Hz, while the clamped-clamped polymer's was slightly higher at 2.75Hz. This small increase in bandwidth did come as a surprise, when considering the order of magnitude difference in natural frequencies between configurations. However, clamping the free end of the cantilever introduced an integrator effect to the frequency response of the clamped-clamped polymer. This effect was attributed as the cause for the nominal bandwidth gain in the clamped-clamped actuator, while the resonant frequency, or actuator length, was concluded to be the limiting factor for bandwidth of the cantilever. There were also discrepancies between the sinusoidal time responses and the frequency response plots. The major cause of these discrepancies was stated to be the nonlinear nature of the ionic polymer material being analyzed as though it were a linear system.

Chapter 5

Conclusions

With the presentation of research completed, this final chapter will review the conclusions made for the different topics discussed in the previous four chapters. The contributions of this work will then be restated, but in more specific terms since the results have already been presented. Following the contributions, suggestions will be made for future work that can be done with ionic polymer actuators.

5.1 Conclusions of Research

Throughout the preceding chapters, conclusions were made about the research results. They will be summarized here again to bring a close to the work. As a quick recap of this thesis, the first chapter provided an introduction to ionic polymer materials and the second chapter discussed their dynamic response characteristics. The new research was presented in Chapters 3 and 4, covering open-loop effects on bandwidth and control techniques, respectively. And now in the fifth chapter, the conclusions will be restated.

From evaluating the humidity effects of a cantilevered and clamped-clamped ionic polymer actuator, it was discovered that the natural frequencies shift increasingly in a linear trend as the material dehydrates. Moreover, the shift is faster at lower humidity levels and slower at higher humidity levels. This is true over the tested range of 60% to 70% relative humidity and continuous actuation for up to 52 minutes. Additionally for the cantilever, a leveling off of the shift was seen as the input was increased. The magnitude of the cantilever follows the opposite trend, decreasing over time. Although the clamped-clamped frequencies also shift linearly with time, a discrepancy is noticed between magnitude shifting of different

testing configurations. This is because the clamped-clamped case shifts in a non-decreasing manner.

Tensioning the clamped-clamped polymer re-emphasized the linearly increasing frequency shifts and non-decreasing magnitude shifts. Also, as the applied tension was increased, the initial frequency increased. In comparing the tensioned effects to uniform beam theory, it was found that the results matched qualitatively, but not quantitatively. Statements were made about the open-loop bandwidth effects, as well, where it was noted that clamped-clamped actuator's bandwidth would increase with time and tension, while the cantilever's would most likely decrease.

In experimenting with different control techniques, it was discovered that integral control can greatly improve the tracking capability of the actuators when compared to the linear quadratic regulator approach. There is also no modeling necessary for the implementation of this control. Taking it one step farther, adaptive control was applied with unsuccessful overall results. These results did demonstrate the effects of increasing the adaptation gain, but the control system performance suffered from reference model inaccuracy and the low voltage tolerance of the polymer.

When considering the effects integral control has on the bandwidth of the actuators, only a nominal gain was achieved when going from the clamped-free to the clamped-clamped configuration. Despite the large increase in natural frequencies noted from changing the testing configuration, an unexpected integrator effect was introduced that limited the closed-loop bandwidth of the clamped-clamped actuator. The factors limiting the bandwidth of the cantilever and clamped-clamped actuators were determined to be the resonant frequency, or length, and the integrator effect, respectively.

With the conclusions of the work discussed, the contributions will now be stated, drawing from the information learned by the research.

5.2 Contributions

Back in the first chapter, the contributions of this research were stated in a broad sense, so as not to invalidate the reading of this thesis. Now that the results have been presented and conclusions have been made, the contributions will be emphasized again, but this time the descriptions will be more specific.

- *Investigate Dehydration Effects.* Linear trends were established for the frequency shift as a function of time, and is independent of boundary conditions. Also, the slope was larger at lower humidity levels and smaller at higher humidities. By increasing the input to the polymer, it was shown that the frequency shifts exhibit a leveling off as they approach a final value. Concerning the peak magnitudes, the cantilever's decrease as the material dehydrates, while those for the clamped-clamped actuator are non-decreasing.
- *Examine Boundary Condition Effects.* In going from clamped-free to clamped-clamped, the natural frequency of the polymer actuator increases by an order of magnitude. Once clamped, applying tension increases the frequencies even more without any ill-effects on magnitude, which does not decrease. This can be correlated to increasing open-loop bandwidth with tension. The same was shown as this actuator dehydrates. The cantilever has the opposite effect because the magnitudes decrease as the frequencies increase. This shows that the cantilever's open-loop bandwidth will not increase as the material dehydrates.
- *Improve Actuator Tracking Capability.* Integral control can be used for short-term tracking of the actuators with a fast response and no steady-state error. Using just an integrator and a gain also requires no model of the system to be developed, only a gain to be adjusted. This makes it much easier to implement and use for various sized actuators. A simple adaptive controller was also used, but to no avail. However, increasing the order of the reference model may more accurately represent the polymer and present a control design that could be used as the polymer dehydrates. The closed-loop bandwidth was also characterized to have little increase when comparing the cantilever to the clamped-clamped actuator. This was because of an integrator effect that clamping both ends of the polymer introduced to the system. The limiting factor of the cantilever polymer was concluded to be the resonance, or length.

5.3 Future Work Recommendations

During the course of performing this research, certain issues arose either from the work itself or from the conclusions that were made. This section will bring attention to some of these issues.

- Repeatability and material inconsistency were often discussed in experimental result sections of this work, where it was noted that material properties often vary across the dimensions of a single polymer specimen. In order for these materials to be produced at the commercial level and implemented into system designs, the manufacturing standards will have to be improved. Researching the manufacturing processes of the base material NafionTM and its electroding could establish certain ranges of property values that can be attained from different processes, with consistency being a key factor.
- Precision control will be an intense field of study for ionic polymers as controllable membranes are more fully realized. As they stand now, the surface roughness for these actuators is on the order of two microns. Sub-wavelength precision is required for optical applications, however. This means that plating methods need to be addressed, where the smoothness of the electrodes is improved by at least one order of magnitude.
- In order to be used for the control of membrane optics in space, current ionic polymers need to be testing to see how they perform in shape control applications. With this baseline material characterized in this way, more insight will be available for future material designers in terms of what needs to be changed to achieve better shape morphing ability.
- As they are now, ionic polymers rely heavily on water to achieve their large bending deflections. However, water both evaporates and freezes in differing air environments. The use of different solvents may be one way to eliminate this environmental limiting factor. By studying the use of solvents with lower freezing temperatures and those that are less susceptible to evaporation, the operating conditions of ionic polymer materials can be increased.
- Because the humidifier used in assessing the hydration effects was limited in the range over which it could operate, it would be very interesting to see what happens at lower and higher humidity levels. In particular, research of the “wet” humidity levels would be useful for showing how much or how little the frequencies and magnitudes will shift as the air contains more and more water. This could possibly create more of a design space in which ionic polymers could be used without suffering too much from

the variable parameters.

- The adaptive control scheme implemented in this research was unsuccessful, for the most part, due to the low order model used. Expanding the use of adaptive control to larger scale models that can more accurately represent the true polymer system may prove helpful in increasing the performance of the actuators. As mentioned before, adaptive control does have great potential with ionic polymers because these materials have variable and uncertain parameters.
- High material compliance is a very favorable feature of ionic polymers and has captured the attention of a variety of engineering fields. However, without a soft sensor to accompany the actuator, the applications will remain limited to research. Development of a soft sensor, to be used in conjunction with the ionic polymer actuator, would increase the practicality of their use. An ionic polymer sensor/actuator pair would be ideal and may not be too far in the future since the sensing capability of ionic polymers is presently under investigation. Regardless of the sensing unit, this would be a great advancement for the system integration of ionic polymers.

Bibliography

Akle, B., 2002, **Multilayer Ionic Transducers**, M.S. Thesis, Virginia Polytechnic Institute and State University.

Arena, P., Bonomo, C., Fortuna, L., and Frasca, M., 2002, *Electro-Active Polymers as CNN Actuators for Locomotion Control*, in: **IEEE International Symposium on Circuits and Systems**, Vol. 4, pp. 281–284.

Bacon, F., **Beama Journal**, Vol. 61, No. 6, 1954.

Bar-Cohen, Y., 2001, *Electroactive Polymers as Artificial Muscles - Reality and Challenges*, in: **42nd AIAA/ASME/ASCE/AHS/ASC Structures, Structural Dynamics, and Materials Conference**, Seattle, WA.

Bennett, M., 2002, **Manufacture and Characterization of Ionic Polymer Transducers Employing Non-Precious Metal Electrodes**, M.S. Thesis, Virginia Polytechnic Institute and State University.

Blevins, R., **Formulas for Natural Frequency and Mode Shape**, Krieger, Malabar, FL, 1979.

Ferrara, L., Shahinpoor, M., Kim, K., Schreyer, B., Keshavarzi, A., Benzel, E., and Lantz, J., 1999, *Use of ionic polymer-metal composites (IPMCs) as a pressure transducer in the human spine*, in: **SPIE Conference on Electroactive Polymer Actuators and Devices**, Vol. 3669, Newport Beach, CA, pp. 394–401.

Franklin, G., Powell, J., and Emami-Naeini, A., **Feedback Control of Dynamic Systems**, Third Edition, Addison-Wesley, Menlo Park, CA, 1994.

- Franklin, G., Powell, J., and Workman, M., **Digital Control of Dynamic Systems**, Third Edition, Addison-Wesley, Menlo Park, CA, 1998.
- Friedland, B., **Control System Design An Introduction to State-Space Methods**, McGraw-Hill, Boston, MA, 1986.
- Grove, W., **Philosophical Magazine**, Vol. 3, No. 14, pp. 139, 1839.
- Guo, S., Sugimoto, K., Fukuda, T., and Oguro, K., 1999, *A New Type of Capsule Medical Micropump*, in: **IEEE/ASME International Conference on Advanced Intelligent Mechatronics**, Atlanta, GA, pp. 55–60.
- Guo, S., Sugimoto, K., Hata, S., Su, J., and Oguro, K., 2000, *A New Type of Underwater Fish-like Microrobot*, in: **IEEE/RSJ International Conference on Intelligent Robots and Systems**, Vol. 2, Takamatsu, Japan, pp. 867–872.
- Inman, D., **Engineering Vibrations**, Second Edition, Prentice-Hall, Upper Saddle River, NJ, 2001.
- Jenkins, C. and Vinogradov, A., 2000, *Active Polymers for Space Applications*, in: **IEEE Aerospace Conference**, Vol. 7, Big Sky, MT, pp. 415–420.
- Kanno, R., Kurata, A., Hattori, M., Tadokoro, S., and Takamori, T., 1994, *Characteristics and Modeling of ICPF Actuator*, Vol. 2, pp. 691–698.
- Keshavarzi, A., Shahinpoor, M., Kim, K., and Lantz, J., 1999, *Blood pressure, pulse rate, and rhythm measurement using ionic polymer-metal composites sensors*, in: **SPIE Conference on Electroactive Polymer Actuators and Devices**, Vol. 3669, Newport Beach, CA, pp. 369–376.
- Laurent, G. and Piat, E., 2001, *Efficiency of Swimming Microrobots using Ionic Polymer Metal Composite Actuators*, in: **IEEE International Conference on Robotics and Automation**, Vol. 4, Seoul, Korea, pp. 3914–3919.
- Leo, D., Newbury, K., Mallavarapu, K., Griffin, S., and Shahinpoor, M., 2001, *Ionic Polymer Devices for Optical Positioning Systems*, in: **AIAA Space Conference**, Vol. 15, Albuquerque, NM, pp. 328–338.

- Mallavarapu, K., 2001, **Feedback Control of Ionic Polymer Actuators**, M.S. Thesis, Virginia Polytechnic Institute and State University.
- Mallavarapu, K. and Leo, D., 2001, *Feedback Control of Resonant Modes in Bending Response of Ionic Polymer Actuators*, in: **ASME/IMECE International Adaptive Structures and Materials Systems Symposium**, New York, NY.
- Nemat-Nasser, S., *Micro-mechanics of Actuation of Ionic Polymer-metal Composites (IPMCs)*, **Applied Physics**, Vol. 95, No. 5, pp. 2899–2915, 2002.
- Newbury, K., 2002, **Characterization, Modeling, and Control of Ionic Polymer Transducers** Ph.D. Thesis, Virginia Polytechnic Institute and State University.
- Oguro, K., Kawami, Y., and Takenaka, H., *Bending of an Ion-Conducting Polymer Film-Electrode Composite by an Electric Stimulus at Low Voltage*, **Trans. Journal of Micro-machine Society**, Vol. 5, pp. 27–30, 1992.
- Onishi, K., Sewa, S., Asaka, K., Fujiwara, N., and Oguro, K., 2000, *Biomimetic Microactuators Based on Polymer Electrolyte/Gold Composite Driven by Low Voltage*, in: **Micro Electro Mechanical Systems**, Miyazaki, Japan, pp. 386–390.
- Popov, V. M., **Hyperstability of Automatic Control Systems**, Springer Verlag, New York, NY, 1973.
- Rossi, D. D., Lorussi, F., Mazzoldi, A., Scilingo, E., and Orsini, P., 2001, *Active Dressware: Wearable Proprioceptive Systems Based on Electroactive Polymers*, in: **IEEE International Symposium on Wearable Computers**, Zurich, Switzerland, pp. 161–162.
- Sadeghipour, K., Salomon, R., and Neogi, S., *Development of a Novel Electrochemically Active Membrane and 'Smart' Material Based Vibration Sensor/Damper*, **Smart Materials and Structures**, Vol. 1, pp. 172–179, 1992.
- Salama, M. and Jenkins, C., 2001, *Intelligent Gossamer Structures: A Review of Recent Developments and Future Trends*, in: **42nd AIAA/ASME/ASCE/AHS/ASC Structures, Structural Dynamics, and Materials Conference**, Seattle, WA.
- Sewa, S., Onishi, K., Asaka, K., Fujiwara, N., and Oguro, K., 1998, *Polymer Actuator*

Driven by Ion Current at Low Voltage, Applied to Catheter System, in: **Micro Electro Mechanical Systems**, Heidelberg, Germany, pp. 148–153.

Shahinpoor, M., *Conceptual Design, Kinematics and Dynamics of Swimming Robotics Structures using Ionic Polymeric Gel Muscles*, **Smart Materials and Structures**, Vol. 1, No. 1, pp. 91–94, 1992.

Shahinpoor, M., Bar-Cohen, Y., Simpson, J., and Smith, J., *Ionic Polymer-Metal Composites (IPMCs) as Biomimetic Sensors, Actuators and Artificial Muscles - A Review*, **Smart Materials and Structures Journal**, Vol. 7, No. 6, pp. R15–R30, 1998.

Slotine, J.-J. and Li, W., **Applied Nonlinear Control**, Prentice-Hall, Upper Saddle River, NJ, 1991.

Tadokoro, S., Fuji, S., Fushimi, M., Kanno, R., Kimura, T., Takamori, T., and Oguro, K., 1998, *Development of a Distributed Actuation Device Consisting of Soft Gel Actuator Elements*, in: **IEEE International Conference on Robotics and Automation**, Vol. 3, Leuven, Belgium, pp. 2155–2160.

Tadokoro, S., Murakami, T., Fuji, S., Kanno, R., Hattori, M., Takamori, T., and Oguro, K., *An Elliptic Friction Drive Element Using an ICPF Actuator*, **IEEE Control Systems**, Vol. 17, No. 3, pp. 60–68, 1997.

Tadokoro, S., Yamagami, S., Ozawa, M., Kimura, T., Takamori, T., and Oguro, K., 1999, *Multi-DOF Device for Soft Micromanipulation Consisting of Soft Gel Actuator Elements*, in: **IEEE International Conference on Robotics and Automation**, Vol. 3, Detroit, MI, pp. 2177–2182.

Thomas, S. and Zalbowitz, M., 1999, “Fuel Cells - Green Power,” Tech. rep., Los Alamos National Laboratory.

Witherspoon, S. and Tung, S., 2002, *Design and Fabrication of an EAP Actuator System for Space Inflatable Structures*, in: **43rd AIAA/ASME/ASCE/AHS/ASC Structures, Structural Dynamics, and Materials Conference**, Denver, CO.

Witherspoon, S., Tung, S., and Roe, L., 2001, *Development of a MEMS-Based Health-Monitoring Module for Space Inflatable Structures*, in: **42nd**

AIAA/ASME/ASCE/AHS/ASC Structures, Structural Dynamics, and
Materials Conference, Seattle, WA.

Appendix A

Humidity Effects Data Plots

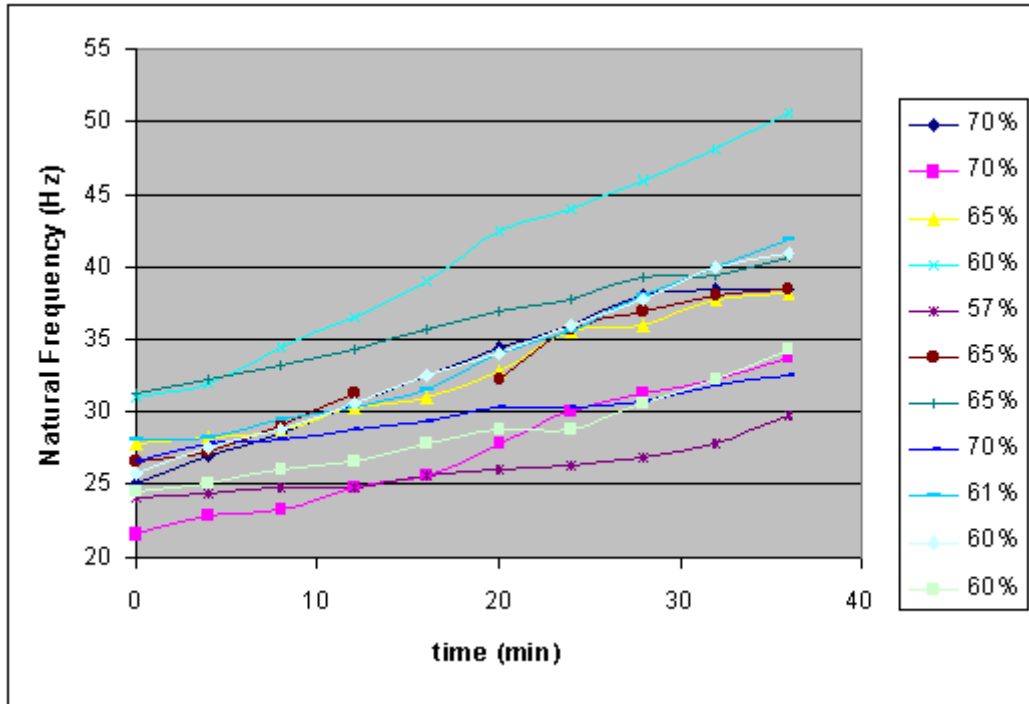


Figure A.1: Natural Frequency Shift as a Function of Time for Cantilever Ionic Polymer with 500mV-rms Input.

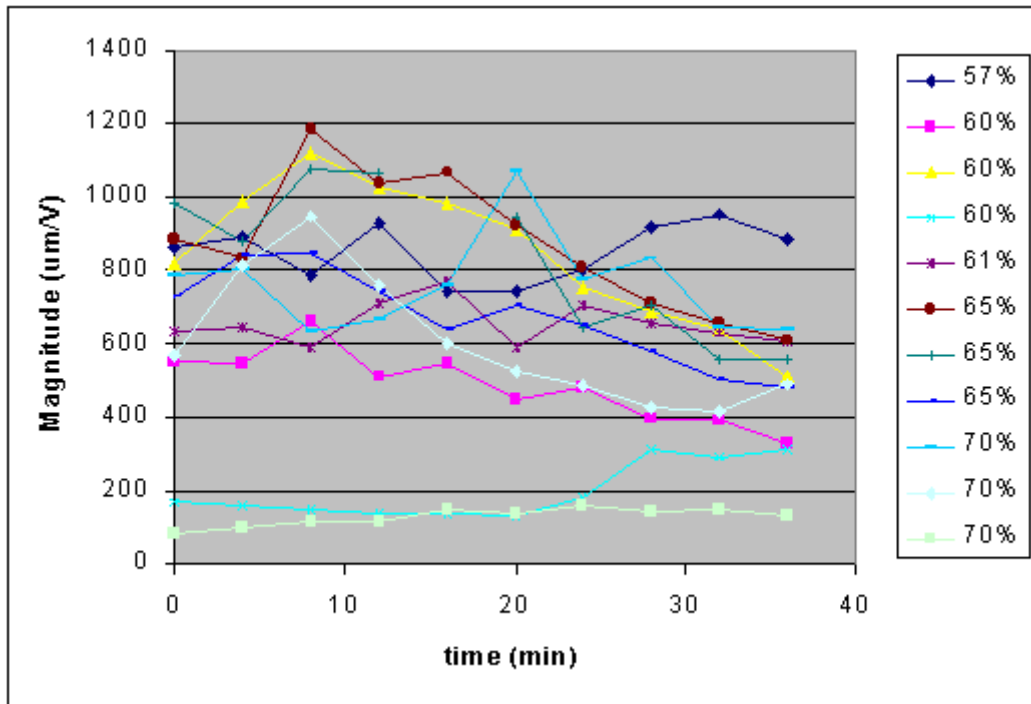


Figure A.2: Magnitude Shift as a Function of Time for Cantilever Ionic Polymer with 500mV-rms Input.

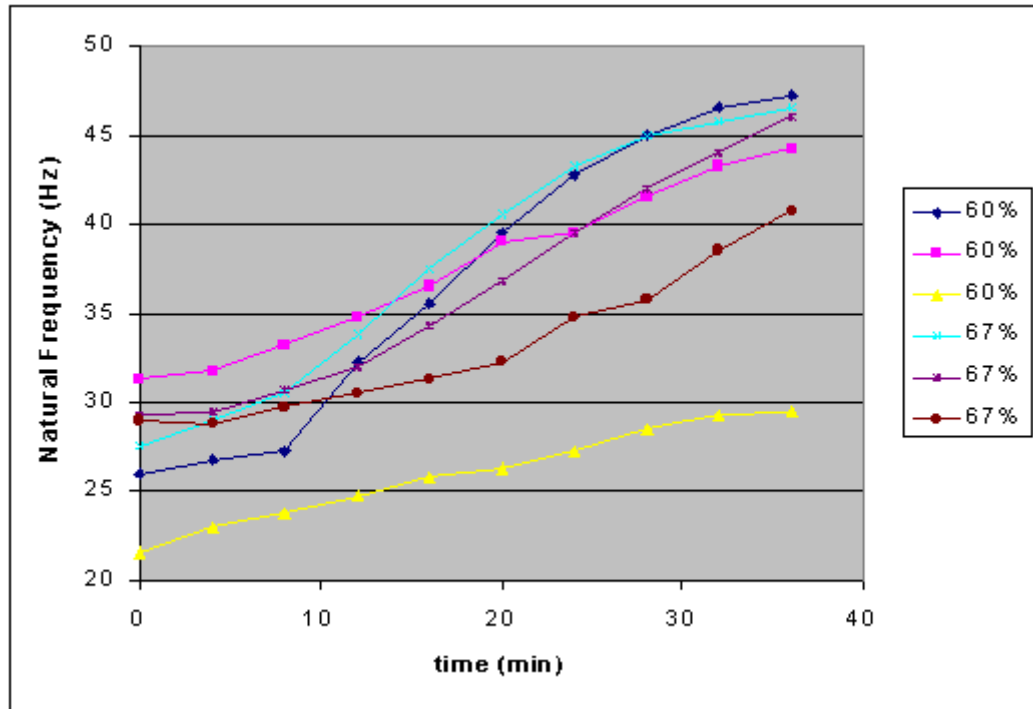


Figure A.3: Natural Frequency Shift as a Function of Time for Cantilever Ionic Polymer with 750mV-rms Input.

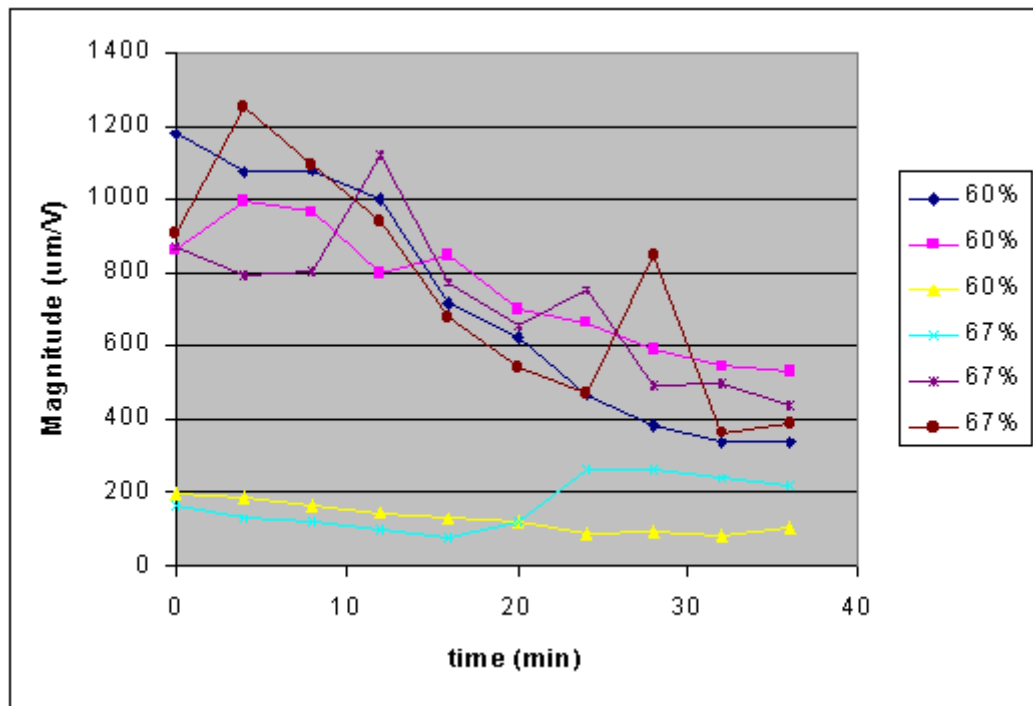


Figure A.4: Magnitude Shift as a Function of Time for Cantilever Ionic Polymer with 750mV-rms Input.

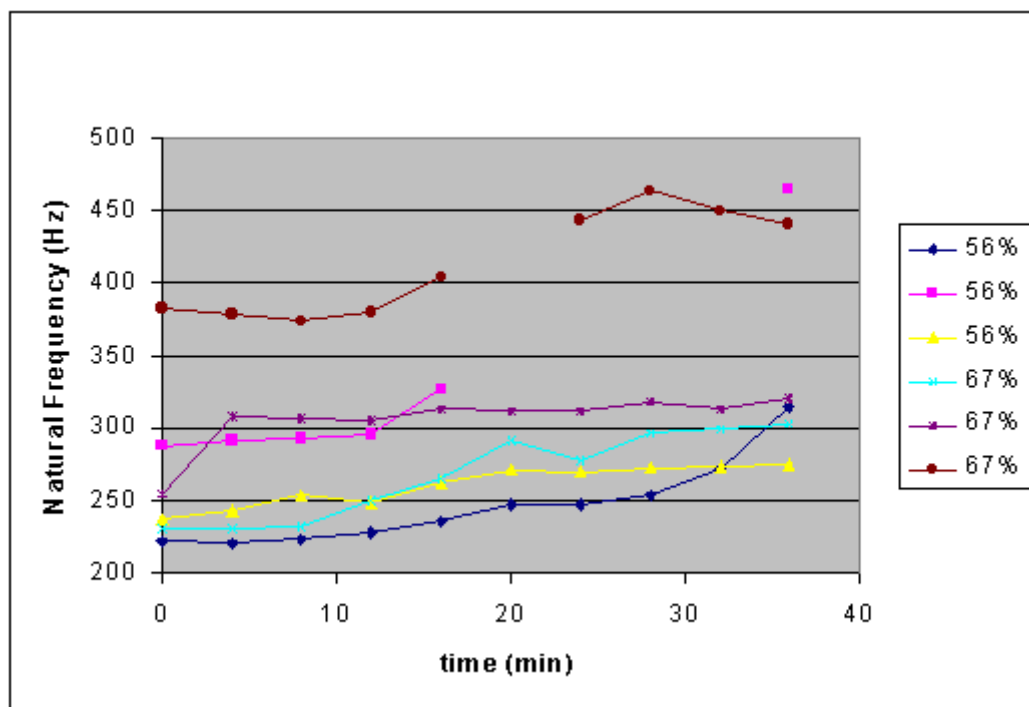


Figure A.5: Natural Frequency Shift as a Function of Time for Clamped-Clamped Ionic Polymer with 500mV-rms Input.

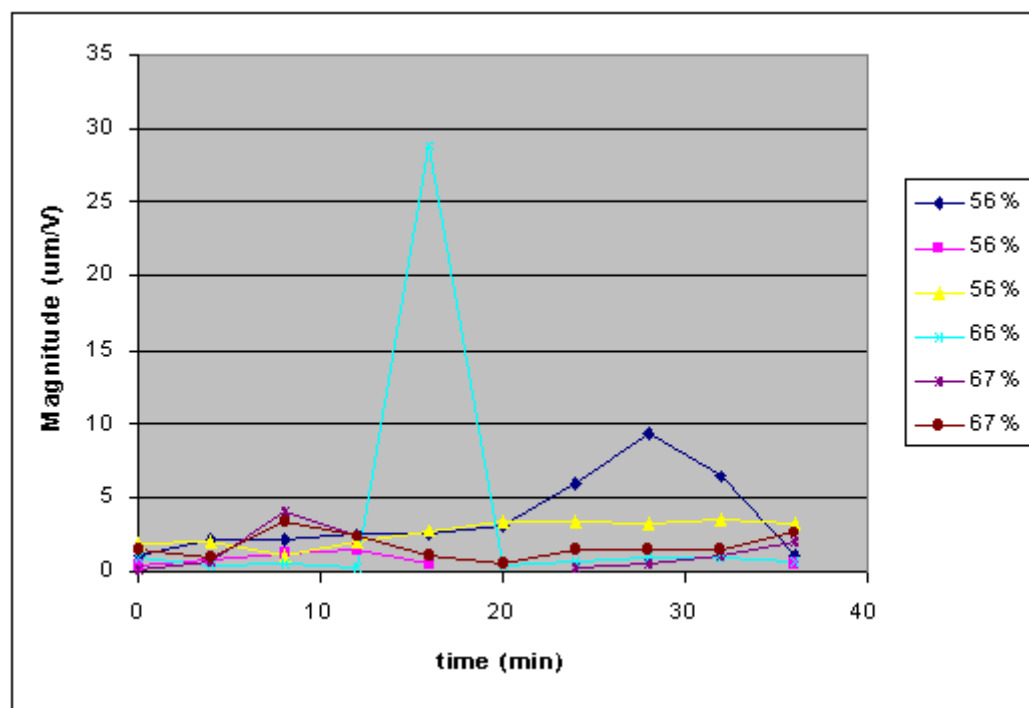


Figure A.6: Magnitude Shift as a Function of Time for Clamped-Clamped Ionic Polymer with 500mV-rms Input.

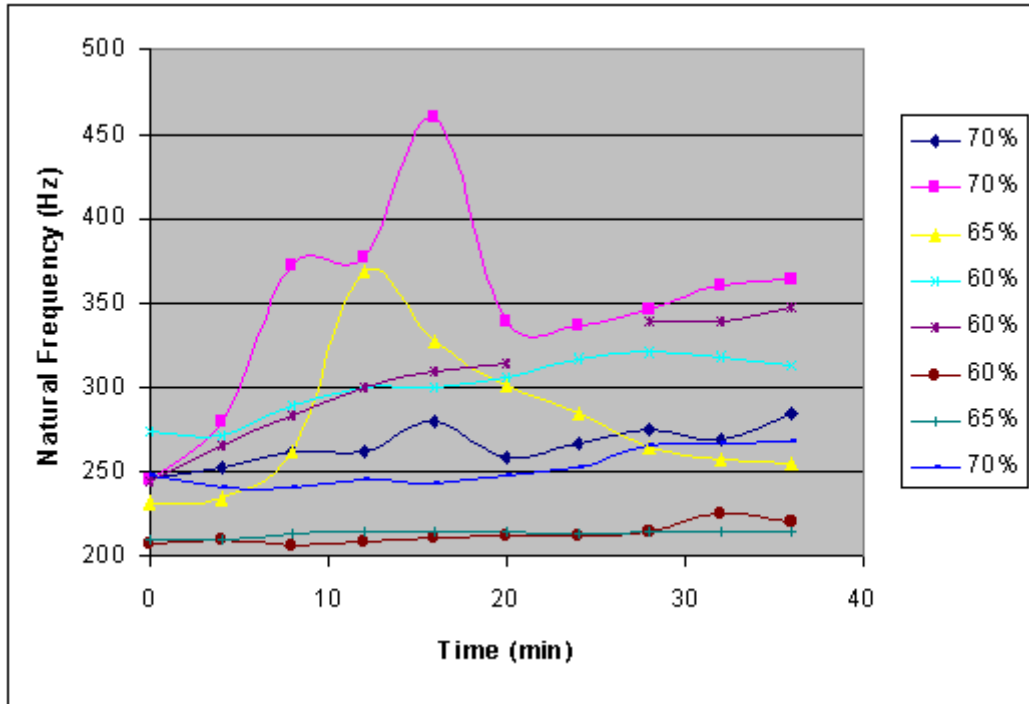


Figure A.7: Natural Frequency Shift as a Function of Time for Clamped-Clamped Ionic Polymer with 1V-rms Input.

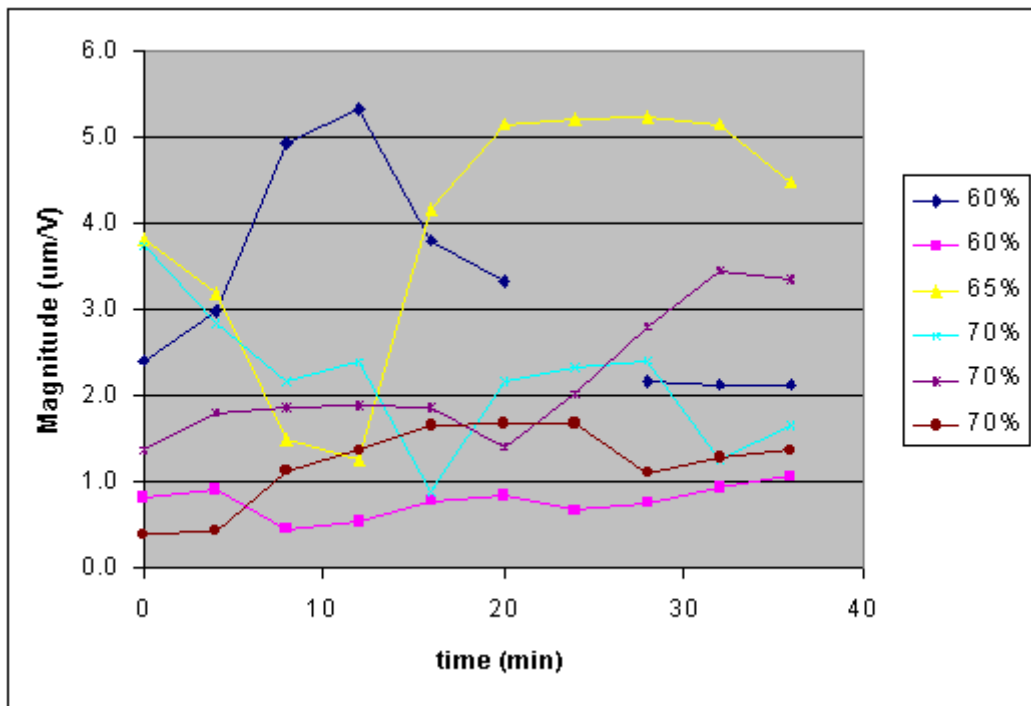


Figure A.8: Magnitude Shift as a Function of Time for Clamped-Clamped Ionic Polymer with 1V-rms Input.

Appendix B

Tension Effects Data Plots

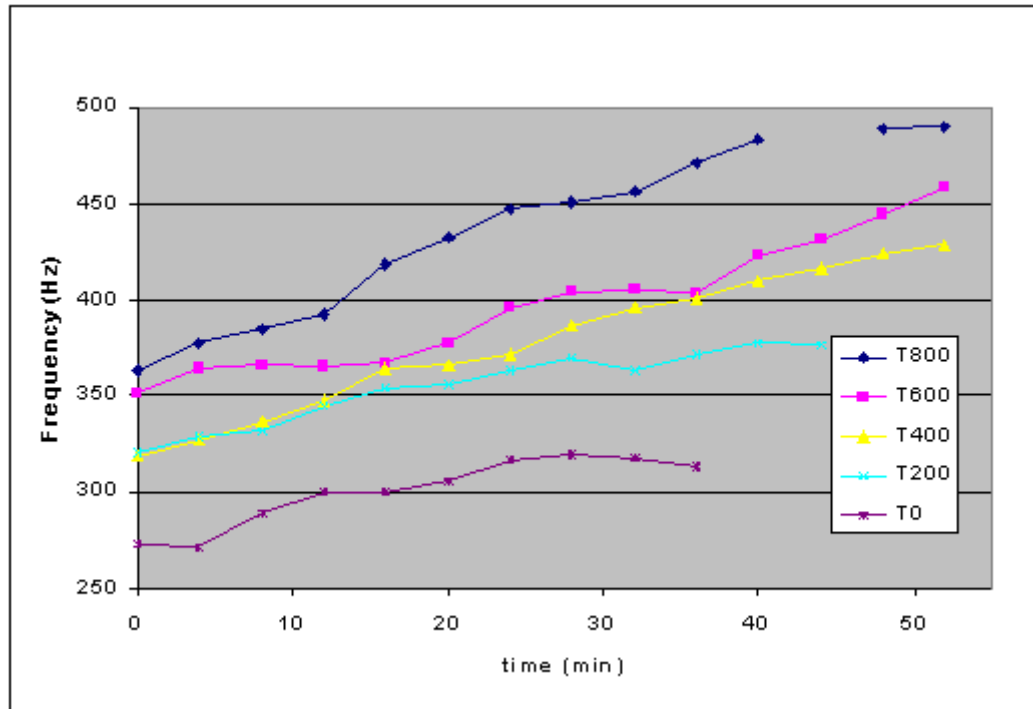


Figure B.1: Natural Frequency Shift as a Function of Time and Tension for Clamped-Clamped Ionic Polymer with 1V-rms Input. Tensions given in milli-Volts.

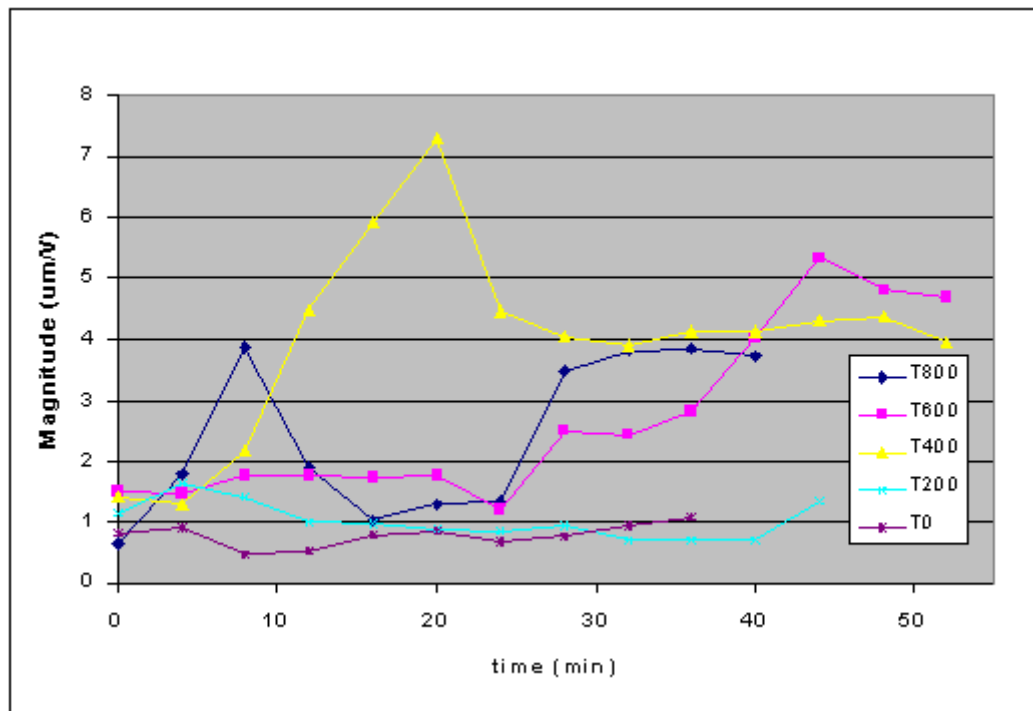


Figure B.2: Magnitude Shift as a Function of Time and Tension for Clamped-Clamped Ionic Polymer with 1V-rms Input. Tensions given in milli-Volts.

Appendix C

Control Scheme Block Diagrams

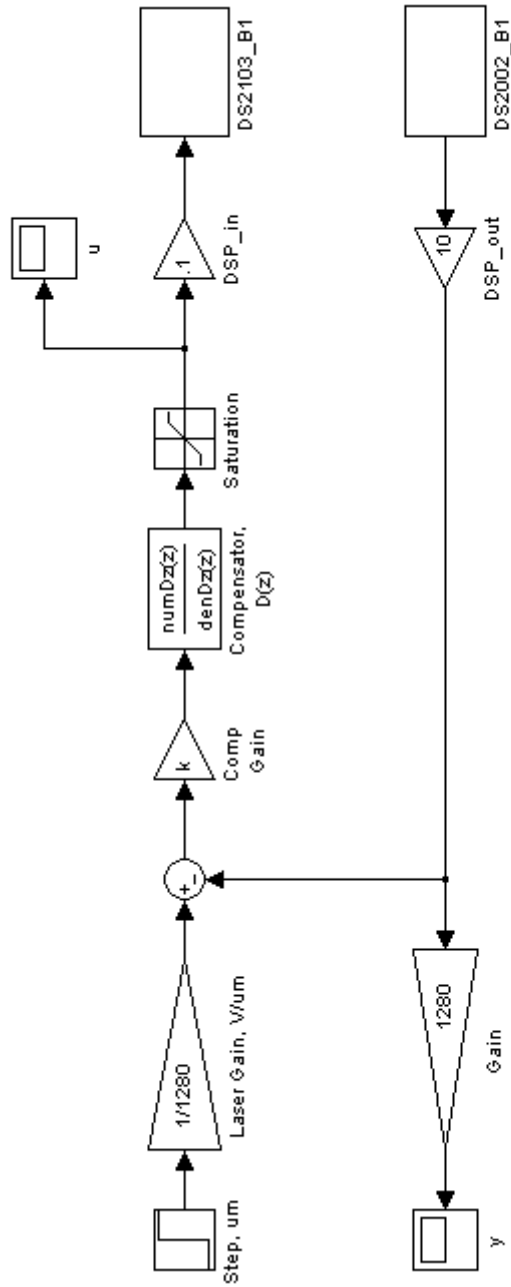


Figure C.1: Proportional-Integral Control Block Diagram.

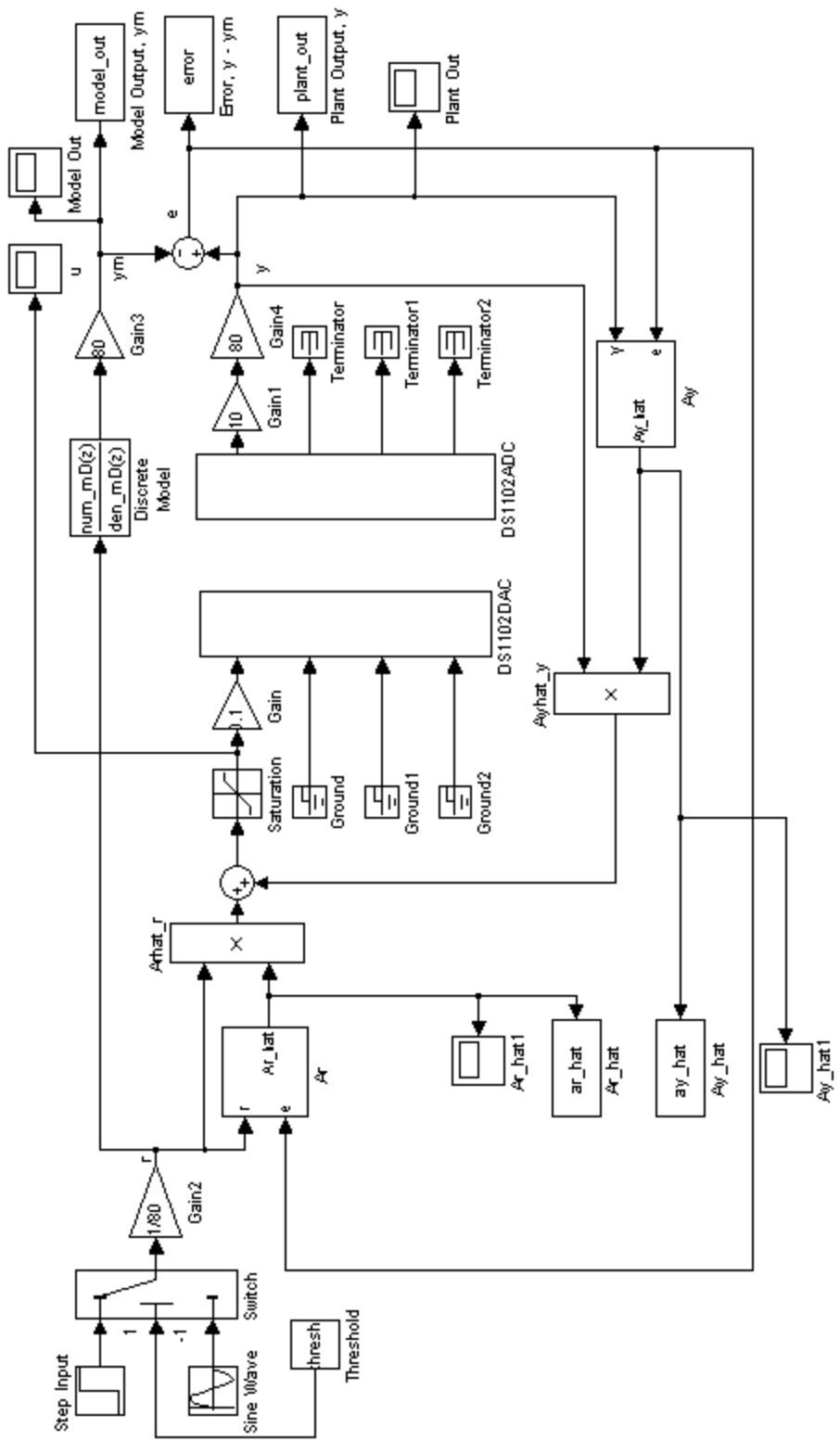


Figure C.2: Model-Reference Adaptive Control Block Diagram.

Vita

Curt Kothera was born on January 4, 1979 to Sharyn and Clark Kothera, in Ravenna, Ohio. At the age of 7, his family moved to Charlotte, North Carolina, where he graduated from Myers Park High School in 1997. Later that year, he attended Virginia Tech, with mechanical engineering being the discipline of choice. The fall semester of his junior year, Curt participated in a study abroad program at Luleå Tekniska Universitet in Luleå, Sweden. Back at Virginia Tech, he was accepted into the 5 year BS/MS program. Curt graduated Summa Cum Laude with a Bachelor of Science degree in Mechanical Engineering in May of 2001. The following summer placed him in Baltimore, Maryland, where he worked for Northrop Grumman's Electronic Sensors and Systems Sector. Returning to his studies in the fall of 2001, Curt worked as a teaching assistant for one semester before starting his graduate research under Dr. Donald J. Leo, in the Center for Intelligent Material Systems and Structures (CIMSS). His research focused on ionic polymer actuators. During the pursuit of his master's degree, Curt was selected for a summer position at the Air Force Research Laboratory in Albuquerque, New Mexico, as part of the Space Scholars Program.

Address: Center for Intelligent Material Systems and Structures
310 Durham Hall
Blacksburg, VA 24061

This thesis was typeset with L^AT_EX 2_ε¹ by the author.

¹L^AT_EX 2_ε is an extension of L^AT_EX. L^AT_EX is a collection of macros for T_EX. T_EX is a trademark of the American Mathematical Society. The macros used in formatting this thesis were written by Greg Walker, Department of Mechanical Engineering, Virginia Tech.